1970

Dielectric Properties Of Pentamethylene-sulfide - Pentamethylene-oxide

Ronald Richard Martin

DIELECTRIC PROPERTIES OF PENTAMETHYLENE SULFIDE-PENTAMETHYLENE OXIDE

by

Ronald R.H. Martin

Department of Chemistry

Submitted in partial fulfillment

of the requirements for the degree of

Doctor of Philosophy

Faculty of Graduate Studies

The University of Western Ontario

London, Canada

October 1969

To My Parents

ABSTRACT

The purpose of this work was to study the dielectric properties of the system pentamethylene sulfide-pentamethylene oxide. Both dielectric studies and other physical measurements showed the system to form a continuous series of solid solutions. A small portion of the pentamethylene sulfide rich region of these solid solutions proved suitable for studies of dielectric dispersion. These studies showed that Hoffman's interpretation of dielectric dispersion in solids (the multi-position, single axis rotator) is probably valid.

PROLOGUE

"The acquistion of exact knowledge is apt to be both tiresome and tedious but it is necessary to any degree of excellence."*

No work can claim intellectual value without clear purpose, be it implied or directly stated. It is my belief that the present work carries with it the clear purpose of examining dielectric relaxation and has specific value in that it lends support to a particular approach to this phenomenon. To claim;however, that this is its sole value would be to take a singularly myopic view of its implications.

At some indefinite period in our mental developement the humanities and the natural sciences parted company and have since moved in separate spheres. That such a move was the inevitable result of increasing disciplinary specialization does nothing to repair the damage of the schism. Man still pursues as a unit a common if indefinite goal.

I submit, then, that this work has a second purpose. It attempts to explore the meaning of one small part of the physical universe in the belief that understanding of the inanimate might lead to understanding of ourselves. Thus even the most insignificant work must be viewed as a contribution to the sum of human knowledge, a thought which is contained in this work and which has made its tedious moments more bearable.

* Bertrand Russell.

ACKNOWLEDGEMENTS

I wish to express my thanks to Dr. Raymond Chan without whose understanding and advice this work would never have been completed. I wish also to acknowledge my indebtedness to my fellow graduate students, in particular my associates William Clayton, Hemming Chew and Shu Chung Liao.

The financial support afforded by Canadian Industries Limited, Ontario Graduate Fellowships and the National Research Council is also gratefully acknowledged.

Errata

There is no page 122. Error in numbering pages.

TABLE OF CONTENTS

LIST OF TABLES

LIST OF FIGURES

CHAPTER I

INTRODUCTION

A. The prime purpose of this work is to study the dielectric dispersion observable in the frequency range from 100 Hz to 100 kHz in the solid system pentamethylene oxide:pentamethylene sulfide. As in the case with many scientific investigations this was by no means clear from the outset and the system was subjected to much examination before such clear purpose was introduced. It is accordingly the desire of the author to set some of the basic concepts of dielectric dispersion, with particular attention to binary, solid, organic systems to serve as a guide to the reader. Certain sections of the discussion which accompanies the results of the present work will deal entirely with other physical aspects of the system under investigation. It is to be stressed that these are complementary to the main work and that the main weight of argument to be used will deal with dispersion. All meaningful discussion of the current results will be found not in this portion of the work but rather in the discussion itself to which the reader sufficiently familiar with dielectric work is immediately referred.

B. Capacitance and the Dielectric Constant

The capacitance of a given conductor is defined such that C, the capacitance, is the proportionality constant between Q, the charge in the medium and V, the potential of the medium such that

$$C = \frac{Q}{V} \qquad (1)$$

The dielectric constant may be defined as the ratio of the capacitance of a given medium to that of free space such that:

$$\epsilon = C/C_o \qquad (2)$$

where ϵ is the dielectric constant, C is the capacitance of the medium and C_o is that of free space. The dielectric constant is thus dimensionless and is unity for free space. It is the fact that it is dependent on the medium, the temperature, and the frequency of measurement that, while casting a shadow on the adjective "constant", makes its value a subject of interest and hence suitable for study.

C. Basis for the Existence of a Dielectric Constant

1) Non-Polar Substances and the Clausius-Mosotti Equation

Figure 1, below, shows a simple parallel-plate capacitor containing a dielectric medium between the plates of a capacitor.

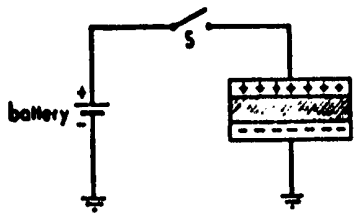

Figure I

If the material between the plates, initially vacuum, is replaced by a non-polar material it will be found that the total charge Q on the plates has increased. Since the voltage supplied is constant in this array, reference to equation (1) clearly shows that the capacitance of the assembly has increased. Equation (2) may now be used to indicate that the dielectric constant of the material between the plates of the capacitor is greater than unity. We now seek an explanation for this phenomenon.

Faraday (1) has pointed out that the molecules of which a dielectric is composed are themselves aggregates of discrete charges and hence are polarizable in an electric field. This property permits a compensating charge to form at the surface of the dielectric in contact with the condenser plates and hence allows the ability of the capacitor to store charge to be enhanced.

This observation, that the material composing a dielectric is polarizable, was used by Clausius* (2) and Mosotti (3) who derived an expression for the dielectric constant of a non-polar dielectric. The result, known as the Clausius-Mosotti (4a) equation is considered next.

Consider the field between the plates of a condenser such as that shown in figure I. The field perpendicular to the plates is given by:

$$E_o = 4\pi\sigma \tag{3}$$

Where σ is the surface charge density on the plates. Introduction of a dielectric material leads to a decrease in the field strength such that:

$$E = 4\pi\sigma/\epsilon \tag{4}$$

This decrease in field strength could have been achieved by reducing σ such that

$$\sigma \frac{(\epsilon - 1)}{\epsilon} = P \tag{5}$$

this latter effect being due to polarization, P, of the dielectric material. We now introduce a new quantity, the electric displacement D defined such that

---

* Reference to the original papers, as in this case, is often a matter of historical rather than real interest. Since the results of these investigations are given with deeper insight in later works I shall always refer to these later and better sources as well.

$$D = 4\pi\sigma \tag{6}$$

Clearly

$$D = \epsilon E \tag{7}$$

Whence

$$D = E + 4\pi P \tag{8}$$

and

$$\epsilon - 1 = \frac{4\pi P}{E} \tag{9}$$

Now the induced electric moment m associated with an individual molecule will be simply

$$m = \alpha_o F \tag{10}$$

Where α_o is the polarizability (which may or may not be isotropic) and F is the field intensity to which the molecule is subjected. It is obvious that the total polarization per unit volume of a molecular assembly will be the sum of the individual moments i.e.

$$P = N_1 m \tag{11}$$

where N_1 is the number of molecules per unit volume.

Consider now a molecule at the centre of a spherical cavity in a dielectric between the plates of a capacitor. The cavity is considered to be small with respect to the volume of dielectric but large compared to the size of the molecule. Our reference molecule is now subjected to an electric field composed of three components:

$$F = F_1 + F_2 + F_3 \tag{12}$$

Where: F_1 is the field due to the charge on the condenser plates, F_2 is

the field due to the polarization of the surface of the spherical cavity and F_3 is the field due to the molecules removed to create the cavity. This latter is taken to be zero and has been rigorously shown to have this value for gases and cubic crystals (5). It may then be shown:

$$F_1 = 4\pi\sigma \tag{13}$$

$$F_2 = -4\pi P + \frac{4\pi}{3} P \tag{14}$$

Whence from (12)

$$F = E + \frac{4\pi P}{3} \tag{15}$$

And using (11), (9) we obtain

$$\frac{\epsilon - 1}{\epsilon + 2} = \frac{4\pi N_1}{3} \alpha_0 \tag{16}$$

Since $N_1 = Nd/M$

where N = Avogadro's number, d is the density and M the molecular weight we have at once:

$$P = \frac{\epsilon - 1}{\epsilon + 2} \frac{M}{d} = \frac{4\pi N}{3} \alpha_0 \tag{17}$$

this latter equation being the desired result. It should be noted with reference to equation (9), (12) and (15) that the field assumed to be acting on a given molecule is:

$$F = \frac{(\epsilon + 2)}{3} E \tag{18}$$

This is the Lorentz field and is not always adequate. This derivation has been carried out for the expressed purpose of introducing the concept of internal field. Its estimation by other means will be discussed later in this work.

The value of equation (17) for substances such as 2,2,4-trimethylpentane (6) and benzene (8) has been demonstrated. It has even been applied to solid cyclohexane with considerable success (9). It has been found however that substances like ethyl bromide in the vapor state have a high polarization which decreases as a linear function of the absolute temperature (10,11). Clearly equation (17), which is independent of temperature, is inadequate in this case. It was Debye (12a) who supplied the necessary correction which we consider next.

It is evident that, in addition to the polarization induced in the molecules as a result of the motion of electrons and nuclei in an applied field, there will be polarization arising from the alignment of molecules having a permanent dipole moment with the field. This dipole moment arises from the fact that, due to different electronegativities of the constituent atoms, there is an unsymmetric distribution of charge in the molecule. The molecule naturally retains its overall electrical neutrality. It is the alignment of these dipoles in the electric field that was considered by Debye.

The potential of a dipole oriented with the axis of an electric field is:

$$U = -\mu F \tag{19}$$

If the dipole makes an angle Θ with the field direction this becomes

$$= -\mu F \cos\Theta \tag{20}$$

Using Boltzmann's distribution function we may write, for the number of dipoles in a certain solid angle $d\Omega$, $A\, e^{-U/kT}\, d\Omega$ where A is a constant dependent on the number of dipoles present. Thus we obtain for the average moment per molecule:

$$\bar{m} = \frac{\int_{Ae} (\mu F/kT)^{\cos\theta} \mu \cos\theta \, d\Omega}{\int_{Ae} (\mu F/kT)^{\cos\theta} \, d\Omega} \qquad (21)$$

After integration this equation yields a Langenvin (13) function which may be expanded to yield:

$$\bar{m} = \frac{\mu^2 F}{3kT} \qquad (22)$$

for small values of $\mu F/kT$, which is invariably the case under normal circumstances.

Recalling equation (10) we are now able to write for equation (22) the average moment due to induced polarization and that due to the permanent dipole moment of a molecule:

$$\bar{m} = \alpha_o F + \frac{\mu^2 F}{3kT} = (\alpha_o + \frac{\mu^2}{3kT})F \qquad (23)$$

setting

$$\alpha = \alpha_o + \frac{\mu^2}{3kT} \qquad (24)$$

We may write for (17):

$$\frac{\epsilon - 1}{\epsilon + 2} \frac{M}{d} = P = \frac{4\pi N\alpha}{3} = \frac{4\pi N}{3} (\alpha_o + \frac{\mu^2}{3kT}) \qquad (25)$$

where (25) is the Clausius-Mosotti-Debye equation. This equation has been verified (8) by a number of workers and is now well established for the gas phase, and dilute solutions (7). It does however suffer from a serious limitation. If for a moment we ignore non-dipole polarization we may write equation (25) as:

$$\frac{\epsilon - 1}{\epsilon + 2} = \frac{4\pi N\mu^2}{9kT} \qquad (26)$$

$$T_c = \frac{4\pi N_1 \mu^2}{9k} \tag{27}$$

whence

$$\frac{\epsilon - 1}{\epsilon + 2} = \frac{T_c}{T} \tag{28}$$

If T_c is equal to T the right hand side of equation (28) must become unity and the dielectric constant must increase without bound.* For water equation (27) yields a T_c of 1,140°K and since the predicted effect does not occur equation (25) must be incorrect.

So far it has been shown that the dielectric constant is due to two effects; induced polarization due to the mobility in an applied field of the charged particles of which molecules are composed and the alignment with the field of molecules having a permanent dipole associated with them. It is proposed that our attention should next be directed to some refinements of equation (25) in order to learn what further evidence of the structure of matter might be obtained from the dielectric constant.

D. Inner Field: The Equations of Onsager and Kirkwood

It was Onsager (14) who proposed that the failure of equation (25) was due to an over-estimation of the field strength within the cavity containing the reference dipole. A qualitative description of Onsager's approach is now given. The reader cannot do better than to refer to Böttcher's (15a) detailed description for further information. Consider Figure 2:

---

* The substance becomes a ferroelectric with spontaneous alignment of dipoles.

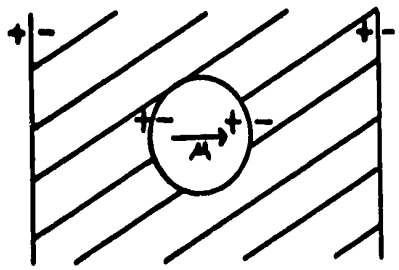

Figure 2

If there is no dipole at the center of the cavity illustrated the field within the cavity will be the Lorentz field as discussed by Mosotti and Debye. The introduction of a dipole to the cavity has the following effects:

(a) The field of the dipole induces further polarization on the surface of the dielectric sphere.

(b) The field acting on the dipole enhances the dipole moment of the polar molecule.

(c) The field of the dipole opposes the external field.

The result of (a) and (b) (which reach an equilibrium value rather than continuing indefinitely) is to increase the strength of the dipole. It should be noted that the increased polarization at the cavity surface is due to the dipole and hence has no effect on the alignment of the dipole, as does the external field. The effect of (c) is to reduce the field strength within the cavity; in fact the net effect of (a), (b) and (c) is to reduce the cavity field. It is this reduction of field strength which leads to elimination of the catastrophic increase in the dielectric constant observed in the Debye equation. Onsager's equation may now be written:

$$\mu_o^2 = \frac{9kT}{4\pi N}\frac{M}{d}\frac{(2\epsilon + n^2)}{3\epsilon(n^2+2)}\frac{(\epsilon+2)}{}\left[\frac{(\epsilon-1)}{(\epsilon+2)} - \frac{(n^2-1)}{(n^2+2)}\right] \qquad (29)$$

where n is the index of refraction measured with sodium D light.*

Fig. 3 (16a) shows the agreement of Onsager's equation

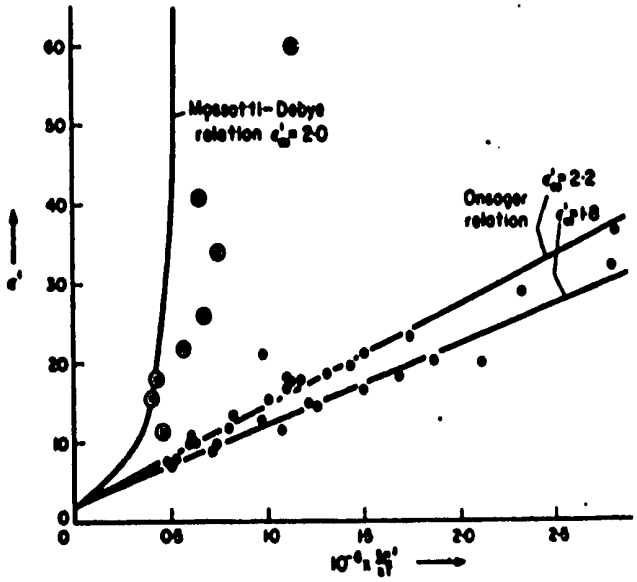

Figure 3

Permittivity (ε') of liquids as a function of s (molecules per cm), μ (dipole moment) and T°K (after R. H. Cole). Points O represent hydroxylic liquids.

with experiment together with the failure of the Clausius-Mosotti-Debye relationship. It is important to note the high and scattered results for hydrogen-bonded compounds. This observation leads to the next improvement in our picture of dielectrics, the Kirkwood (17) equation.

The fault Kirkwood sought to correct may be best appreciated if we consider the environment immediately surrounding our reference dipole. In the Clausius-Mosotti development the reference molecule was in a cavity large compared to the molecule but small compared to the volume of dielectric. Onsager considered the cavity to be of molecular dimensions but considered the material surrounding the molecule to be homogeneous. Kirkwood has restored the molecularity of the system by considering discrete nearest-neighbor interactions between the reference dipoles and

---

* Strictly the index of refraction at infinite frequency but sodium D light is used by most authors.

its neighbors. Kirkwood's result is:

$$g\mu^2 = \frac{9kT}{4\pi Nd}\left[\frac{(\epsilon-1)(2\epsilon+1)}{9\epsilon} - \frac{n_D^2-1}{n_D^2+2}\right] \tag{30}$$

The principal difference between this equation and that of Onsager is the term g, the so-called g-factor. It is included in order to account for the alteration of the dipole moment of the molecule under consideration as a result of interaction with its nearest neighbours. We have

$$\mu\bar{\mu} = g\mu^2 \tag{31}$$

where μ is the regular dipole moment and $\bar{\mu}$ is the altered one. Kirkwood writes:

$$g = 1 + z\,\overline{\cos\psi} \tag{32}$$

where z is the number of nearest neighbours and

$$\overline{\cos\psi} = \int \cos\psi\; e^{-W/kT}\, d\Theta \tag{33}$$

Here ψ is the angle between neighboring dipole pairs, W is the hindering potential preventing dipole orientation with the applied field, the integral of $e^{-W/kT}$ being normalized to unity. In the case of liquids z is related to the radial distribution function. If solids are considered the integral in equation (33) is replaced by a sum over specific angles and potential barriers. With solids z can be determined, at least in principle, from X-ray data. Thus, theoretically at least, g and hence ϵ can be determined. It is more usual however to estimate g by insertion of measured values into equation (30). Typical results are shown in tables (18) I and II.

TABLE I. Dielectric constants of the normal alcohols at 20°C.

	g(obs.)	g(calc.)	ϵ(obs.)	ϵ(calc.)
Methyl alcohol	2.94	2.57	32.8	29.2
Ethyl alcohol	3.04	2.57	24.6	21.3
n-Propyl alcohol	3.07	2.57	19.5	17.3
n-Butyl alcohol	3.21	2.57	18.0	14.6
n-Amyl alcohol	3.43	2.57	15.8	12.8

TABLE II. Correlation parameters of several polar liquids.

	t (°C)	$\mu.10^{18}$ (Debye)	ϵ (observed)	g (observed)
Hydrogen cyanide	20	2.80	116	4.1
Hydrogen fluoride	0	(1.8)	83.6	3.1
Hydrogen peroxide	0	2.13	91	2.8
Ammonia	15	1.48	17.8	1.3
Ethyl ether	20	1.15	4.4	1.7
Acetone	20	2.85	21.5	1.1
Nitrobenzene	20	3.90	36.1	1.1
Ethyl bromide	20	1.80	9.4	1.1
Pyridine	20	2.20	12.5	0.9
Benzonitrile	20	3.90	25.2	0.8

Materials with g factors greater than one are often referred to as associated, those with g = one are called normal liquids and will be found to obey Onsager's equation. Examples of g factors less than one

have been observed and this last effect has been ascribed to an antiparallel arrangement of dipoles (19a).

In summary we now have three equations for the dielectric constant (25), (29) and (30). These constitute progressively better approximations of ϵ. There are, of course, other equations mostly containing empirical approximations of the inner field or allowing for molecular geometry (anisotropy of α) but these do not lead to great improvement and are not necessary to a basic theoretical understanding of dielectric constant.

E. Relation Between the Dielectric Constant and the Index of Refraction.

Maxwell (20) first supplied the relationship between the dielectric constant and the refractive index. Maxwell's equation is:

$$n^2 = \epsilon b \tag{34}$$

where b is the magnetic permeability of the medium. In cases where b is close to one (for diamagnetic substances) we write:

$$n^2 = \epsilon \tag{35}$$

It will be immediately obvious to the reader familiar with dielectric measurements that this relation is often far from true. Consider the case of ethyl alcohol with $n_D^{20^\circ} = 1.36$ and $\epsilon = 24.6$. The resolution of this difference lies in a recognition of the fact that the dielectric constant is a function of frequency of the electric field and before equation (35) can be true the dielectric constant must be measured at the same frequency as the index of refraction. The reason for this difference may be readily appreciated if we consider the polarizability as expressed in equations (17) and (25). From our development of

Debye's equation it is obvious that we have added a term to the polarizability expressed by equation (17). Because of the need to account for additional polarization as a result of alignment of permanent dipoles in the system we may then write:

$$P_{total} = P_{induced} + P_{dipole} \tag{36}$$

Now at the normal frequencies at which the index of refraction is measured the electric field changes too rapidly for the dipoles to follow and we observe a much lower dielectric constant. It is in fact observed that the dielectric constant measured in the microwave region is often (but not always) identical to the square of the index of refraction measured by the sodium D line.

Let us digress briefly to consider the nature of equation (36) when P dipole is zero. It was stated earlier in this work that induced polarization was due to the mobility of elementary charged particles making up the atoms of a dielectric. We may thus write for equation (36) with P dipole zero:

$$P_{induced} = P_E + P_A \tag{37}$$

where P_E is the polarization due to mobility of electrons and P_A is due to motion of the positively charged nuclei. It is possible to separate these terms in the following way. Insertion of equation (35) into equation (17) yields:* (21,22)

$$\frac{n^2-1}{n^2+2}\left(\frac{M}{d}\right) = [R] \tag{38}$$

---

* Note this formula was derived independently and without reference to a discussion such as that given above by Lorentz and Lorentz (see references).

where R is the molar refraction. Since the index of refraction is often measured at frequencies sufficiently high that atomic polarization does not contribute appreciably it may be desirable to have an estimate of both the electronic and atomic polarization. This is often obtained by extrapolating the index of refraction to infinite wavelength with the aid of the Cauchy* relationship:

$$n = n_\infty + \frac{a}{\lambda^2} \tag{39}$$

where λ is the wavelength at which the measurement is made, n the observed index of refraction, n_∞ the index of refraction at infinite wavelength and a is constant. Measurement of n at two different wavelengths thus allows calculation of n_∞ from the relation:

$$n_\infty = \frac{\lambda_1^2 n_1 - \lambda_2^2 n_2}{\lambda_1^2 - \lambda_2^2} \tag{40}$$

This result combined with equations (38) and (17) allows the evaluation of the electronic and atomic polarization from index of refraction measurements in the optical region. In practice use of equation (40) is difficult allowing many errors in measurement to accumulate in P_A which is small at any rate. It has become common practice to assign P_A arbitrarily somewhere between 5 and 15 percent of the total induced polarization.

It has been mentioned that the dielectric constant at microwave frequencies does not always agree well with n_D^2. There has been considerable discussion as to the significance of this difference. Poley (23) has reported significant differences** between the high frequency

---

* This approach is discussed in detail in Böttcher (15a), page 255.

** These differences are supplied in Whalley's paper.

dielectric constant and n_D^2. He has suggested that this is due to a high frequency polar relaxation process. Smyth (24) later studied the same substances examined by Poley and found much better agreement between the two values. Such controversy regarding the value of the high frequency dielectric constant is common and illustrates the experimental difficulties involved. However Whalley (25) points out that in the particularly well documented* case of water $n_D^2 \doteq 1.78$, high frequency dielectric constant $\doteq 5.5$ the discrepancy is due to the contribution of vibrating dipoles which at high frequencies will still contribute to the dielectric constant as the vibrations allow the dipoles to contribute to the polarization.

F. Dielectric Dispersion - The Debye Formulation

It has been repeatedly stated in this work that the dielectric constant often varies with the frequency of the applied electric field used to measure it. The term dispersion is applied to the change in any physical property with the frequency of the force applied to measure it. Such dispersion is due to the relaxation time of the material where the relaxation time is said to be due to the delayed response of the system to an applied force. In the present case a force, in the form of an electric field, will be applied to a dielectric and the time required for the system to respond, in this case become polarized,** will be studied.

---

* Suitable references are supplied in Whalley's paper.

** Strictly speaking, it is the time required for the polarization to decay to within $1/e$ of its equilibrium value after the removal of the polarizing field.

A typical example of the variation of dielectric constant with frequency (26) for a real system is shown in Figure 4.

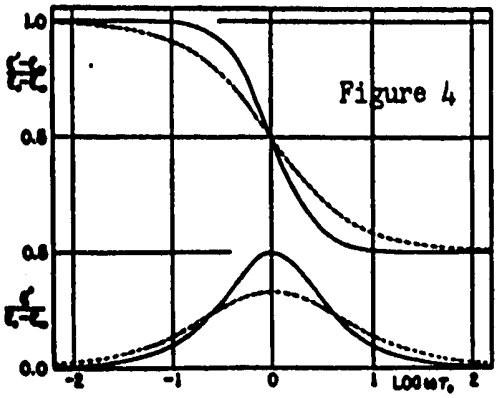

Figure 4

Before beginning an examination in detail of dielectric dispersion it will be necessary to define certain symbols and relationships. These are: ϵ_o = static dielectric constant i.e. the dielectric constant of the sample in a constant field.

ϵ_∞ = high frequency dielectric constant i.e. the dielectric constant in a field oscillating sufficiently rapidly that orientational polarization does not occur.

ϵ^* = the complex dielectric constant. This term is introduced in analogy to the real and imaginary parts of an oscillating electric field. It is defined such that:

$$\epsilon^* = \epsilon' - i\epsilon'' \tag{41}$$

ϵ' is the measured dielectric constant and ϵ'' (the imaginary part) is a measure of the energy loss in the sample as a result of the relaxation process.

We shall now begin a consideration of Debye's (12b) formulation of relaxation in dielectrics. Kauzmann(26) has shown:

$$dP_{(t)}/dt = 4\pi kP_{(t)} = -k_o P_{(t)} \tag{42}$$

where $P_{(t)}$ is polarization at time t and k_o is the rate at which dipoles jump from one orientation to another. This leads to a simple exponential function for the rate of decay of polarization after the removal of the field:

$$P_{(t)} = P_o e^{-k_o t} \tag{43}$$

where P_o is the initial polarization. The relaxation time τ is then defined as the time required for the polarization to fall to 1/e of its initial value, hence:

$$\tau = 1/k_o \tag{44}$$

Kauzmann develops equation (42) further to yield:

$$dP/dt = -\tfrac{1}{2} \left\langle k \varphi^2 \right\rangle_{av} (P - \frac{No\mu^2}{3kT} F) \tag{45}$$

or

$$\frac{dP}{dt} = -\tfrac{1}{2} \left\langle k\varphi^2 \right\rangle_{av} (P - No\, a_\mu F) \tag{46}$$

where a_μ is polarizability due to dipole orientation and $\left\langle k\varphi^2 \right\rangle_{av}$ dt is the mean square angle moved in an interval of time dt defined by

$$\left\langle k\varphi^2 \right\rangle_{av} = \int \varphi^2 k_o(\varphi) d\Omega \tag{47}$$

At this point I beg the reader's indulgence. I wish to digress to show where Kauzmann and Debye part company, since the result of their difference of opinion leads to an interpretation of τ to which I shall have occasion to refer later.

Kauzmann has considered k to be a measure of the frequency with which molecular jumps to new orientations occur. Debye assumed k was a measure

of the probability of finding the molecule in a new orientation after a set time interval. Under this latter condition Einstein (27) has shown:

$$\int \varphi^2 k_o(\varphi) d\Omega = \langle k\varphi^2 \rangle_{av} = 4kT/\zeta \tag{48}$$

where $\langle k\varphi^2 \rangle_{av}$ is the mean square deviation of angle per unit time and ζ is the average coefficient of frictional resistance opposing angular rotation. The torque which then leads to an angular velocity of $d\theta/dt$ thus is:

$$T = \zeta \, d\theta/dt \tag{49}$$

Let us now consider the dipole to be a sphere of radius a immersed in a homogeneous medium of viscosity η. Stokes' law now yields:

$$\zeta = 8\pi\eta a^3 \tag{50}$$

Substitution in (46) yields

$$\frac{dP}{dt} = -\frac{1}{\tau}(P - N_o \alpha_\mu F) \tag{51}$$

where

$$\tau = 4\pi\eta a^3/kT \tag{52}$$

Further reference will be made to equation (52).

Let us now end the present digression and return essentially to equation (46) and write, for the decay of polarization due to dipole orientation after removal of the field:

$$\frac{dP}{dt} = -k_o(P_\mu - N_o \alpha_\mu F) \tag{53}$$

Now, using the Lorentz field we write:

$$F = \frac{4\pi}{3}\left(\frac{\epsilon_\infty + 2}{3}\right)P_\mu \tag{54}$$

so that

$$\frac{dP_\mu}{dt} = -k_o \left(\frac{\epsilon_o+2}{\epsilon_o+2}\right)P_\mu \quad = -k_o' P_\mu \tag{55}$$

where $k_o'^{-1}$ is often referred to as the macroscopic relaxation time, τ, which obviously differs from the molecular relaxation rate k_o^{-1}. Since the exact difference depends on the form of the inner field which is used and the difference is usually small (28) the latter value for τ will be used without further comment in this paper. Now, in the interest of brevity we write

$$dP/dt = -k_o' \left[P_\mu - N_o \alpha_\mu \left(\frac{\epsilon_o+2}{3}\right) E \right] \tag{56}$$

where $E = R\left[E_o e^{i\omega t}\right]$ and $P_\mu = R\left[P_o e^{i\omega t}\right]$ and is periodic with the same frequency as E, further

$$P_{oT} = P_{o\mu} + P_{oel} = \frac{N_o \alpha_\mu}{1 + i\omega\tau} \left(\frac{\epsilon_o + 2}{3}\right) E_o$$

$$+ \alpha_{el} \left(E_o + \frac{4\pi}{3} P_{oT}\right) \tag{57}$$

Knowing $4\pi P_{oT} = (\epsilon - 1)E_o$ and employing equation (41) we obtain the Debye dispersion relations:

$$\epsilon' - \epsilon_\infty = \quad = \frac{\epsilon_o - \epsilon_\infty}{1 + (\omega\tau)^2} \tag{58}$$

$$\epsilon'' = \frac{(\epsilon_o - \epsilon_\infty)}{1 + (\omega\tau)^2} \omega\tau \tag{59}$$

A simpler derivation of (58) and (59) may be found in Davies (16).

C. Discussion of Debye Formulation - Some Additional Equations:

In older literature particularly it was conventional to display dielectric dispersion data by plotting either ϵ' and/or ϵ'' against frequency. This procedure together with the Debye representation has already been shown in Figure 4. A more convenient method has been suggested by Cole and Cole (29), not surprisingly this approach has become known as a Cole-Cole plot. It consists of plotting ϵ'' against ϵ'. It may be seen by eliminating $\omega\tau$ from (58) and (59) to obtain:

$$\left[\epsilon' - \frac{\epsilon_o+\epsilon_\infty}{2}\right]^2 + [\epsilon'']^2 = \left[\frac{\epsilon_o-\epsilon_\infty}{2}\right]^2 \qquad (60)$$

Now note that (60) is the equation of a circle with displaced center, i.e. of the form:

$$(x-a)^2 + y^2 = R^2 \qquad (61)$$

where

$$x = \epsilon'$$

$$a = \frac{\epsilon_o+\epsilon_\infty}{2}$$

$$y = \epsilon''$$

$$R = \frac{\epsilon_o-\epsilon_\infty}{2}$$

One further point remains to be examined before continuing with a discussion of the form of the dispersion. That is an expression of τ, the relaxation time in terms of the frequency at which the dielectric absorption is a maximum. From equation (59) we have:

$$\frac{d\epsilon''}{d\omega} = \left[\frac{(\epsilon_o-\epsilon_\infty)}{1+(\omega\tau)^2}\right]\left[1\ \frac{-2\omega^2\tau^2}{1+\omega^2\tau^2}\right] \qquad (62)$$

Setting the second bracket equal to zero we have at once:

$$\omega_c = 1/\tau_o^* \tag{63}$$

This allows a determination of the relaxation time from a knowledge of the frequency dependence of ϵ''.

Really excellent agreement with experiment has been achieved in a number of cases (30). There are, however, numerous exceptions - as might well be expected since the facile analysis employed by Debye can hardly be expected to apply to a large number of real systems.

Figure 5 (29) shows Cole-Cole plots for a number of systems which do not conform to equations (58) and (59):

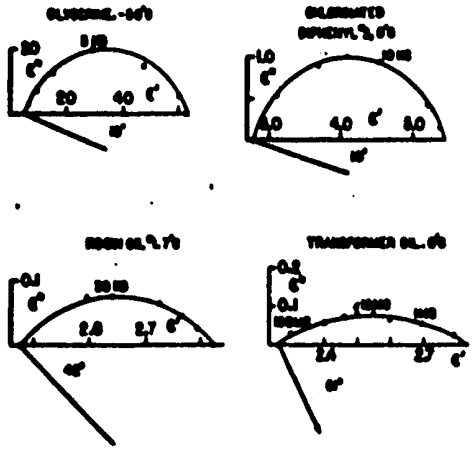

FIG. 5 Complex dielectric constants of liquids.

For these systems Cole and Cole (29) have supplied an empirical equation, which is modification of that given by Debye. It is:

$$(\epsilon' - i\epsilon'') - \epsilon_\infty = (\epsilon_o - \epsilon_\infty)/\left[1+(i\omega\tau_o)^{1-\alpha}\right] \tag{64}$$

---

* The subscript used with τ i.e. τ_o is introduced here because the deviations from Debye behavior are thought to be due to a distribution of relaxation times about a critical value τ_o.

Separation of real and imaginary parts of equation (64) yields:

$$\epsilon' - \epsilon_\infty = \frac{(\epsilon_o - \epsilon_\infty)\left[1 + (\omega\tau_o)^{1-\alpha}\sin(\tfrac{1}{2}\alpha\pi)\right]}{1 + 2(\omega\tau_o)^{1-\alpha}\sin(\tfrac{1}{2}\alpha\pi) + (\omega\tau_o)^{2(1-\alpha)}}$$

$$= \tfrac{1}{2}(\epsilon_o - \epsilon_\infty)\left[1 - \frac{\sinh(1-\alpha)x}{\cosh(1-\alpha)x + \sin(\tfrac{1}{2}\alpha\pi)}\right] \qquad (65)$$

$$\epsilon'' = \frac{(\epsilon_o - \epsilon_\infty)(\omega\tau_o)^{1-\alpha}\cos(\tfrac{1}{2}\alpha\pi)}{1 + 2(\omega\tau_o)^{1-\alpha}\sin(\tfrac{1}{2}\alpha\pi) + (\omega\tau_o)^{2(1-\alpha)}}$$

$$= \frac{\tfrac{1}{2}(\epsilon_o - \epsilon_\infty)\cos(\tfrac{1}{2}\alpha\pi)}{\cosh(1-\alpha)x + \sin(\tfrac{1}{2}\alpha\pi)} \qquad (66)$$

where $x = \ln(\omega\tau_o)$. α is a number between 0 and 1, the former value reducing the expression to the original Debye formulation. As shown in Figure 5 this representation results in a symmetric arc representation of the dispersion with $\alpha\,\pi/2$ being the angle between the ϵ' axis and the radius of the circle forming the symmetric arc, drawn $\perp$ to the tangent of the curve at $\epsilon'' = 0$. The parameter α can best be described as an index of the amount by which the observed dispersion differs from "ideal" Debye representation.

The value of the Cole symmetric arc lies in its ability to reproduce the data found for a great many liquid and solid systems. As a successful empirical relationship it serves as something of a marker allowing theoreticians to seek, from a molecular or other model to generate an equation of the same form thus giving physical meaning to the observed parameters. The extent to which this has been done for the symmetric arc and for the following types of empirical relationships will be dis-

cussed along with the dispersion results observed in this work.

The third type of frequently observed dispersion is the Cole-Davidson* (31) skewed-arc shown in Figure 6 (32).

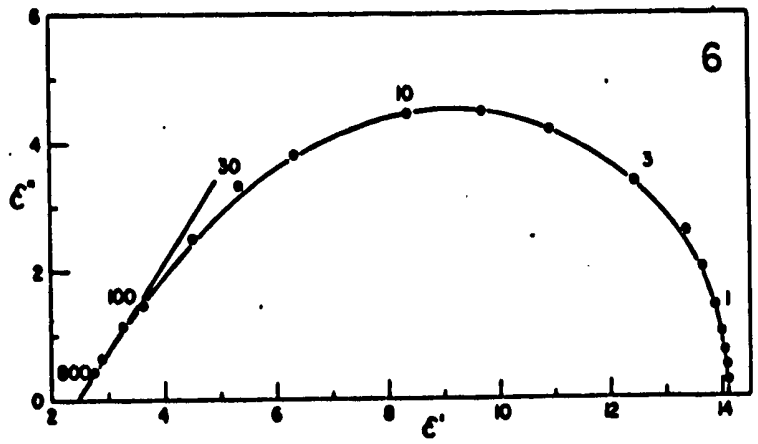

Figure 6. Tetrahydrofurfuryl alcohol at -105.9°C. Skewed-arc locus is drawn for $\beta = 0.592$. Numbers beside points are frequencies in kc/sec.

Reference shall be made to this formulation as the Davidson formulation or the skewed-arc.

Once again the equation used in an empirical one. Its form is:

$$(\epsilon' - \epsilon'') - \epsilon_\infty = (\epsilon_0 - \epsilon_\infty)/(1 + i\omega\tau_0)^\beta \qquad (67)$$

Separation of real and imaginary parts yields:

$$\frac{\epsilon' - \epsilon_\infty}{\epsilon_0 - \epsilon_\infty} = (\cos\phi)^\beta \cos\beta\phi \qquad (68)$$

$$\frac{\epsilon''}{\epsilon_0 - \epsilon_\infty} = (\cos\phi)^\beta \sin\beta\phi \qquad (69)$$

---

* We now have two empirical functions. They shall be referred to in the following ways:
Cole-Cole = Symmetric arc = Cole
Cole-Davidson = Skewed arc = Davidson
This being done in the interest of variety and/or brevity. It is believed that no confusion should arise.

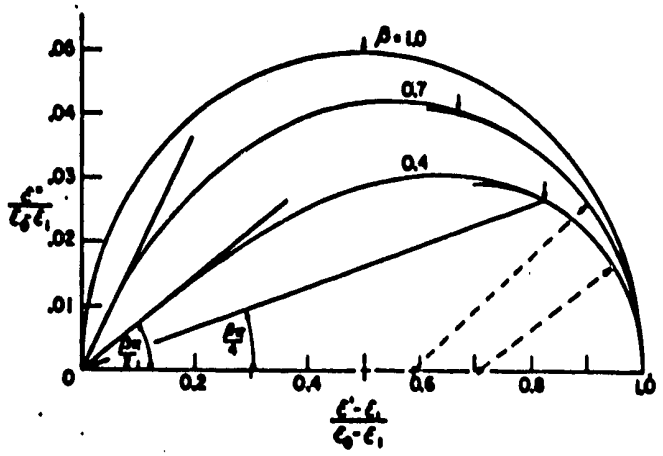

Skewed-arc loci on the complex dielectric constant plane. Arrows indicate frequencies at which $f = f_{max}$. broken lines the radii of circular arcs which coincide with the loci at low frequencies.

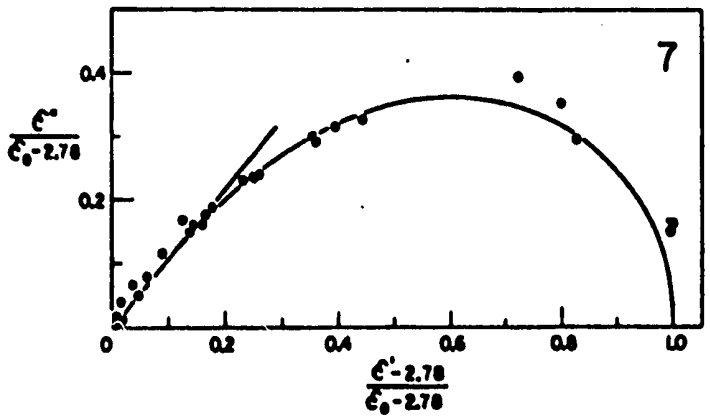

Aggregate plot for 2-methyl-2,4-pentanediol at temperatures between -45 and -79 C and frequencies of I, I0, 30, and I00 kc/sec. Locus is drawn with $\beta = 0.525$.

Figure 7

where $\phi = \tan^{-1}\omega\tau_0$ and β is a parameter such that $\beta \leq 1$. When $\beta = 1$ equation (67), once again, reduces to Debye's result. Figure 7 shows the effect of varying β and illustrates the geometric interpretation of $\beta(\pi/2)$ as the angle between the linear high frequency portion of the function and the ϵ' axis.

Finally let us consider the type of relaxation behavior evidenced by Figure 8 (33).

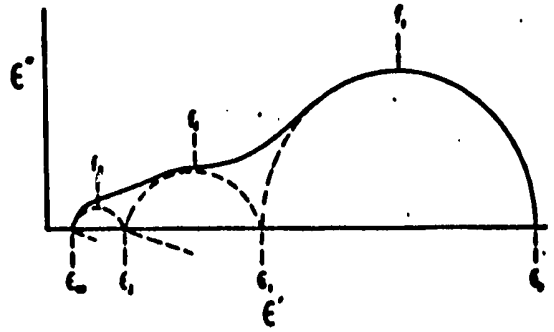

FIG. 8 Schematic dielectric constant locus for overlapping dispersions.

This type of so-called multiple dispersion is considered to be, as shown, the sum of several independent dispersions. Figure 9 (33) shows resolution of such dispersion in n-propanol.

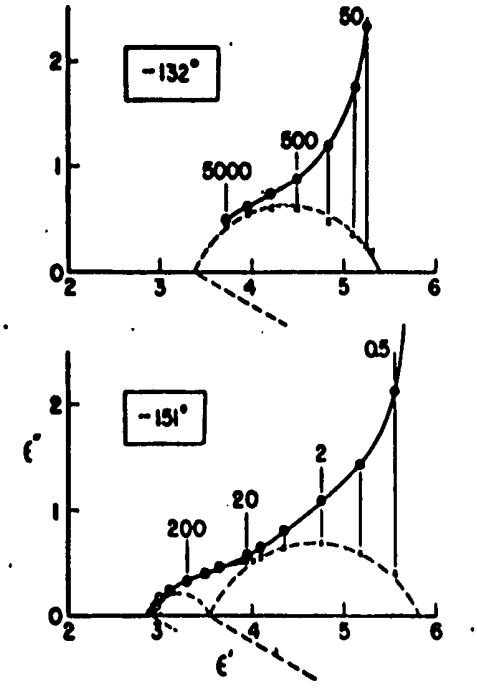

FIG. 9 High frequency portions of complex dielectric constant loci for n-propanol at −132° and −151°. Circles are measured values, crosses are values obtained by subtraction of contributions from the low frequency dispersion. Indicated frequencies are in kc/sec.

This behavior seems to occur most frequently in glasses, solids and solutions of two different rotating species. Detailed discussion will be reserved for that accompanying our own results.

H. Rate Theory of Dielectric Relaxation.

The so-called Absolute Rate Theory of Eyring (34) has been applied to dielectric relaxation (26,35). Reference should now be made to Figure 10 which may be regarded as the energy of a dipole in an electric field as a function of its position. Here it is considered that the dipole may be aligned either with the field or against it and that there is some energy barrier which must be overcome by the molecule, which requires a considerable amount of energy to surmount this barrier.

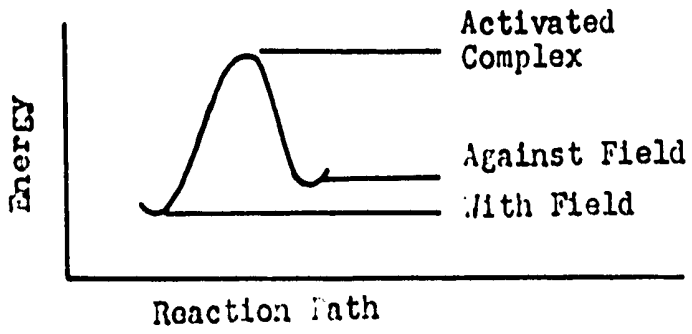

Figure 10

Now a molecule, having reached the top of the energy barrier between the two stable positions may be said to be an "activated complex" similar to that described by Eyring. Now we may write, for the number of molecules crossing the barrier in unit time,

$$\#\text{ of molecules} = jN^{*}z \tag{70}$$

where N^{*} is the number of activated complexes present, z is the rate at which the activated complex decays in the desired direction, j is the transmission coefficient measuring the number of complexes which, having started to decay in the right direction, get turned around and return to the

initial position.

If we now calculate the number of activated complexes present by assuming thermodynamic equilibrium between the activated complex and reactants* we may proceed by assuming that this equilibrium may be represented by the ratio of the partition function of the activated complex to that of the reactant molecules. Thus:**

$$\text{Equilibrium constant} = F_o' / \prod_i F_i \tag{71}$$

Now let us abstract from F_o' the translational degree of freedom corresponding to motion of the activated molecule into the "product" state (i.e. alignment with the field) we thus have:

$$F_o' = F_o^* (2\pi m^* kT)^{\frac{1}{2}} \frac{l}{h} \tag{72}$$

where m^* = inertial mass moving along the reaction coordinate and l is the linear dimension of this coordinate.

Now, the mean velocity along the reaction coordinate in the desired direction is

$$\bar{v} = (kT/2\pi m^*)^{\frac{1}{2}} \tag{73}$$

and thus we find for z of equation (70)

$$z = \frac{\bar{v}}{l} = \frac{kT}{(2\pi m^*)^{\frac{1}{2}}} l^{-1} \tag{74}$$

Combining the last five equations we now write for the reaction rate k_o:

$$k_o = j \left(\frac{kT}{h}\right) \left(\frac{F_o^*}{F_o}\right) \tag{75}$$

---

* By reactant we mean dipoles not aligned with the field.

** N* will be N (# of reactant molecules), times equilibrium const.

where $F_o = \prod_i F_i$

Now $\frac{F_o^*}{F_o}$ is itself an equilibrium constant. From thermodynamics we write:

$$K = \frac{F_o^*}{F_o} = e^{-\Delta G^\ddagger/RT} \tag{76}$$

$$= e^{\Delta S^\ddagger/R} e^{-\Delta H^\ddagger/RT} \tag{77}$$

where $\Delta G^\ddagger$, $\Delta S^\ddagger$ and $\Delta H^\ddagger$ are, respectively, the molar free energy, entropy and enthalpy required to enter the transition state. The reaction rate may now be written:

$$k_o = j \frac{kT}{h} e^{-\Delta G^\ddagger/RT} \tag{78}$$

$$= j \frac{kT}{h} e^{\Delta S^\ddagger/R} e^{-\Delta H^\ddagger/RT} \tag{79}$$

Since $1/k_o = \tau_o$, the relaxation time, much of the above thermodynamic data is obtainable from knowledge of τ_o. Consider (assuming $j = 1$)

$$\tau_o = \frac{h}{kT} e^{\Delta H^\ddagger/RT} e^{-\Delta S^\ddagger/R} \tag{80}$$

Whence

$$\ln \tau_o = \frac{1}{T} \frac{\Delta H^\ddagger}{R} - \ln T + \left(\ln \frac{h}{k} - \frac{\Delta S^\ddagger}{R}\right) \tag{81}$$

It may be seen that $\Delta H^\ddagger$ may be obtained from (81) by plotting $\ln \tau_o T$ vs $1/T$ but sufficiently accurate results have so far been achieved with plots of $\ln \tau_o$ vs $1/T$. (26)*

This type of analysis will be discussed further in the light of the results of the present work.

---

* In this work a plot of $\ln T\tau_o$ vs $1/T$ will be used.

CHAPTER II

EXPERIMENTAL

A. Introduction

The prime object of this investigation has been examination of the dielectric relaxation process in the mutual solid solutions of pentamethylene sulfide and pentamethylene oxide. It was immediately obvious that certain physical information about the system would prove useful and not all of this information was available in the literature. The experimental section of this paper thus contains a description of all procedures used to obtain the required physical properties of this system, together with a detailed outline of the methods used to study the dielectric constant.

B. Materials

The pentamethylene sulfide used was supplied by the Aldrich Chemical Company Inc. It was certified reagent grade and was reported by the supplier to have $n_D^{26} = 1.5050$. This material was purified by distillation through a twelve inch Vigreaux column from calcium hydride, the portion boiling between 141-142°C being retained, a literature value of 141.75°C having been reported (36). After this procedure the index of refraction was found to be $n_D^{18} = 1.5047$. This agreed well with the quoted value and that of Lydia Reinisch (37) who reported $n_D^{18} = 1.5046$. Gas chromatography showed the compound to be free of volatile impurities. The

sample was stored in sealed flasks covered with aluminum foil in a vacuum desiccator partially filled with silica gel. The pentamethylene oxide was supplied by K and K Laboratories of Plainsview, New York and was reported by the supplier to have $n_D^{20} = 1.4200$. This compound was purified in the same manner as that used for pentamethylene sulfide and was stored in the same way. The product was found to have $n_D^{25} = 1.4176$ which compared favorably with reported values in the literature, i.e., $n_D^{21} = 1.4211$ (38), $n_D^{30} = 1.4157$ (39) and $n_D^{30} = 1.4159$ (40). The additional literature values were sought because the product was found to boil at 87°C, the fraction between 87 and 88°C being collected. This was in good agreement with Allen and Hibbert (38) but contrasted with a second literature value (41) of 81-82. It seems reasonable to conclude that the latter is in error.

During the course of this work it became necessary to recover pure starting materials from solution. The wide separation of boiling points allowed this to be done using the distillation apparatus described. The purity of the products was insured by the same physical tests already outlined. In a final test a Beckman Infrared Spectrometer was used to obtain spectra of both the starting materials and recovered products. In all cases the spectra were found to be indistinguishable.

C. Density Measurements

The density of pentamethylene sulfide and pentamethylene oxide together with that of a series of their mutual solutions was determined in the liquid state.

The density measurements were carried out using a double stem pycnometer calibrated with thrice distilled water.

The temperature of the sample was obtained by immersion in a water

bath maintained at the desired temperature by a Sargent Thermoniter. Readings of sample volume were taken starting one hour after the pycnometer was placed in the water bath and were continued at ten minute intervals till a constant value was obtained.

These results are recorded and discussed in Chapter III Section B.

D. Index of Refraction

The index of refraction of the pure components and a series of their solutions was determined using an Abbe-3L Refractometer supplied by Bausch and Lomb, thermostated at 25°C. Results are recorded and discussed in Chapter III Section C.

E. Measurement of Dipole Moment

The dipole moments of both pentamethylene sulfide and pentamethylene oxide were measured using a WTW DM01 Dipole Meter with carbon tetrachloride as solvent, employing the Guggenheim-Smith equation (42,43).

The carbon tetrachloride was purified in the same manner as the pentamethylene oxide.

The results are recorded and discussed in Chapter III, Section D.

F. Differential Thermal Analysis

Differential thermal analysis was carried out on pure pentamethylene sulfide and pentamethylene oxide together with a series of their mutual solutions at ten mole percent intervals.

The solutions of appropriate concentrations were prepared using the densities of the pure components to ascertain the required volumes of pure material which were then mixed using a syringe accurate to within 0.001 ml.

This analysis was carried out using an array of copper-constantan thermocouples which permitted the measurement of both the temperature of the sample and that of a naphthalene reference. The output of the thermocouples was recorded as a continuous function of time on a two-pen recorder.

The sample and its naphthalene reference were located in separate glass tubes inserted in symmetrically drilled holes in an aluminum control block. The entire assembly was then placed in a fifteen liter stainless steel Dewar where heating and cooling took place. The assembly is shown in Figure IIand is similar to that used by McMillan and Los (44).

Cooling of the assembly was initiated by the addition of liquid nitrogen to the Dewar containing the aluminum block; heating by allowing the liquid nitrogen to evaporate overnight. The average cooling rate was $2^{\circ}C$ per minute while heating took place at $0.5^{\circ}C$ per minute. Since the heating results were more consistent and reproducible than the cooling results which were complicated by supercooling, the former are regarded as being closer to equilibrium values and are quoted exclusively.

Transitions in the solid state of the compounds under study often involve changes in the molecule's orientation relative to its neighbors. It was feared that dissolved gas molecules might lubricate the lattice (45) and alter the transition temperature observed. To avoid this difficulty selected samples were condensed into the measuring cell and sealed under vacuum. Since no changes in the transitions were observed the practice was discontinued.

The sealing technique used is clearly illustrated in Figure 12. It proved useful for the reasons just outlined and because it allowed the

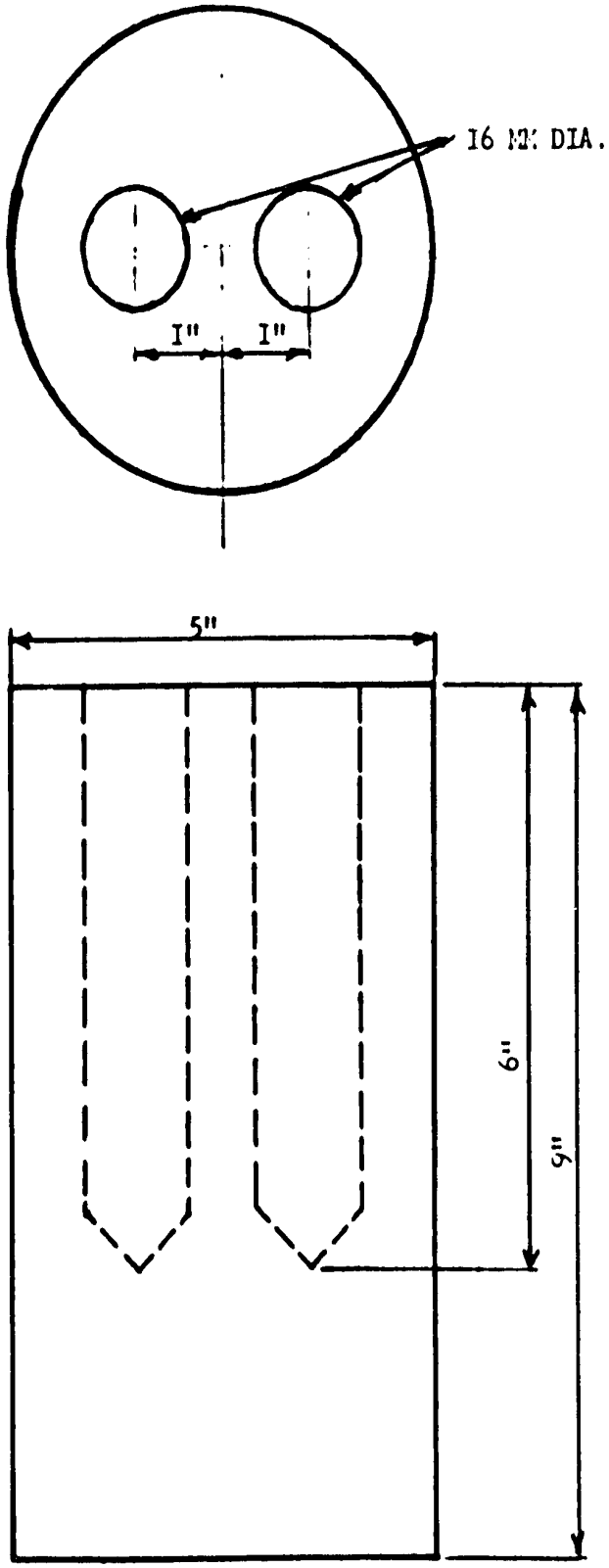

Figure II.

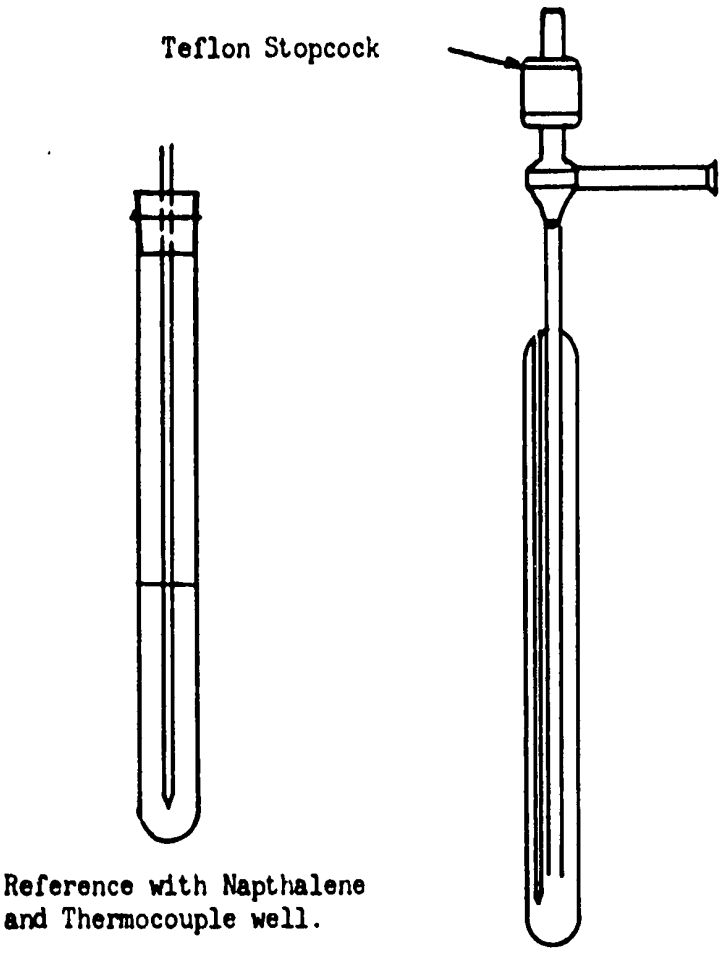
Teflon Stopcock
Reference with Napthalene and Thermocouple well.
Sample with Thermocouple well and sample entry port.

Figure I2

identification of a mysterious and persistent peak at -186°C which became very strong after prolonged cooling. This was absent in the sealed samples and was thus readily identifiable as the boiling point of liquid oxygen which had condensed into the sample tube. In a final run degeneration of the rubber o-rings apparently allowed condensation of oxygen to take place and further condensation of water allowed ice to seal the tube. During heating the sample tube exploded with considerable violence. This incident showed the need for caution in the simplest of laboratory practices.

This superficially simple analysis was beset by difficulties. The most important question was whether or not equilibrium had been reached in the crystal. It was thought that programmed heating would improve the results but the necessity of measuring the difference between the temperature of the sample and that of a reference as the result of a thermal event required that heating or cooling be sufficiently rapid to allow a temperature difference to develop. To minimize the equilibrium problem, the sample was first cooled to liquid nitrogen temperature, heated to just below its melting point, then cooled again and maintained at -196°C for at least two hours before the heating run took place. This annealing plus the apparently optimal heating rate was used to minimize errors and should yield adequate results, particularly at high temperatures. The results are outlined and discussed in Chapter III Section E.

G. Thermodynamic Studies

Thermodynamic studies of this system consisted of measurements of

the enthalpy changes occuring in the pure components and in solution during temperature changes. These measurements were obtained by the use of a Perkin-Elmer Differential Scanning Calorimeter-1B. This instrument is constructed in such a manner that the sample and a reference are maintained at the same temperature during programmed heating and cooling. Any thermal event in the sample appears as an increment in the amount of power required to maintain the sample at the same temperature as that of the reference. A signal proportional to the differential power is transmitted to a recorder pen. The integral of the resulting peak is thus proportional to the corresponding enthalpy change in the sample.

Unfortunately the instrument was designed primarily for operation at temperatures greater than 25°C and it is only with the greatest difficulty that it can be induced to operate at lower temperatures. After calibration of the instrument with suitable standard materials, in this case benzene, carbon tetrachloride and pentamethylene sulfide* and cyclohexane it was found that useful thermodynamic data could be obtained down to about -100°C.

The data obtained from this section are reported and discussed in Chapter III Section F.

H. Dielectric Constant Measurements of Liquid at 30°C.

The dielectric constants of the pure liquids were measured, together with a series of their solutions.

The cell used is shown in Figure 13 and consists of a glass envelope containing a series of metal concentric cylinder capacitors. The array

---

* This compound was used for comparison with the data available on it in McCollough's (36) very complete paper dealing with it.

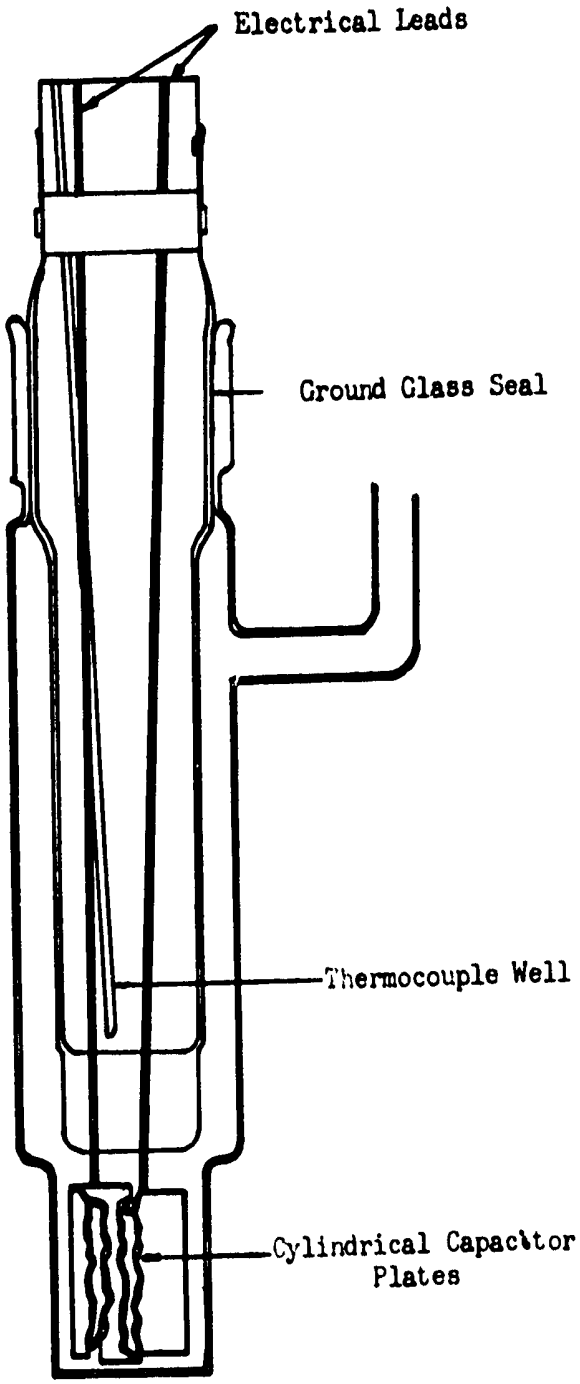
Electrical Leads
Ground Glass Seal
Thermocouple Well
Cylindrical Capacitor Plates

Figure 13

was found to have a cell constant of 9.3 and is unique in that it was the only dielectric cell used in this work which was two-terminal, accordingly the leads were co-axial with outer sheath grounded and were taped in place through the entire series of runs. The cell was immersed in an oil bath, thermostated to within ± .01° C of the desired termperatures. Measurements were made only after the cell had been in situ for twelve hours.

Results are recorded and discussed in Chapter III Section G.

I. Measurement of Dielectric Constant

The prime purpose of this investigation was to obtain meaningful data of the dielectric constant of the system under investigation. Measurement of the dielectric constant of solid systems has always been difficult. The basic problems encountered were:

(a) Sample geometry. The avoidance of the formation of cracks and voids (46,47) within the sample and separation of the sample from the walls of the vessel as a result of thermal expansion and contraction.

(b) Temperature control over long periods required for measurement.

(c) Insurance that equilibrium has been attained in the crystal (48).

These are the only sources of difficulty listed since they are peculiar to this system. Routine sources of error in capacitance measurement such as the elimination of lead capacitances were dealt with using standard methods.

I 1) Continuous Recording Method

The cell used is shown in Figure 14. It was a fully guarded, parallel disc type with a measured cell constant of 0.51. This cell was insulated with one half inch of polystyrene foam and connected to a General Radio type 1605-A impedance comparator so that the voltage appearing across the impedance difference detector as a result of bridge imbalance could be recorded on a double pen recorder which was also used to record sample temperature.

The value of the dielectric constant was then determined at some convenient temperature by placing a standard variable capacitor in parallel with the cell. Capacitance as a function of temperature was then determined by using the standard capacitor to produce the same degree of imbalance as that observed in the system at any given temperature.

Cooling of the cell was effected by adding liquid nitrogen to a Dewar flask containing the insulated cell, heating by allowing the liquid N_2 to evaporate. Both heating and cooling rates were approximately one degree per minute.

Before results were obtained the sample was first cooled to liquid nitrogen temperature, then heated to within $5^{\circ}C$ of its melting point. A measuring run was then taken. The cycling process was the only concession made to equilibrium in the system. The results and their value are discussed in Chapter III Section H.

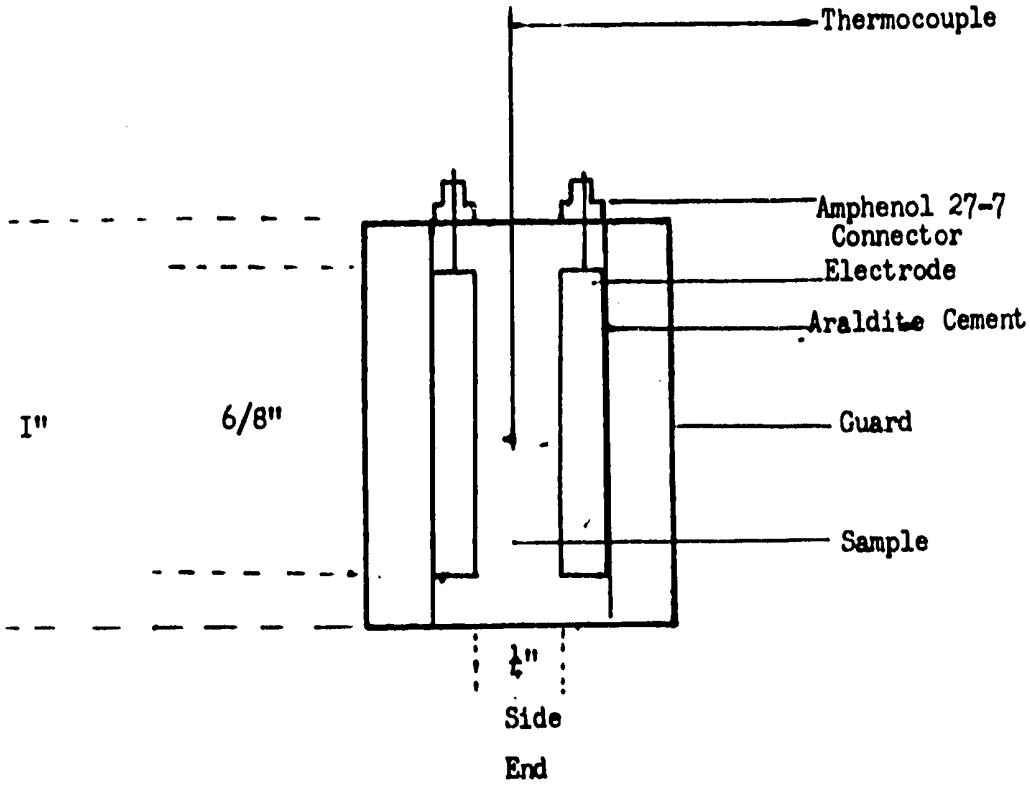

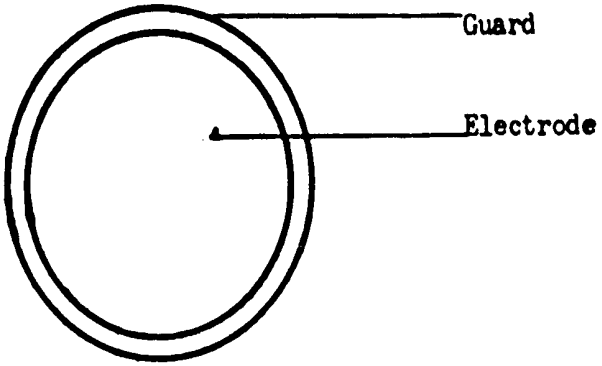

Top

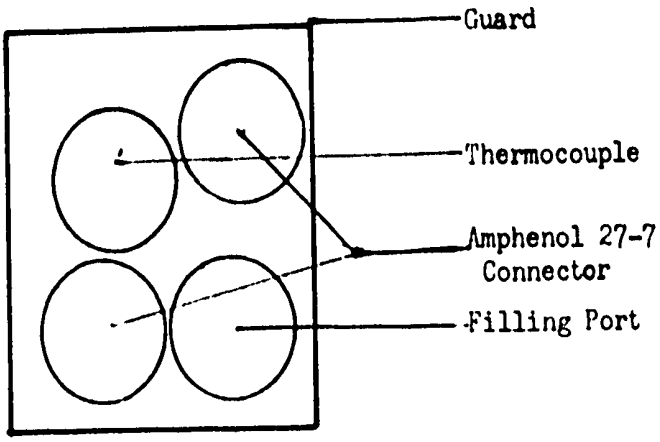

Figure 14

I II) Dielectric Analysis, Co-Axial Cylindar Cell

The cell used is shown in Figure 15[a]. It had a measured cell constant of 1.65. The coaxial cylinder electrode arrangement is similar to that used by Davidson and Cole (31). The cell was filled and introduced into a copper tube wound with heater wire, this assembly being placed in the center of a metal can containing polyurethan foam insulation. The entire assembly was then placed in a stainless steel Dewar and cooled to liquid nitrogen temperature. It was next warmed to just below the melting point of the sample and was then re-cooled to liquid nitrogen temperature. Temperature was controlled by a heater wire wrapped around the cell; the power input to the heating was regulated by the thermocouple voltage. This cycling was employed to anneal the sample and thus eliminate cracks and voids within it (46,47). Finally measurements of the dielectric constant were made at 100 Hz, 1kHz, 10kHz and 100 kHz at temperature intervals suitable for determining the points of phase transition and the dielectric constant in any phase.

Measurements were made on either the General Radio, Capacitance Measuring Assembly Type 1610-A or Type 1615-A, the latter of which is a transformer ratio-arm capacitance bridge. The results are considered in Chapter III Section I.

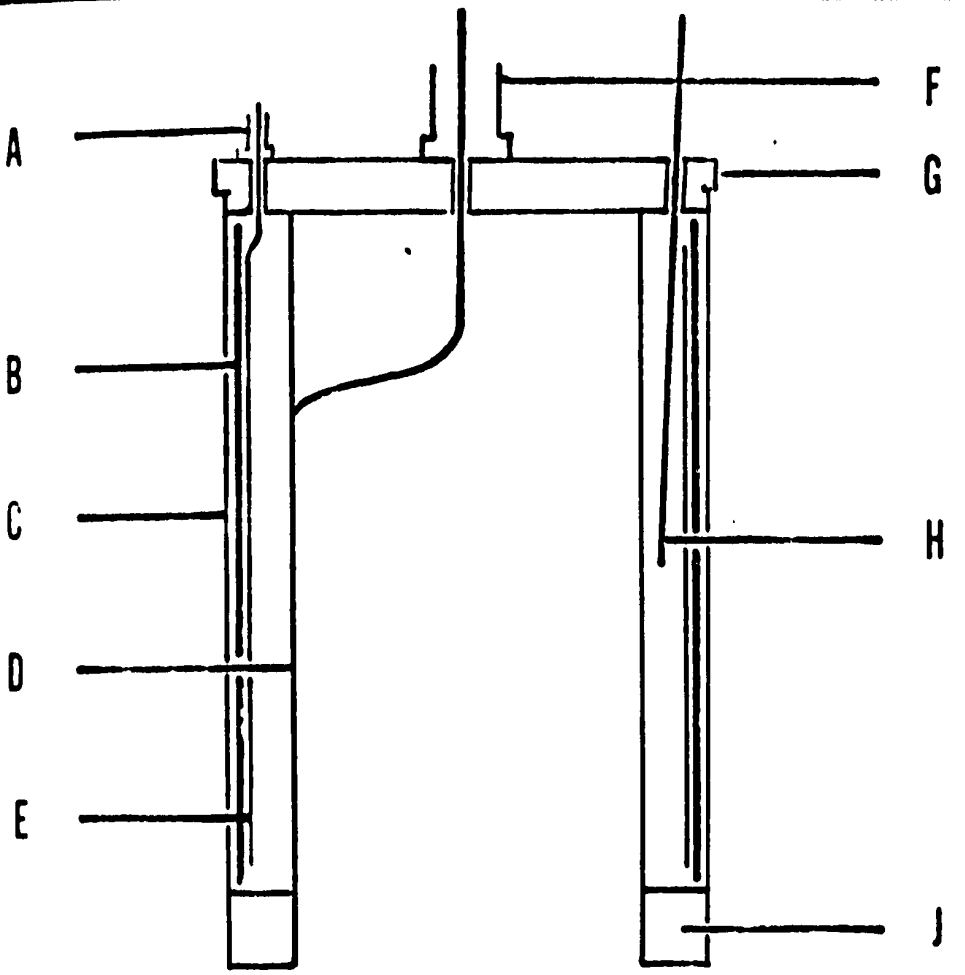

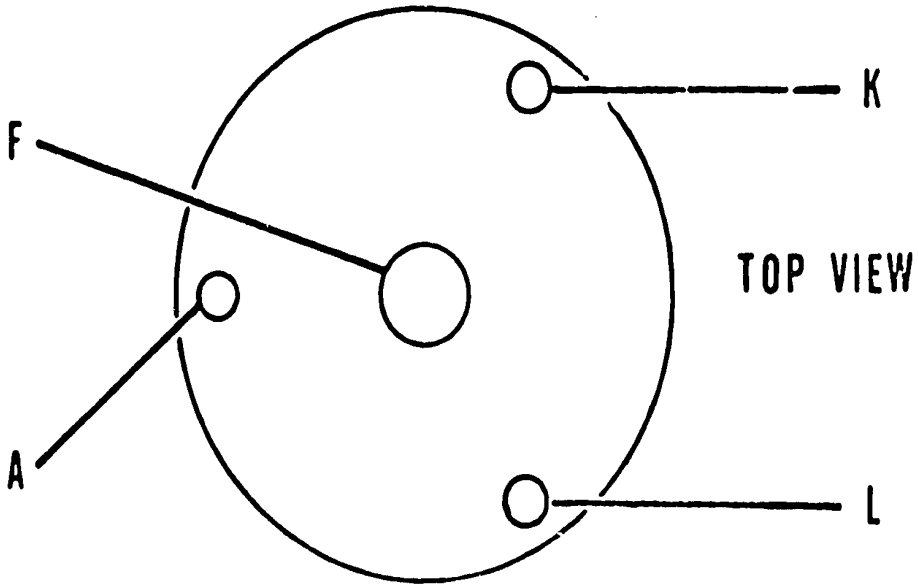

Figure 15[a]. Three-terminal dielectric cell. A, Amphenol subminax connector for high electrode lead; B, Teflon insulation; C, guard electrode; D, low electrode; E, high electrode; F, BNC connector for low electrode lead; G, top plate; H, L. & N. duplex copper-constantan thermocouple; J, base ring; K, thermocouple entry; L, sample entry. Top plate and base ring are in direct contact with guard electrode but insulated from low electrode by Araldite cement.

I III) Final Dielectric Measurements, The Spring Load System

The difficulties involved in the measurement of dielectric constants of solids have already been outlined. This final approach employs a refined cell, together with an improved temperature control system.

The new cell shown in Figure 15[b] is a three terminal, fully guarded co-axial cylinder arrangement with the added refinement that a modest, constant pressure was applied to the sample at all times by a simple piston arrangement. This pressure was estimated to be 12 atmospheres. It was hoped that this arrangement would insure that the sample completely filled the space between the electrodes and that formation of cracks within the sample was minimal or eliminated. The success of this arrangement has been demonstrated in this laboratory (49).

Temperature control was refined. The cell was fitted into a metal tube which was itself insulated from its surroundings by one inch of urethane foam. This metal tube thus served as a heat shield. A thermocouple was then used to sense the shield temperature, this temperature being maintained by a heater wire wound around the outside of the metal tube. The desired shield temperature was set by a Philips recorder which switched the heaters on and off according to whether the shield temperature was too high or too low. Selection of an optimal voltage input to the heater coils kept the shield temperature fluctuation to within $\pm$ 0.5°C. A second thermocouple in more intimate contact with the sample registered a change of less than .01°C during any given measurement.

The treatment of the sample was also improved. After the usual cycling procedure the cell was allowed to warm slowly to the desired temperature and was maintained there until no appreciable drift in the capacitance was

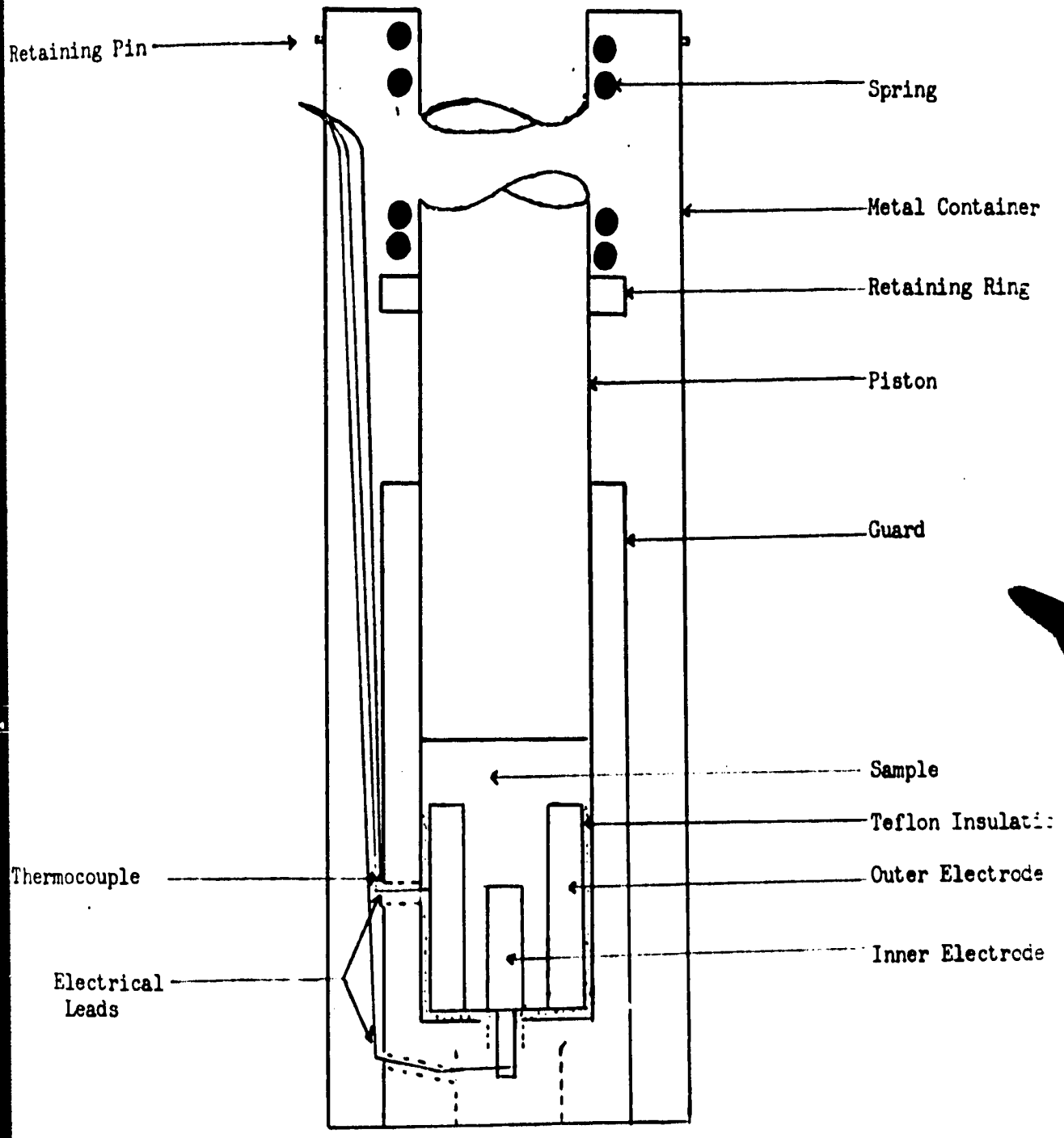
Retaining Pin
Spring
Metal Container
Retaining Ring
Piston
Guard
Sample
Teflon Insulati
Thermocouple
Outer Electrode
Inner Electrode
Electrical Leads

Figure 15b

observed. This procedure took between one and eight hours.

Results are discussed in Chapter III Section K.

CHAPTER III

RESULTS AND DISCUSSION

A. Introduction

The compounds of chief interest in this work are pentamethylene sulfide, also called thiacyclohexane, having the molecular formula $C_5H_{10}S$*; and pentamethylene oxide, also called tetrahydropyran, having the molecular formula $C_5H_{10}O$. Figure 16 shows the structure of the two compounds which shall be referred to as PMS and PMO respectively.

It was found convenient in the experimental portion of this work to describe each procedure separately. This format will be extended to the discussion of the results. In an effort to insure unity a final chapter will be devoted to conclusions. It is felt, however, that the sequence of results presented here is logical and will lend itself to easy reading.

PMS PMO

FIG. 16**

*A third name was found in the literature for this compound. It is tetrahydrothiapyran.

**Both have been found to exist in the chair form (36,53).

B. Liquid Densities

Figures 17-19 show plots of the densities of pure PMO, PMS and their mutual solutions as a function of temperature.

The agreement with existing literature values for the pure components appears to be good although there is some scatter of literature results. These results are tabulated for easy comparison.

TABLE III

Compound	Density	Temperature	Reference
PMO	.8744	30°C	(40)
PMO	.8742	30°C	(39)
PMO	.8735	30°C	this work
PMO	.8693	35°C	(39)
PMO	.8686	35°C	(50)
PMO	.8682	35°C	this work
PMO	.8840	20°C	(41)
PMO	.8839	20°C	this work
PMS	.9849	20°C	(41)
PMS	.9857	20°C	this work

Finally, Figure 20 shows a plot of density vs. mole fraction for the system at 20°C. The plot may be seen to be linear and hence indicates no significant interaction between the components of the solution. This indicated that the components would probably form a continuous

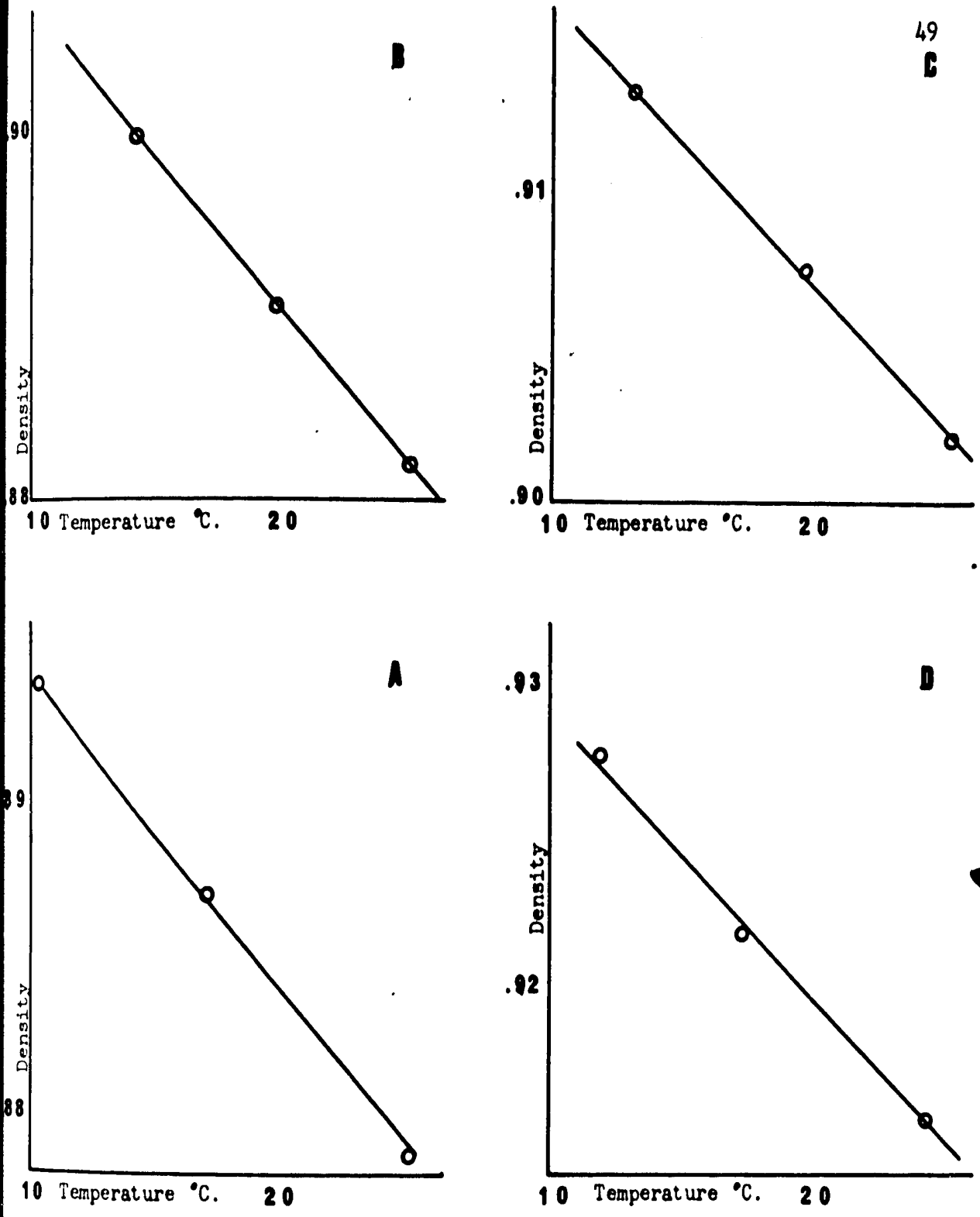

Figure 17. A = 100% PMO B = 91.43% PMO C = 67.02% PMO D = 79.01% PMO

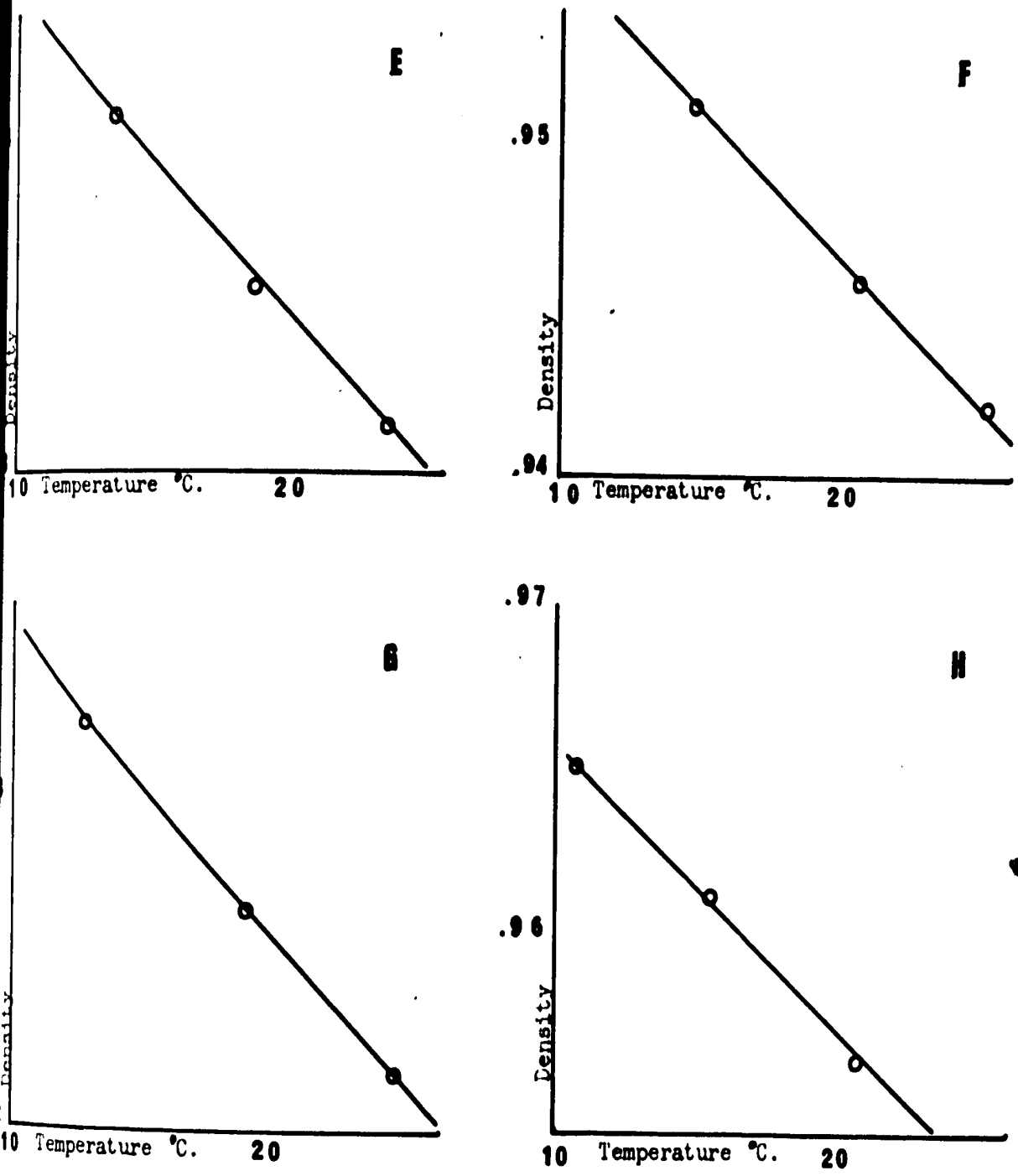

Figure I8. E = 5I.03% PMO F = 39.92% PMO G = 60.26% PMO H = 29.80% PMO

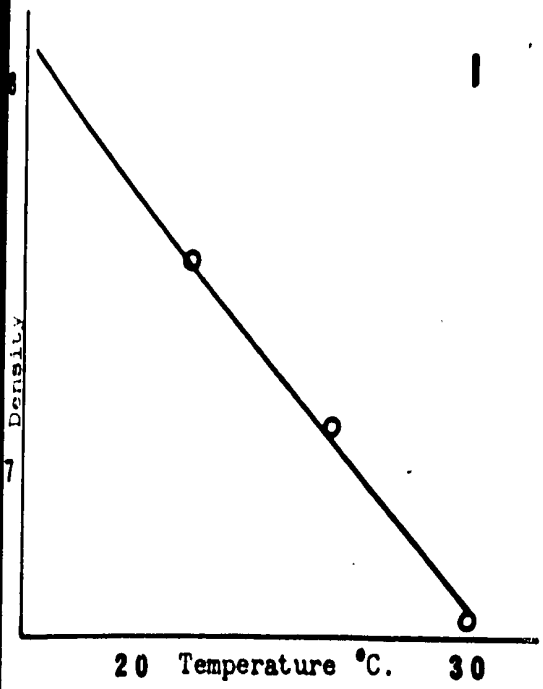

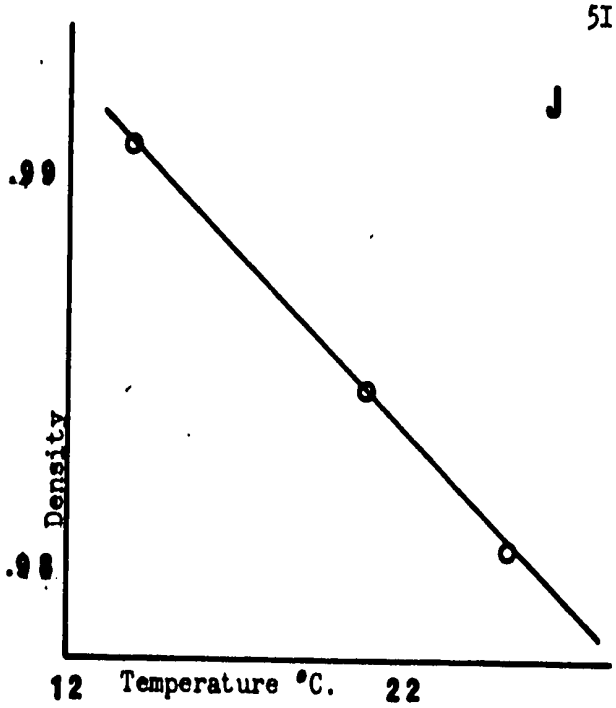

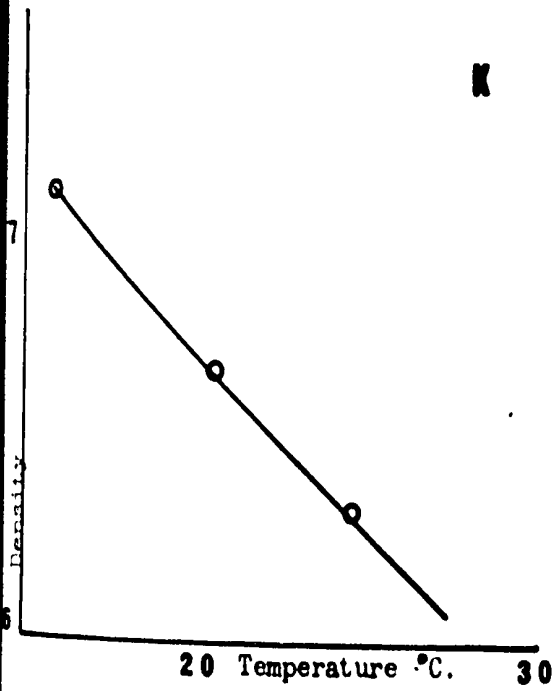

Figure 19. I = 10.62% PMO J = 100% PMS K = 18.12% PMO

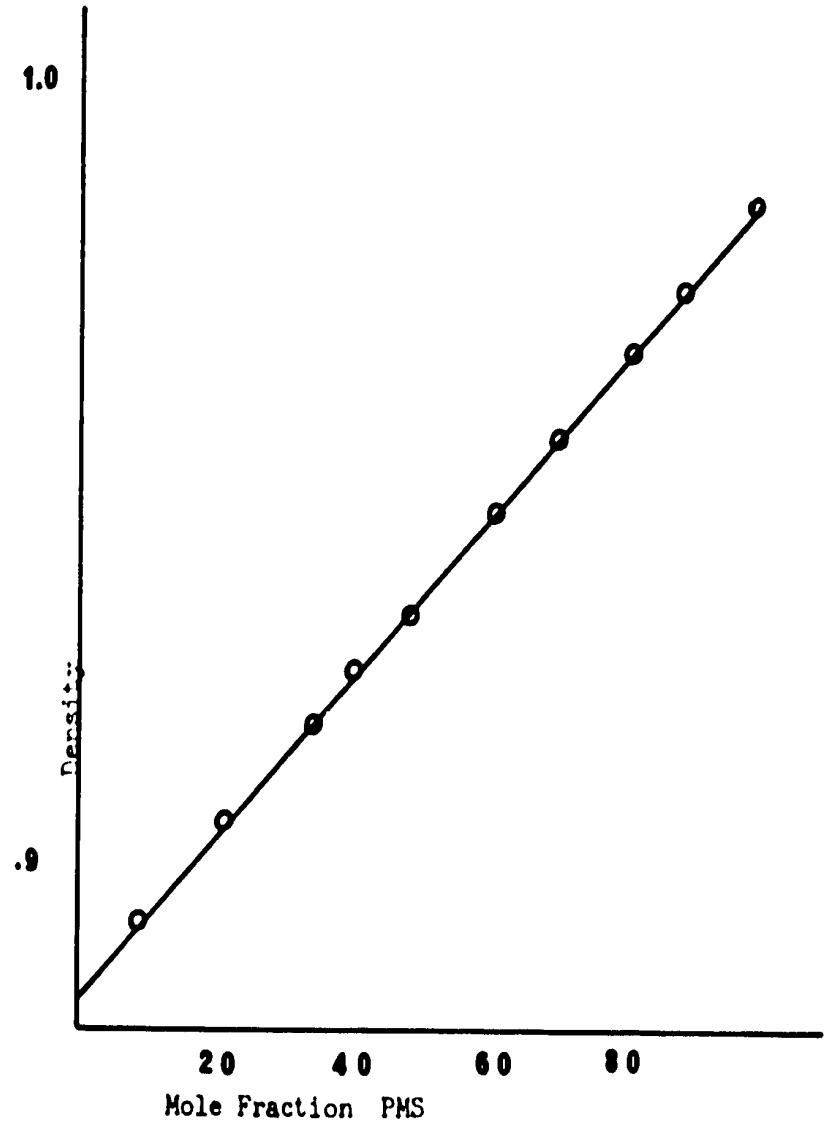

Figure 20

series of solid solutions suitable for study in this work.

Further support for this conclusion was found in the value of α defined such that:

$$\alpha = \frac{1}{V} \left(\frac{dV}{dT}\right)_p$$

This was found to be independent of concentration having the value:

$$\alpha = (9.5 \pm 0.5) \times 10^{-5} \ ^\circ C^{-1}$$

C. Index of Refraction

The recorded indices of refraction are shown in Table IV

TABLE IV

% PMO	%PMS	n_D T=25°C
100	0	1.4176
90.7	9.3	1.4270
80.05	19.05	1.4366
71.27	28.73	1.4443
61.46	38.54	1.4559
51.54	48.47	1.4633
41.47	58.53	1.4711
31.30	68.70	1.4784
20.99	79.01	1.4871
10.56	89.44	1.4939
0	100	1.5047

The results are linear in concentration, as might be expected since only strong ionic fields seem to be capable of changing individual refractive indices in solution. Though this linear behaviour is common (51) it might be regarded as further proof that we are dealing with an almost ideal solution. It is perhaps interesting to note that in the reference quoted this behaviour is used as an argument against the participation of electrons in a hydrogen bond since this effect was observed in alcohols. That is to say the refractive indices of alcohol solutions were linear in concentration.

D. Dipole Moment Measurements

If an electrically neutral assembly of charges is examined and it is found that the centers of charge for positive and negative charges do not coincide it is often convenient to define the dipole moment of the assembly such that

$$\mu = ed \qquad (1)$$

where μ is the electric dipole, e is the magnitude of the charge at one of the charge centers and d is the distance between them.

The fact that many molecules behave as if they had permanent dipole moments is due to four basic factors:

(a) The assymetry of charge in the bonding electrons arising from the electronegativity difference between the two atoms concerned.

(b) The homopolar dipole arising from the unequal size of the orbitals of the two atoms bonded.

(c) The assymmetry of the atomic orbitals involved in the bond arising from the hybrid character of these orbitals.

(d) The assymmetry of the orbitals of the lone-pair electrons arising from hybridization.

The measurement of the dipole moment can be made in the vapor phase using Debye's equation or with very great accuracy using microwave techniques. The fact that not all compounds of interest can be obtained in the vapor phase has led to the widespread use of dipole moments obtained from solution data, the easiest technique being that outlined in the experimental section of this work. The fact that solution results do not agree with vapor data as well as might be hoped is due to so-called solvent effects which might be anticipated from the discussion of the inner field in the introduction. For a fuller discussion of this effect the reader could do worse than refer to reference (19b). Our work, carried out in carbon tetrachloride solution is in excellent agreement with literature values tabulated below in Table V.

TABLE V

Compound	μ(D)	Solvent	Reference
PMO	1.64	CCl_4	this work
PMO	1.63	liq.	52(a)
PMO	1.55	benzene	52(a)
PMO	1.63	benzene	52(a)
PMO	1.89	benzene	52(a)
PMO	1.74	vapor	53
PMS	1.78	none quoted	52(b)
PMS	1.71	benzene	52(b)
PMS	1.81	CCl_4	this work

One tends to reject the value of 1.89 since it appears high, particularly when compared with the value of 1.74 for the vapor. It is gratifying to note for PMO:

$$\frac{\mu \text{ our value}}{\mu \text{ vapor}} = .94$$

This agreement is as good as can be expected.

E. Differential Thermal Analysis

Before considering the results obtained in this work it is necessary to examine the nature of the system we are investigating. In 1938 Timmermans (54) described a class of components having the

descriptive name "molecules globulaire"*. He has elaborated this work in a historical review of the subject made somewhat later, referring to the solid state of these compounds as"plastic crystals" (55). These solids are characterized in this paper by:

(a) A low entropy of fusion (i.e. less than 5 e.u.)

(b) A relatively high melting point (n-pentane, which is non-globular, melts at -141°C while tetramethylmethane, which is globular, melts at -16 °C).

(c) High vapor pressure of the high temperature solid phase.

(d) High plasticity of the high temperature solid phase; the high temperature form of C_2Cl_6 will flow through a hole under a pressure one-tenth of that required to make its low temperature form flow through the same hole (55).

(e) The majority, if not all, of these compounds had a high temperature phase which was a cubic lattice and hence these compounds tend to form solid solutions on mixing.

Pauling (56) is credited with the first suggestion that certain units in solid lattice may be capable of rotation or at least of rapidly changing their orientation in a crystal lattice in such a manner that they could be said to possess "orientational" disorder in the solid. Workers were quick to seize on the suggestion that these solids may have a certain degree of disorder and that this property might explain the low entropy of fusion observed in plastic crystals. As an example

---

*This means the electron envelope is more or less spherical.

let us consider cyclohexane (49), which exists in two solid phases, the high temperature form of which exhibits plastic behaviour, the low temperature form does not. We have

	ΔS_{trans}	ΔS_{fusion}	ΔS_T	$+\Delta S_F$
Cyclohexane	8.59	2.24	10.83	

Thus the suggestion that plastic behaviour is due to orientational disorder appears to stand on firm ground. Further investigation showed that plastic phases gave X-ray diffraction patterns which, while adequate to define the crystal structure, were diffuse in nature, indicating both orientational and some translational disorder in these crystals.

Other physical properties supported this view. Line narrowing of nuclear magnetic resonance absorption lines was observed in certain crystals (57), a fact which is consistent with the view that the molecular units forming the crystal lattice may have considerable freedom to rotate about their center of gravity.

Dielectric measurements on polar, plastic crystals shows that the dielectric constant does not drop rapidly on freezing as with "normal" polar substances. See Figures 21 and 22 below (58).

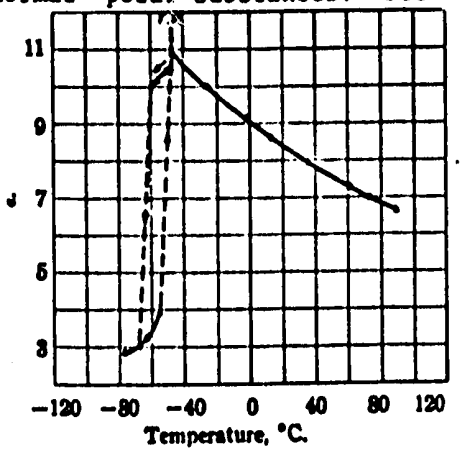

Fig. 21 -Dielectric constant of chlorocyclohexane.

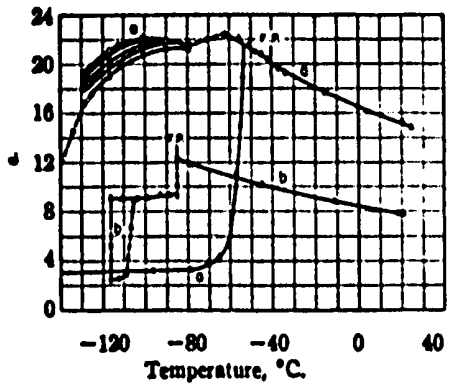

Fig. 22-Dielectric properties of (a) cyclohexanone and (b) cyclohexyl fluoroform.

Further plastic phases often exhibit dielectric dispersion.

It may then be considered to be well established that certain compounds possess orientational freedom in the solid state. This implies at least some degree of translational freedom, also behaviour such as that shown in Figure 23 (55) will help to illustrate the differences between globular molecules and normal behaviour. Throughout this work we shall refer to solids of this type (i.e. globular molecules) as plastic solids and because the distinguishing characteristic of such materials is the ability of the molecular units to achieve different orientations in the lattice in their high temperature forms we shall refer to such phases as rotator* phases.

During the past few years a considerable amount of work has been done on organic plastic systems. Several workers have constructed phase diagrams of binary systems using varying combinations of the properties mentioned (i.e. n.m.r., dielectric work), note for instance references (59) and (60). With these facts in mind we shall now begin a study of the differential thermal analysis of the present system.

TableVI below records the observed transition temperatures while Figure 24 shows representative thermograms.

---

*The term is perhaps misleading since the molecules do not rotate freely as in the gas phase but the term is widely used in the literature and is descriptive.

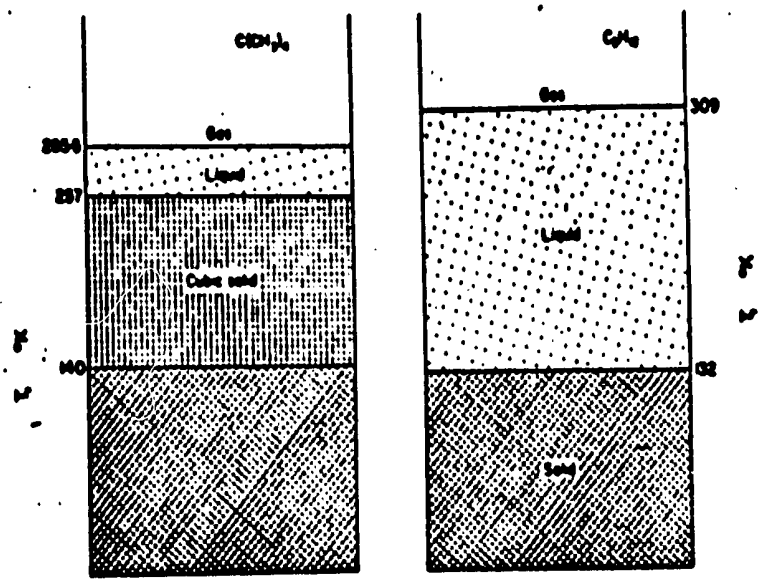

FIG. 23 Phases for neopentane (globular) compared with those for normal pentane (non-globular).

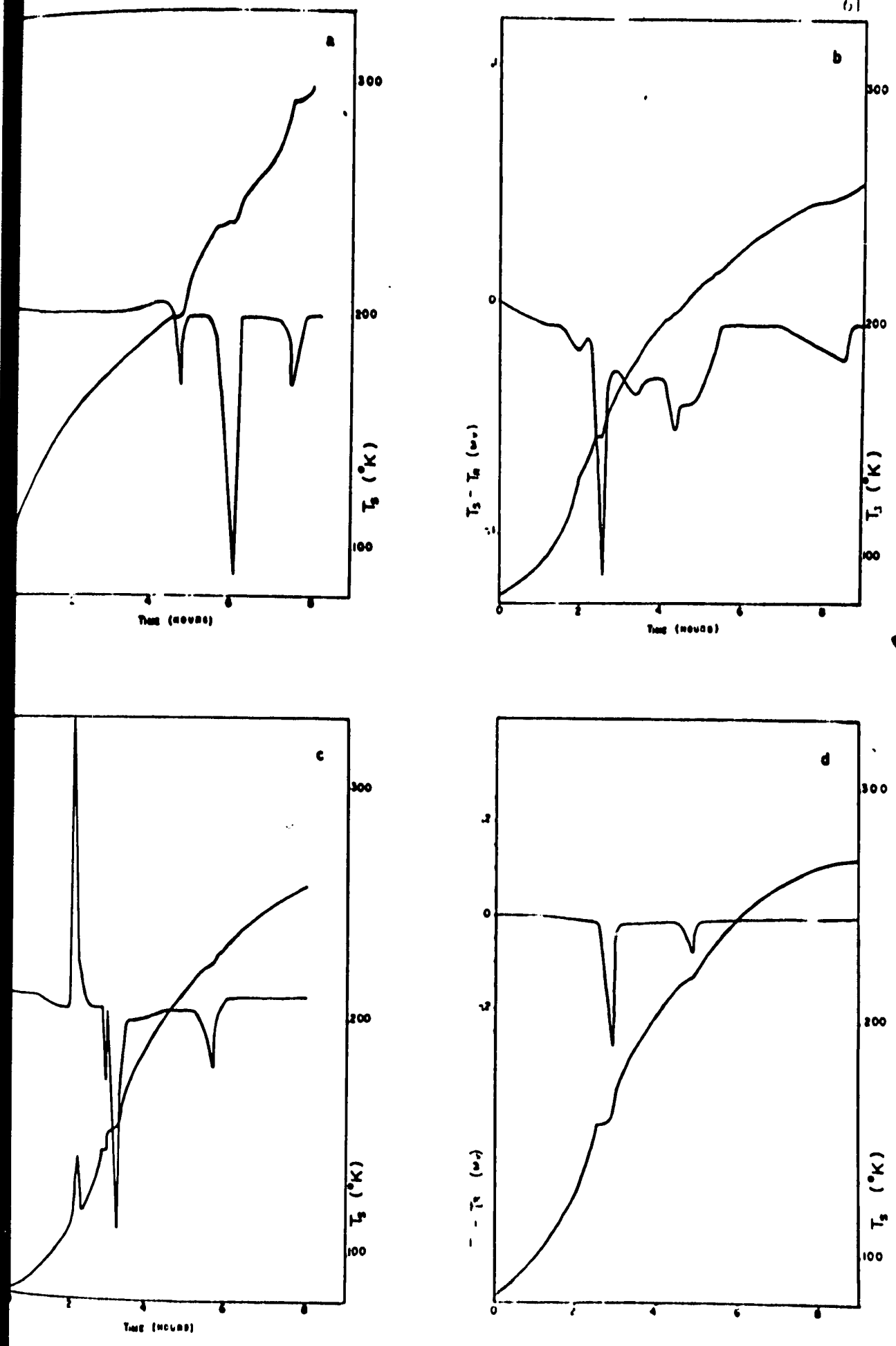

Figure 24. Thermograms for: (a) pure dibutylcyclohexane; (b) 40% and (c) 10% dibutylcyclohexane; (d) pure tetrahydro-

TABLE VI

OBSERVED TRANSITIONS IN PMO, PMS SYSTEMS (^{o}K)

% $C_5H_{10}O$	0	10	20	30	40	50	60	70	80	90	100
Melting points	292	277	266	257	248	242	234	228	223	220	219
CD	240	223	218	216	214						
EF				198	203	203	202	199	190		
GH	200	188	180	176							
IJ			150	148	150	146	150	148	147	150	157
KL					113	127	128	130	128	128	
MN									113	113	
% $C_5H_{10}S$	100	90	80	70	60	50	40	30	20	10	0

It is indeed most tempting to attempt to construct a phase diagram from these data but it has been pointed out by Sherwood (48) that the physical properties of organic solids often are not reproducible and are subject to differences depending on the heating rate and annealing time. Thus the low temperature data must be regarded with suspicion. Previous attempts at such work (references 59, 60) could be described as speculative. A considerable amount of information may be gleaned, however, from plotting the data of Table VI as done in Figure 25. This latter plot and similar ones later constructed on the basis of dielectric data will be coyly referred to as a temperature-composition diagram.

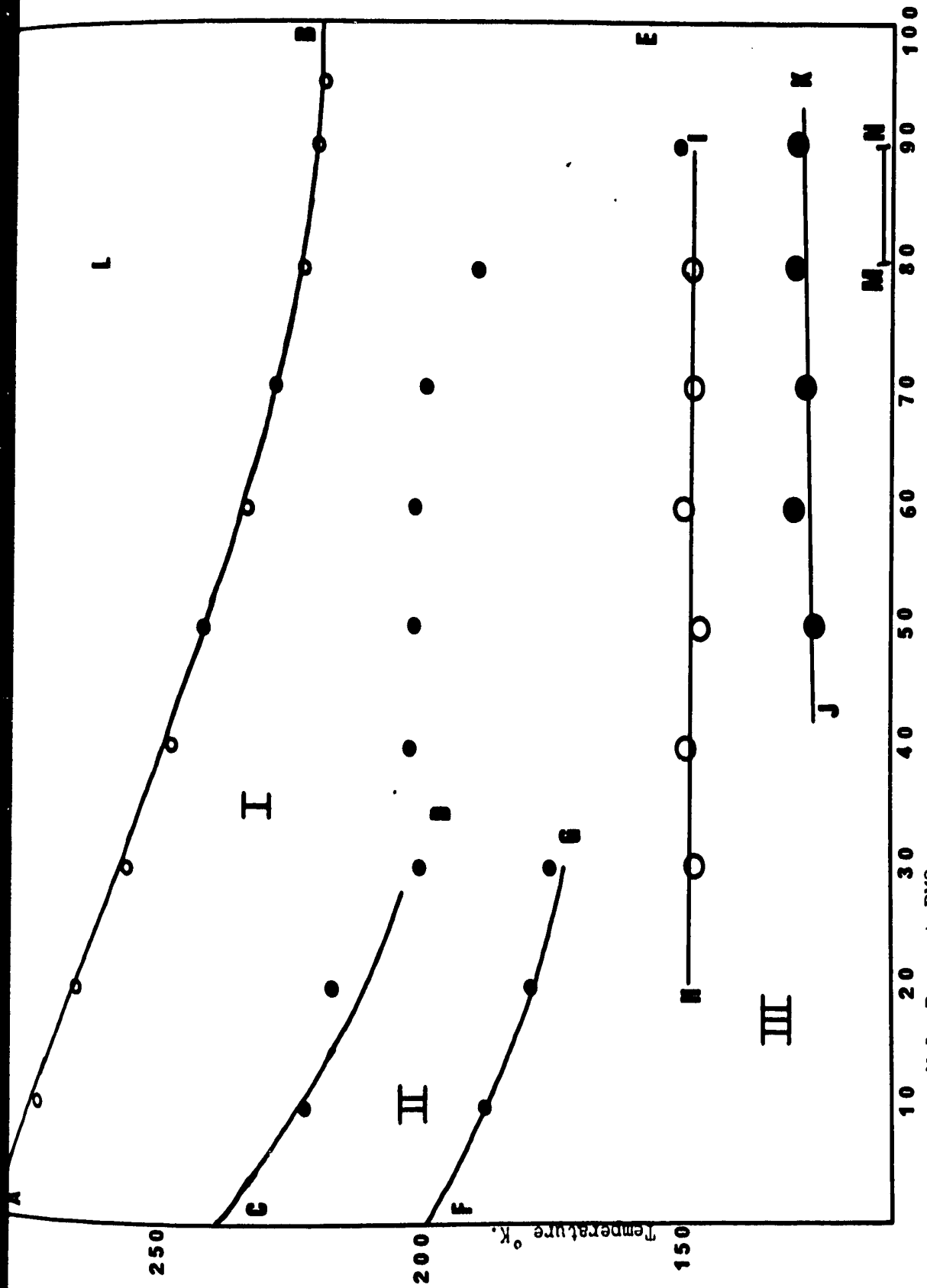
Temperature °K.
250
200
150
10
20
30
40
50
60
70
80
90
100
Mole Percent PMO
A
B
C
D
E
F
G
H
I
J
K
L
M
N
I
II
III

Figure 25

For pure PMS two solid phases were found in agreement with McCullough et al (36). These authors also reported a lambda-type transition in their heat capacity data at 207°K. This was not observed in the present work but it must be borne in mind that simple analysis of this type could hardly be expected to show second order transitions. PMO has been found in the present work to exist in only two crystal modifications.

The line AB represents the melting points of the solutions. It shows no appreciable separation of the liquidus and solidus curves and no evidence of compound formation.

The line CD is a reproducible transition which persists strongly as long as the solution is PMS rich. DE is a fanciful representation of what might be the fate of this line as the PMO concentration is increased.

FG follows the second transition in PMS. It is clear up to 80% PMS, after which it seems to vanish more or less gradually.

The line HI is drawn only to call attention to a series of transitions, the nature of which is unclear, JK serves the same purpose.

MN is drawn between two strong, reproducible peaks of exothermic nature observed on heating. Since such behaviour normally shows transition from a metastable to a stable phase this may be regarded as evidence that true equilibrium has not been attained below 150°K.

The solid portion of the diagram may now be roughly divided into three regions labeled I, II and III. I is bounded by ABEC, II by CDGF and III is the remaining solid portion of the diagram. The nature of these regions will be further examined and elucidated in the work that follows.

F. Thermodynamic Studies

TableVII records the heats of fusion and transition, together with the corresponding entropy changes, observed by the techniques outlined, in this section. The salient features to be noted are:

(i) ΔH and ΔS are available for fusion throughout the entire composition range.

(ii) ΔH and ΔS for transition from the high temperature phase to the next lowest phase is available only from 100-50% PMS and in pure PMO. At intermediate values the transitions were difficult to observe and the ΔH peaks finally obtained showed fine structure. This appears to be due to the poor low temperature response of the instrument and only those values regarded as being remotely accurate are recorded.

(iii) The second solid transition observed in PMS yields ΔH and ΔS values only up to around 90% PMS. After this a peak is still visible till about 70% but it is spread over a wide temperature region and cannot be regarded as a source of accurate data. After 70% the transition is no longer visible.

Attention should first be directed to the fact that the entropies of fusion are all about two, the lowest being 1.61 e.u. This is taken as evidence that the solid formed is plastic in nature also,

$$\Delta S_{\text{fusion PMS}} + \Delta S_{\text{trans I PMS}} + \Delta S_{\text{trans II PMS}} = 11.20$$

TABLE VII

COMP	ΔH_f	ΔS_f	$\Delta H_{trans\ I}$	$\Delta S_{trans\ I}$	$\Delta H_{trans\ II}$	$\Delta S_{trans\ II}$
100% PMS	575.0	1.97	1900.0	7.92	262	1.31
89.44% PMS	562.5	2.03	1562.0	7.00	200.1	1.07
79.01% PMS	511.2	1.92	1068.9	4.90		
68.7% PMS	459.0	1.79	910.0	4.39		
58.53% PMS	429.0	1.73	723.5	3.50		
48.47% PMS	406.0	1.68	446.0	2.19		
38.54% PMS	383.0	1.64				
28.73% PMS	389.5	1.71				
20.0% PMS	360.0	1.61				
10.0% PMS	371.5	1.69				
100% PMS	390.7	1.78	1500	9.8		

Units of ΔH are cal/mole, ΔS e.u./mole

and

$$\Delta S_{\text{fusion PMO}} + \Delta S_{\text{trans PMO}} = 11.58$$

The clear implication is that the loss of positional and orientational entropy between the liquid and the lowest temperature solid phases of PMS and PMO is the same. This fact (together with the observation of low entropy of fusion and an intermediate solid phase) also indicates that there is a region of the crystals which exhibits plastic behaviour.

Fig. 26 shows a plot of the liquidus and solidus lines calculated from relations due to Prigogine (82) assuming the activity coefficients of the components are unity. [Although the calculated separation of the liquidus and solidus lines is small, as expected, it is still significant and agreement with experiment is poor, i.e. there is no observed separation of liquidus and solidus lines]. Calculation of the activities is possible, with the known experimental data, but the aim of this study of the melting characteristics has now served its twofold purpose. It has established:

(1) There is no evidence of eutectic behaviour.

(2) The first solid phase appears to be plastic in nature.

The study of the solid-solid transitions was less satisfying. Using the present equipment the upper transition could be seen at all concentrations (except around 80% PMO) but yielded reliable data only in pure PMO and 50-100% PMS. Similarly the second transition originating

in PMS was visible to 70% PMS and yielded useful data only at 100 and 90% PMS. These results were used to infer that in Figure 25 a region bounded roughly by the figure AFGB is suitable for detailed dielectric study.

As a brief aside Seki (59) uses regular solution theory to write:

$$RT_o \ln x + w(1-x)^2 = \Delta H \left[1 - \frac{T_o}{T} \right] \qquad (82)$$

where T_o is the transition temperature of component one when its mole fraction, x, is unity. ΔH is the enthalpy of transition of pure x and T is the transition temperature of the solution. Since w is related to the heat of mixing, it was hoped that a low w (Seki found 350 cal $mole^{-1}$ for methyl iodide in carbon tetrachloride) would indicate compatability of the two components of our system. Both solid lines shown in Figure 26 are fitted with w = 900 cal $mole^{-1}$ but the shape of the curve both for our work and Seki's proved to be so insensitive to w that our attempts to explore this parameter were abandoned.

G. Dielectric Constant at Thirty Degrees Celsius

Reynolds (61) has made a survey of the major formulae for the dielectric constant of liquid mixtures and has found them all to be special cases of the general relation:

$$(\epsilon - \epsilon_1)\, \delta_1 f_1 + (\epsilon - \epsilon_2)\, \delta_2 f_2 = 0 \qquad (83)$$

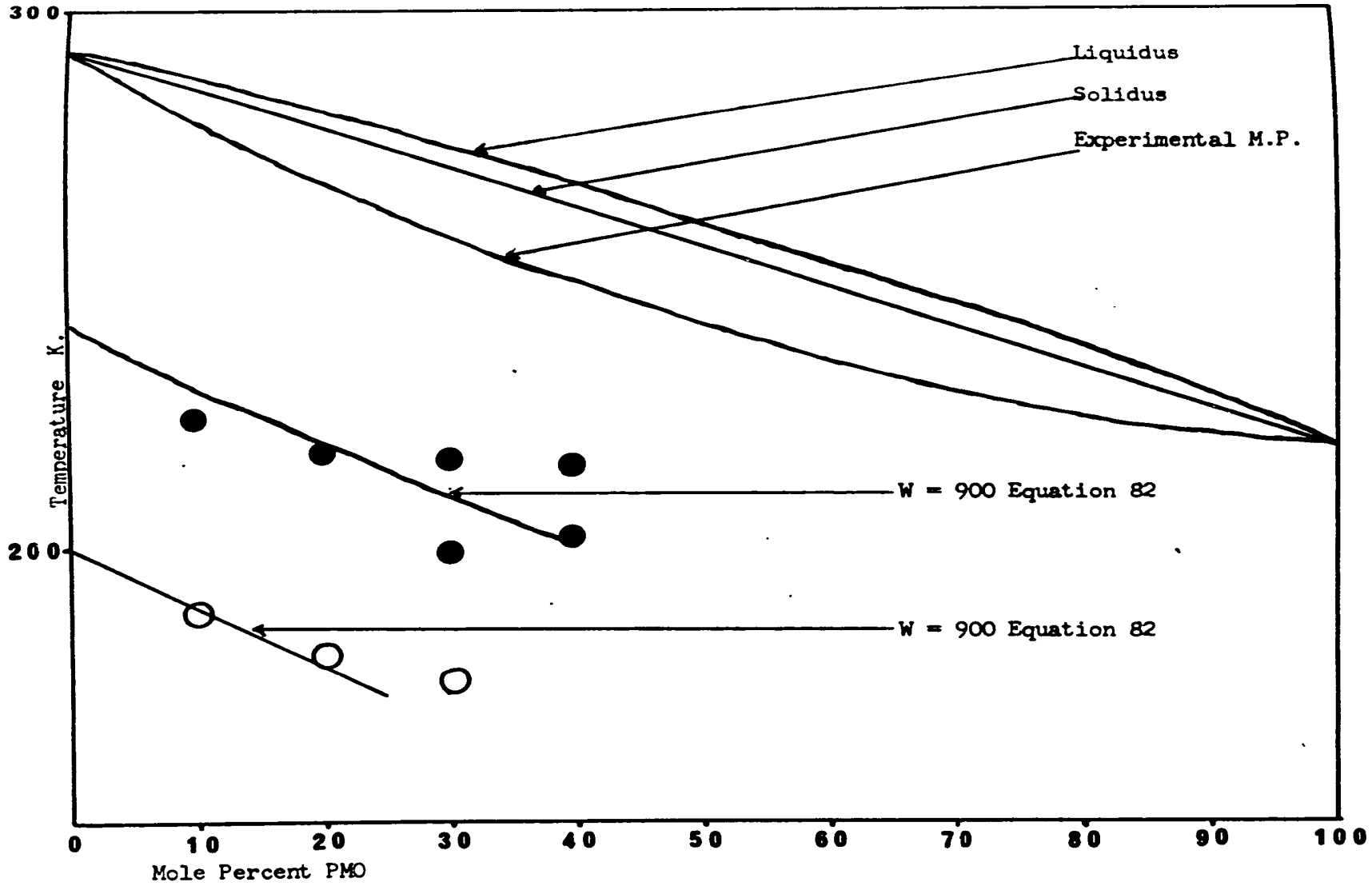
300
200
Temperature K.
Liquidus
Solidus
Experimental M.P.
W = 900 Equation 82
W = 900 Equation 82
0
10
20
30
40
50
60
70
80
90
100
Mole Percent PMO

Figure 26

where ϵ = dielectric constant of the mixture

ϵ_1 = dielectric constant of pure 1

ϵ_2 = dielectric constant of pure 2

δ_1 = vol. fraction of pure 1

δ_2 = vol. fraction of pure 2

$f_1 = \bar{E}_1/\bar{E} \quad f_2 = \bar{E}_2/\bar{E}$

and

$$\bar{E} = \frac{1}{V}\int_V E dV = \frac{1}{V}\left[\int_{V_1} E_1 dV_1 + \int_{V_2} E_2 dV_2\right]$$

$$= \delta_1 \bar{E}_1 + \delta_2 \bar{E}_2$$

Here E is the internal field. Deviations from (83) occur when approximations must be made for the f's.

Fig. 27 shows the results of this experiment plotted against volume fraction. The startling linear result agrees almost exactly with (83). This leads to the conclusion that the internal fields in PMS-PMO and their mutual solutions are closely similar.

When Onsager's equation was applied to pure PMS the dipole moment was found to be 1.55 D, somewhat low. Kirkwood's equation however yielded g = 1.2. Thus with Kirkwood g close to unity and the ratio of Onsager's value to the solution value being about .81 we may conclude that PMS is a "normal" liquid, i.e. one closely following Onsager's equation. PMO treated similarly yields μ = 1.470, g = 1.1 and appears also to behave as a normal liquid.

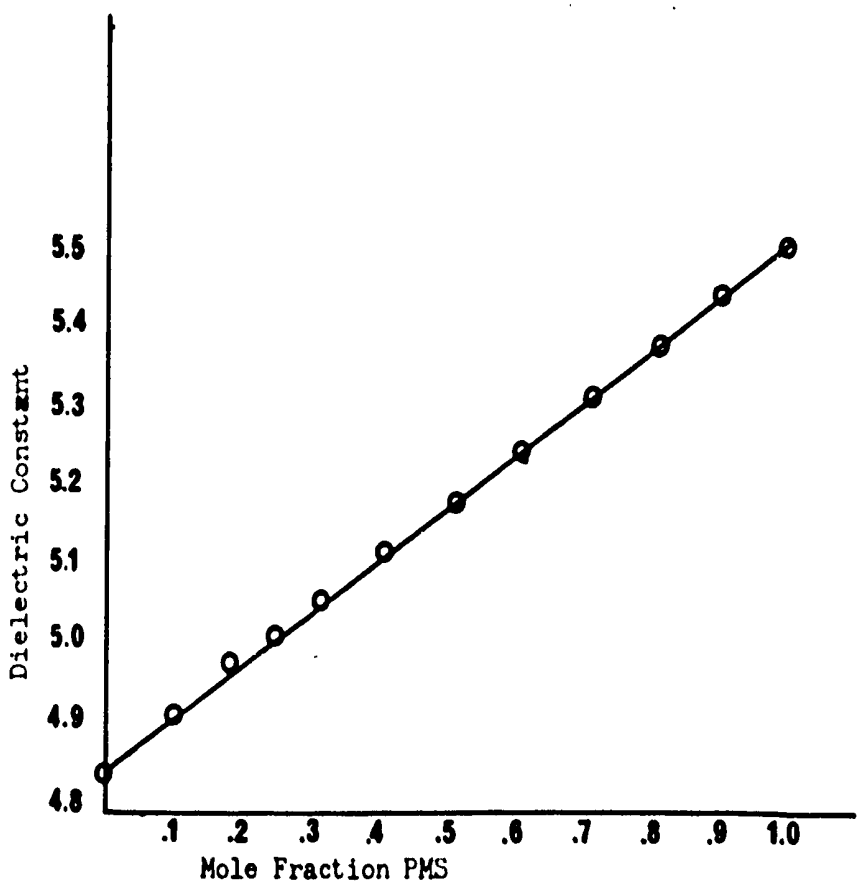
Dielectric Constant
5.5
5.4
5.3
5.2
5.1
5.0
4.9
4.8
.1
.2
.3
.4
.5
.6
.7
.8
.9
1.0
Mole Fraction PMS

Figure 27

The only conclusion to be reached here is that the two components of our system appear to be compatible and should form the solid. solutions observed.

H. Continuous Recording Dielectric Constant

Since the density and often the degree of orientational freedom of the molecules in a substance undergo a discontinuous change during a phase transition, dielectric constant measurements have been used to examine phase changes. Several authors (4c) have used this technique to study solid-solid transitions. These measurements were made using a continuous recording method to determine whether or not the system was in fact suitable for study via dielectric constant analysis.

The results are shown in Figures 28 to 32 at selected compositions and the resulting temperature-composition diagram is shown in figure 33.

That these results are crude at this point cannot be disputed and it would be unwise to attach undue significance to them. However, three points do require attention, in order of importance they are:

(1) The temperature-composition diagram resulting from this work substantially agrees with the previous D.T.A. and D.S.C. results reported.

(2) Considerable hysteresis is observed at the various transitions.

(3) The exothermic reaction previously reported (in the D.T.A. work) shows up as a sudden rise in dielectric constant to near the liquid value followed after about thirty seconds by a return to its low

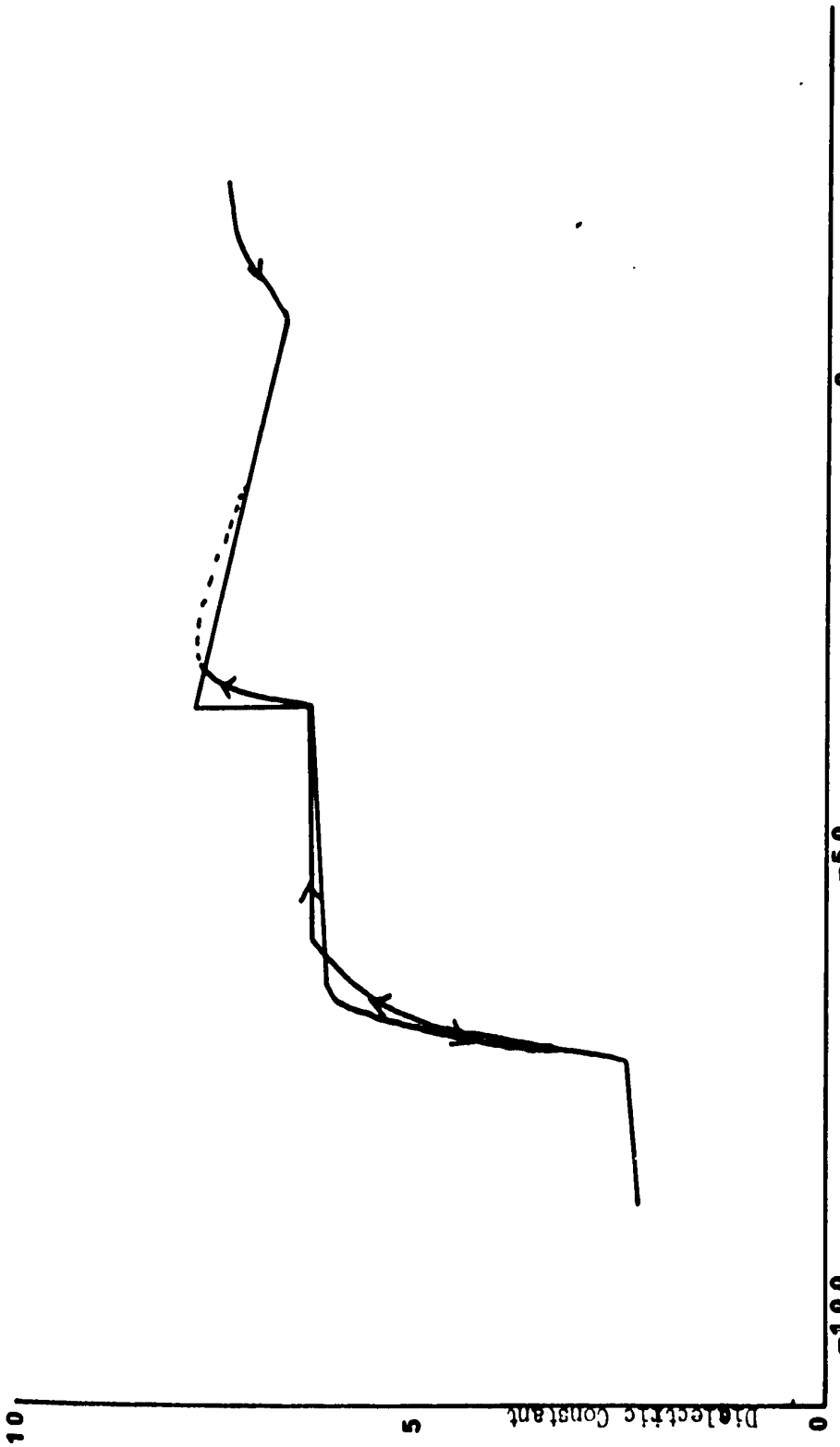

Figure 28

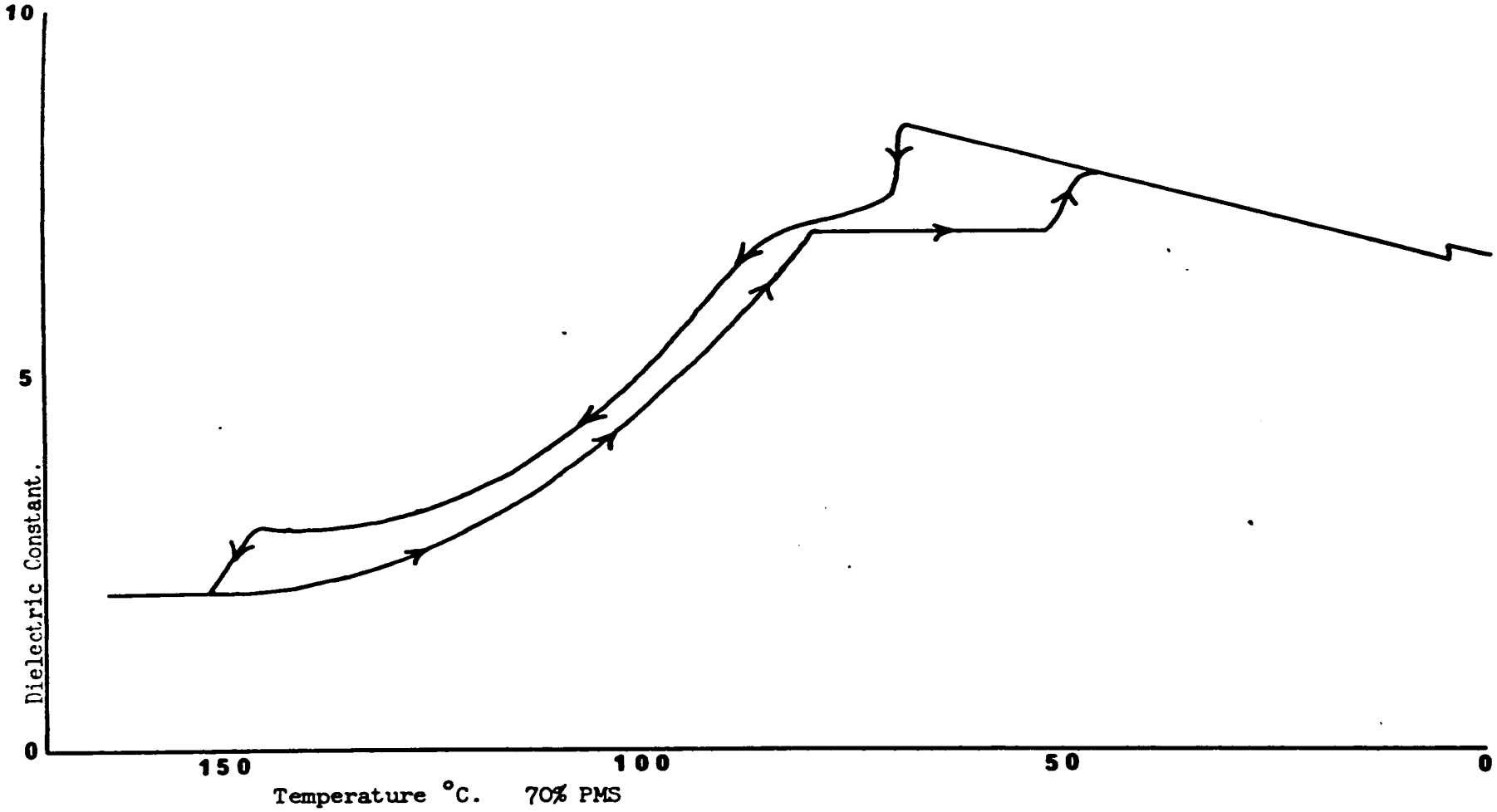

Figure 29

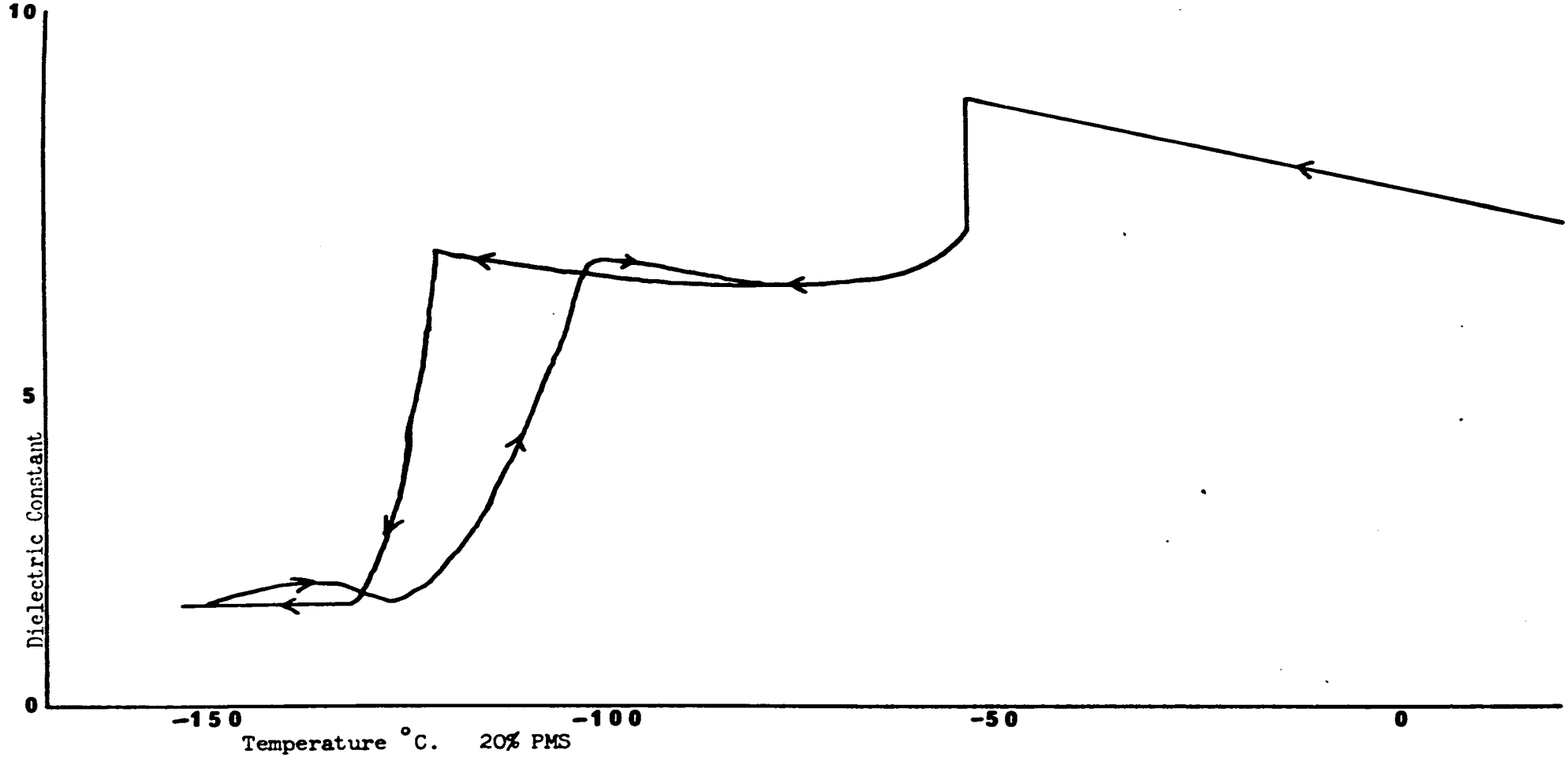

Figure 30

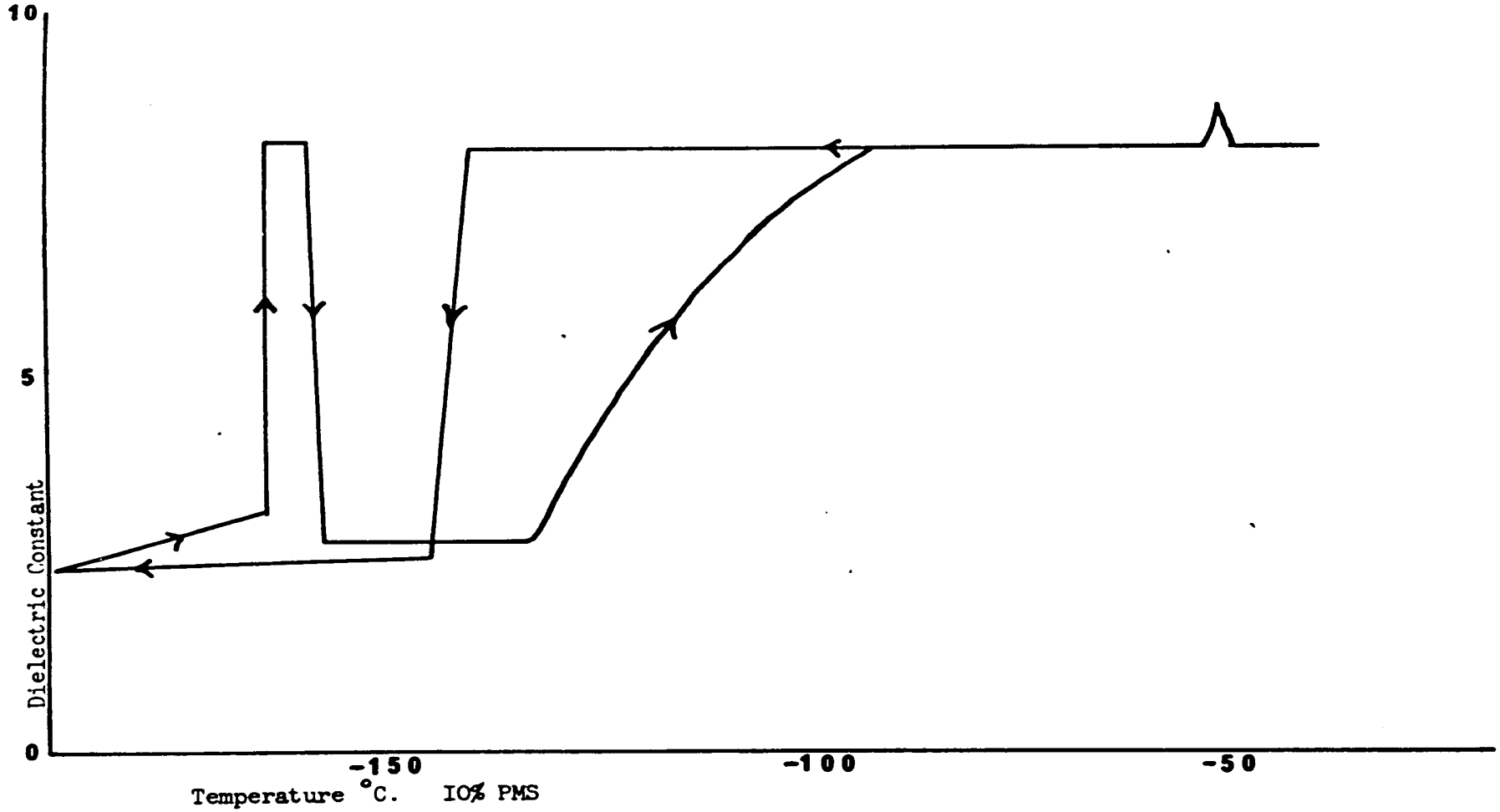

Figure 3I

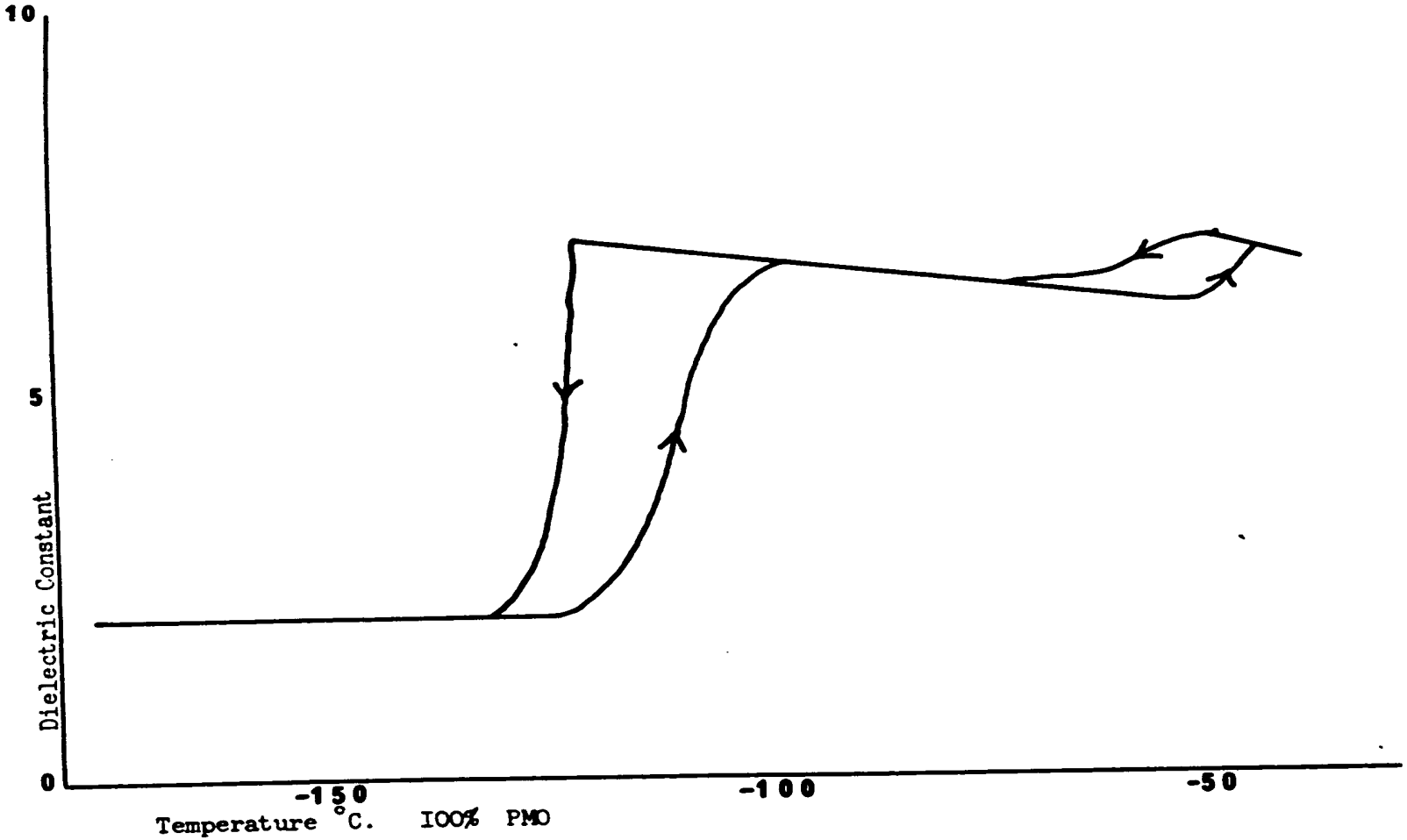

Figure 32

Figure 33

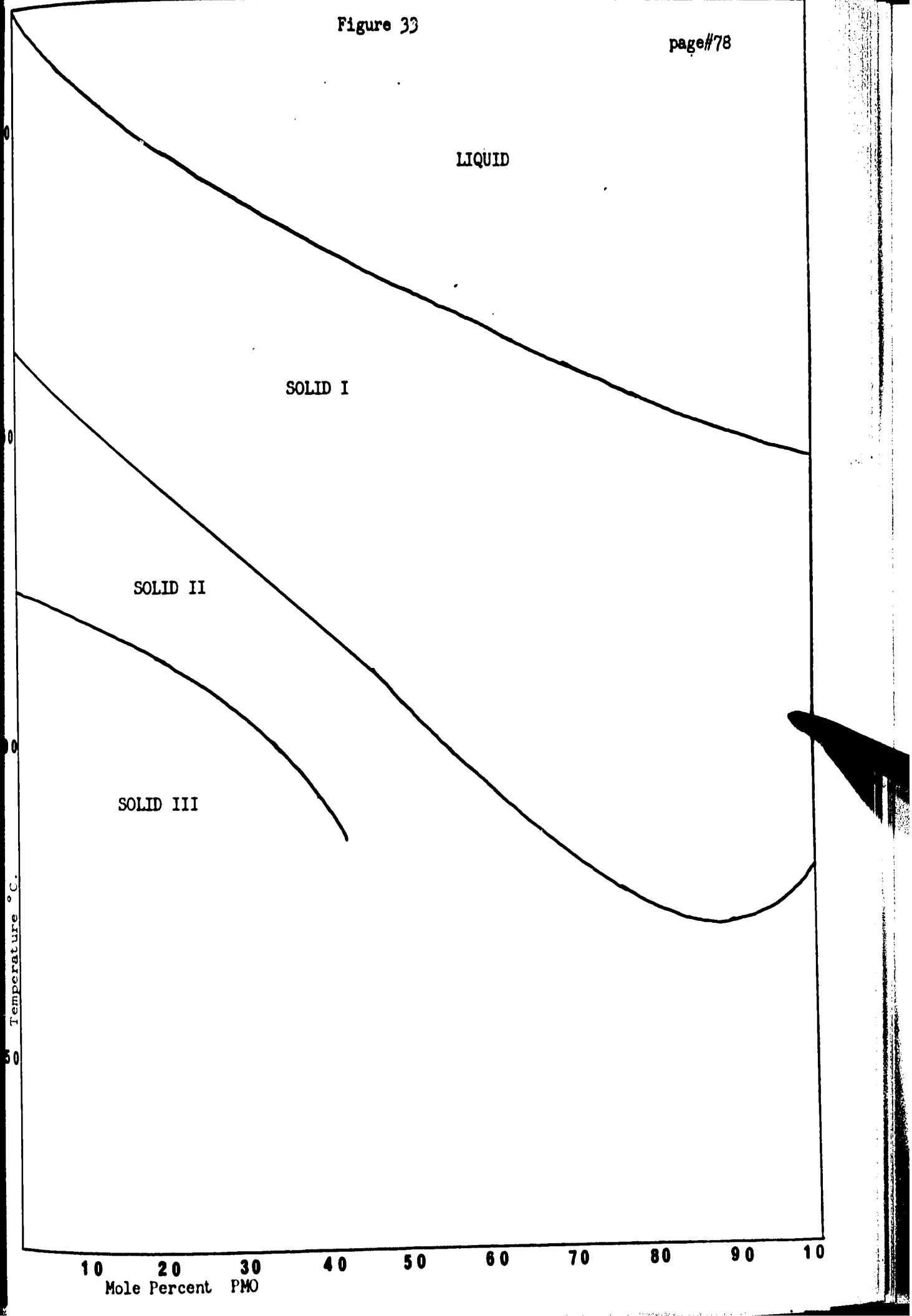
LIQUID
SOLID I
SOLID II
SOLID III
Temperature °C.
10
20
30
40
50
60
70
80
90
10
Mole Percent PMO

value. This is thought to be due to localized melting as a result of the heat liberated during the transition.

The single major conclusion of this section is that the system is suitable for dielectric analysis.

I. Second Dielectric Analysis

This analysis used an improved cell and temperature control apparatus. The results are shown in Figures 34 and 35. Two points are immediately evident. These are:

(1) The expected phase transitions are visible as discontinuities in the dielectric constant vs temperature curve of the pure components, but this is not always clearly the case at intermediate concentrations.

(2) There is always (except in pure PMO) a region in which dielectric dispersion is seen to occur in the frequency range of 10^2-10^5 Hz. Examination of Figures 25 and 33 will show the transitions observed to be in good agreement with our previous work.

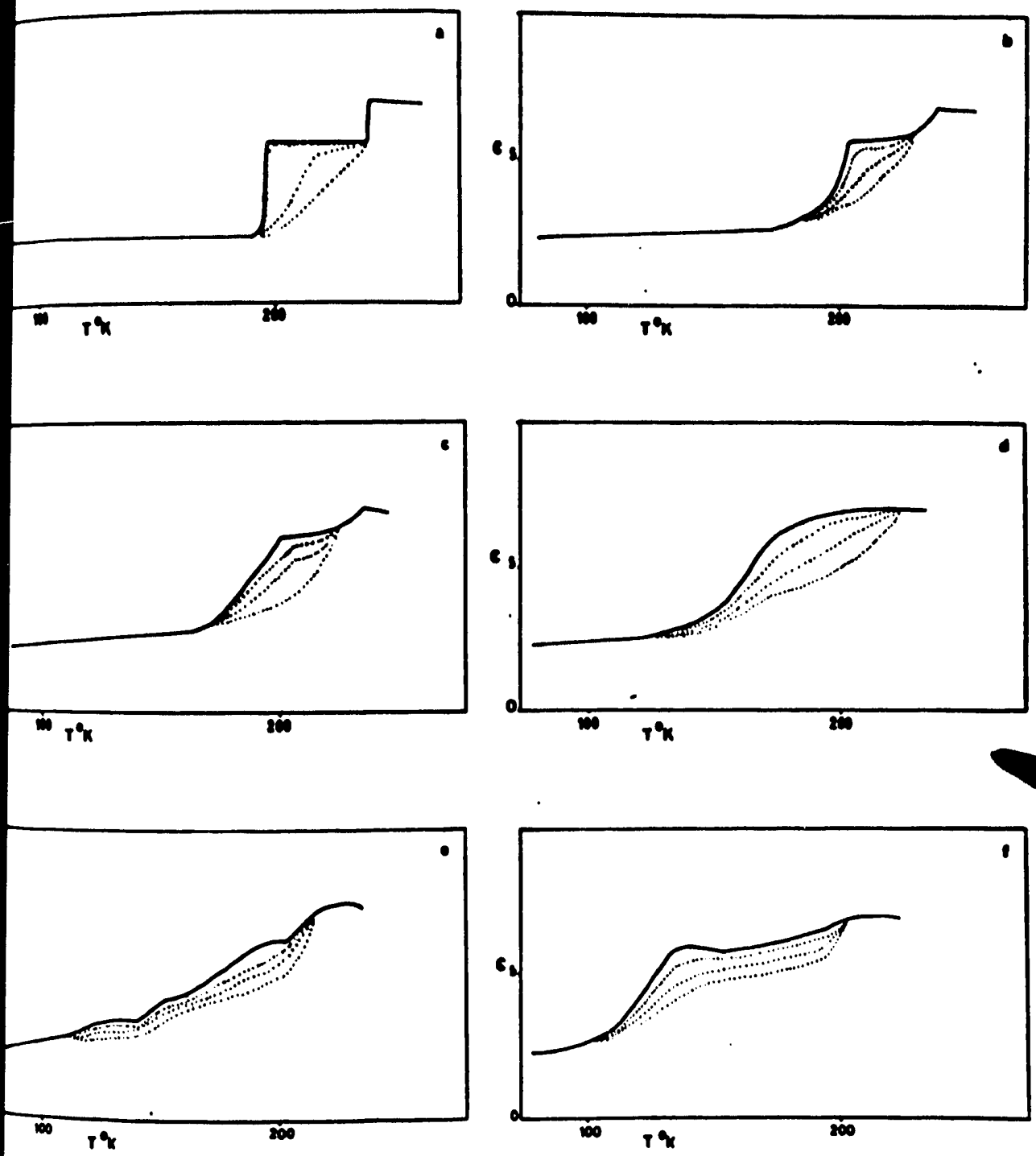

Figure 34 (a) 100% (b) 90% (c) 80 (d) 70 % (e) 60% (f) 50% PMS . In the dispersion region the 4 lines represent , from top to bottom, dielectric constants measured at 100 Hz, 1kHz, 10kHz, and 100kHz respectively.

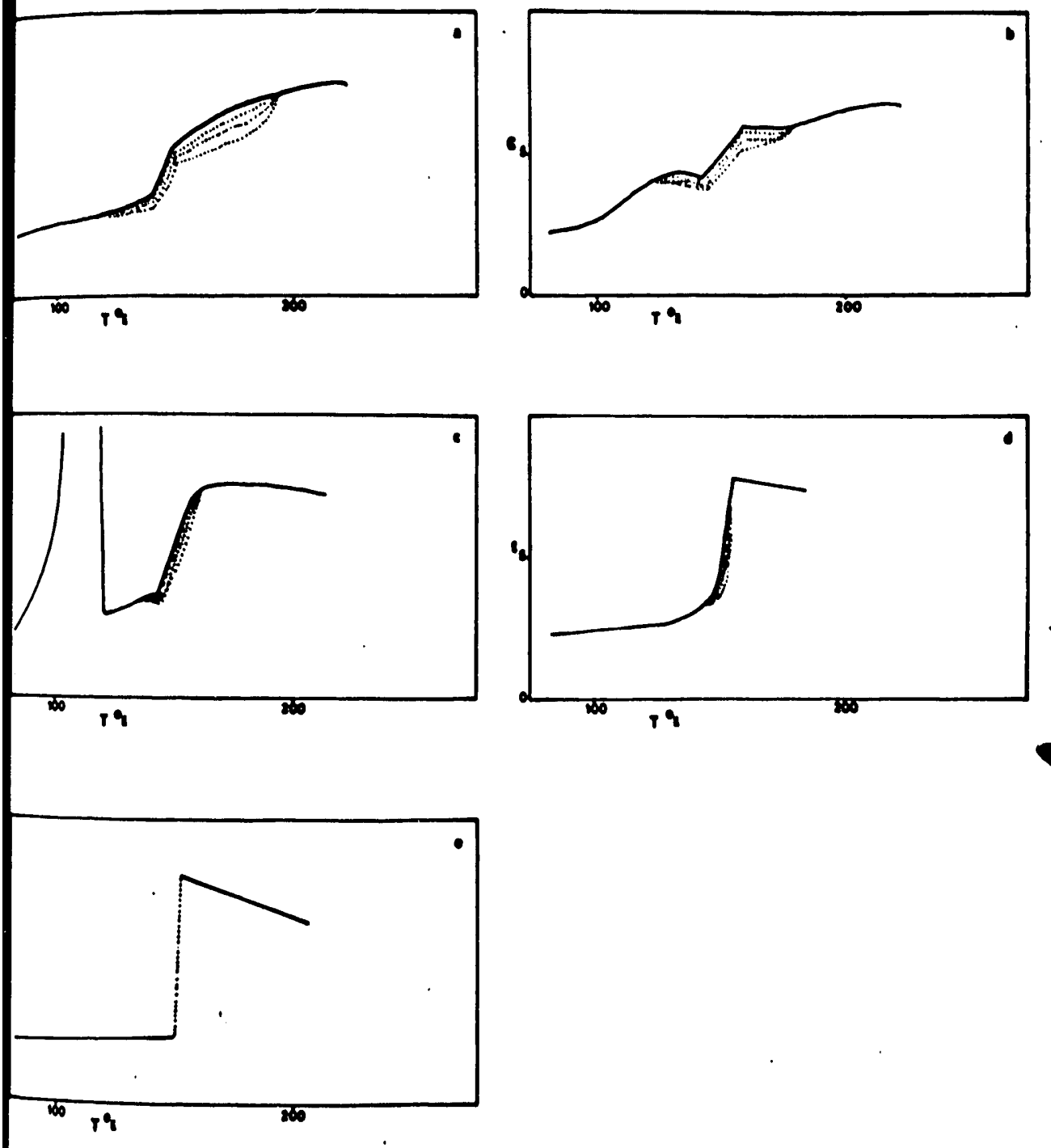

Figure 35 (a) 40% (b) 30% (c) 20% (d) 10% PMS and (e) 100% PMO

TABLE VIII

Temperature at which dielectric dispersion in the frequency range of 100 Hz-100kHz is first observed to appear and disappear in the system thiacyclohexane-tetrahydropyran.

% $C_5H_{10}O$	Appearance of dispersion(°K)	Disappearance of dispersion(°K)
0	198	239
10	185	230
20	174	224
30	124	222
40	113	213
50	103	204
60	118	193
70	130	180
80	140	163
90	144	154
100	153	157

Table VIIIlists the temperatures at which dielectric dispersion first appears and disappears at the frequencies used. These points are plotted in Figure 36 and superposition of this Figure on Figure 25 will show this event to coincide with regions of known or suspected phase

Figure 36

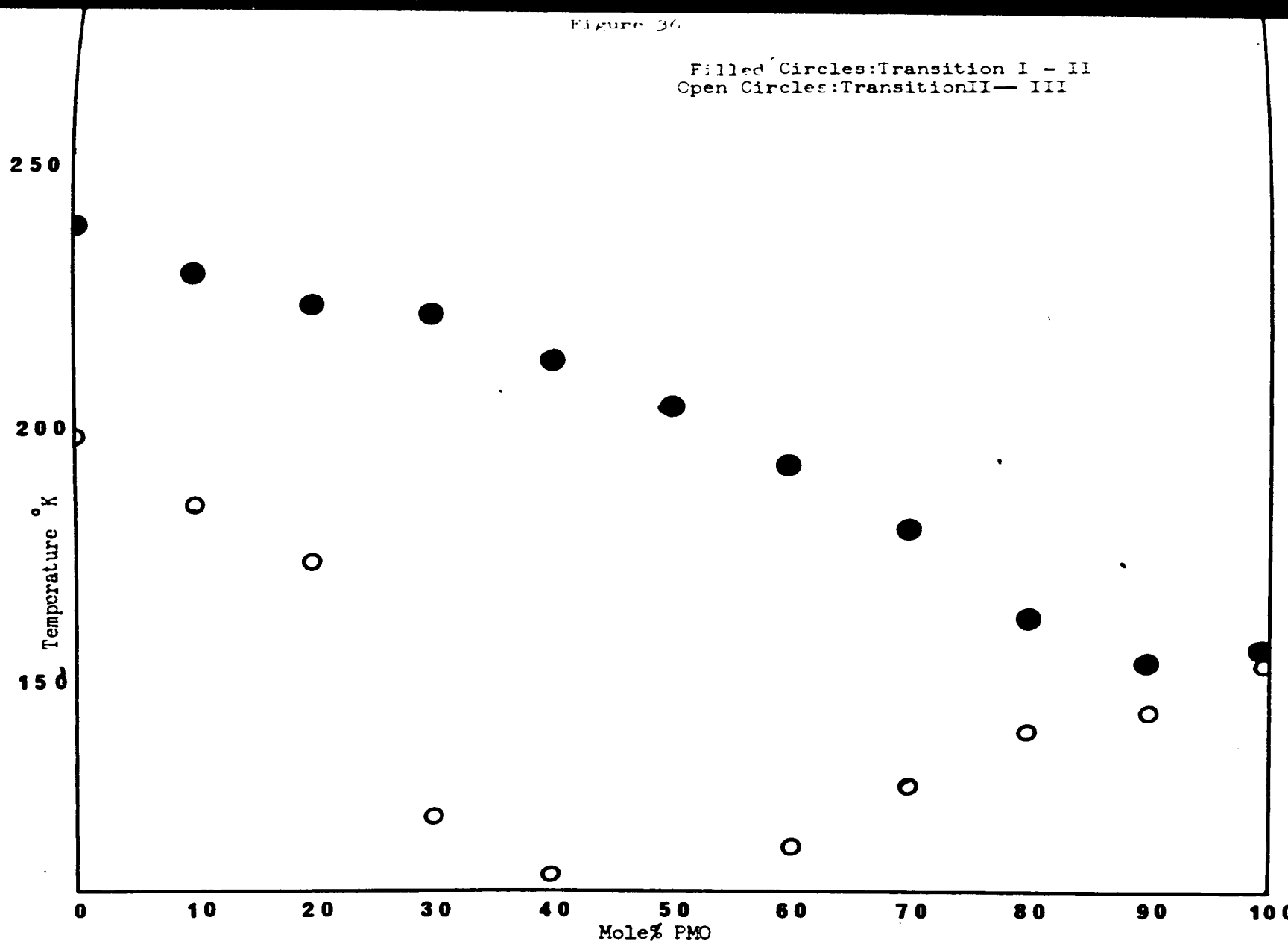
Filled Circles:Transition I - II
Open Circles:TransitionII— III
250
200
150
Temperature °K
0
10
20
30
40
50
60
70
80
90
100
Mole% PMO

transitions. On the basis of the previous discussion of the terms rotation and non-rotation we now divide the temperature composition diagram into three regions, labelled in figure 25 I, II and III corresponding to regions of free rotation, hindered rotation (i.e. showing dielectric dispersion in our frequency region) and non-rotation respectively.

Throughout this portion of the work it was difficult to control the temperature to within $\pm$ 1°C for more than thirty minutes. Considerable drift was often noted in dielectric constant during this time. Once again we are forced to concentrate on the region labelled II in figure 25 and to remain in the PMS rich region of the diagram. Let us now discuss the implications of our results to date.

J. Interpretation of Initial Results

We wish here to comment on the results to date and test the range of their validity. Consider first the two pure substances. The detailed study of PMS of McCullough et al agrees well with our own results, except for the lambda point discovered by him and his associates. It has already been pointed out that this phenomenon lies outside this work and was not observed by other workers engaged in dielectric studies. The two solids labelled I and II in figure 25 have been found to exhibit considerable freedom and the lower phase (II) has been investigated by several workers (36,37). X-ray work has shown (67) the first phase (I) to be simple cubic, optically isotropic and plastic in nature. All other reported physical properties are in agreement with our own work.

PMO agrees well with available physical data though none has been found other than our own for the solid material. Our work clearly shows it to exist in two crystal modifications, the upper of which is plastic in nature. This latter statement is supported by:

(1) Low entropy of fusion.

(2) $\Delta S_{fus} + \Delta S_{trans}$ for PMO $= \sum \Delta S_{trans} + \Delta S_{fusion}$ for PMS

(3) No dielectric dispersion observed in the high dielectric constant high temperature phase.

It is thus concluded, after the above results are compared with the solution data, that the two components form a continuous series of solid solutions. The low temperature region of the resulting temperature-composition diagram is difficult to interpret mainly due to the difficulty in reaching equilibrium. There then remain the high temperature solid phases. Only one of these shows dielectric dispersion in the region of frequency available to us. It is therefore resolved to begin a study with more sophisticated equipment of the regions labelled I and II in figure 25. The region labelled I will be used only to test various equations for the dielectric constant of rotating solids. Region II will be the subject of the major portion of this work, and will be used to study the dielectric constant as a function of frequency, temperature and composition.

K.(I) Dielectric Results from the Spring Loaded Cell

The results of this section will be ordered in the following way: the results obtained at each concentration will be advanced and discussed in some detail. In this manner we shall begin in 100% PMS and

progressing to lower concentrations of PMS we shall be able to observe (hopefully) systematic changes which will yield information about the factors affecting the dielectric constant of the solid solution and the shape of the observed dispersion. As far as is possible the features of each concentration will be examined in the same order to permit easy reading and comparison.

K.(II) 100% PMS

(a) Comparison with Previous Results

First it might be wise to clear up a minor point. The question might well be asked if the transition temperatures are significantly affected in the spring-loaded system. This possibility arising from the well-known Clausius-Clapeyron equation which has the form:

$$\frac{dP}{dT} = \frac{\Delta H}{T\Delta V} \qquad (83)$$

Perusal of Bridgman's work (62) will show that a reasonable average change of one degree Celsius might be expected for every sixty atmospheres applied pressure. Further other work in this laboratory (63) indicates that for PMS forty atmospheres pressure might be expected to bring about this change. It is thus reasonable to assume that the modest pressures used will have no effect in displacing the regions of interest in our present work. Table IX now shows the effect of the pressure cell on the measured values of ϵ' compared with the previous results. In this section the values of the previous work were obtained from figures 34 to 35 and the spring-loaded values from the raw data.

TABLE IX

	T(°C)	Previous ϵ'	Pressure ϵ'
Phase I (Freely rotating at 100 kHz)	-7.4	6.9	7.5
	-22.5	6.9	7.8
	-30.5	6.9	8.1
Phase II (hindered rot. at 1 kHz)	-37.3	5.7	8.1
	-45.1	5.7	7.8
Phase III (no rot. at 1 kHz)	-107.6	2.2	2.5

A simplistic model due to Chan (9) shows that the formation of cracks due to sample shrinkage can lead to a lowering of the measured dielectric constant. The spring loaded cell was devised specifically to correct this. Table IX clearly shows that considerable success has been achieved. The pressure cell values are consistently higher than those obtained without this refinement and in phase I give better values for the dipole moment of PMS than do the previous results. There is, however, reason to believe (63) the dielectric constant, at least at low frequencies, in the upper portion of phase II should be higher than that of phase I. It seems reasonable, then, to conclude that the pressure cell used here is a vast improvement over previous methods but is not perfect.

K.(IIb) METHOD

It is possible, by a suitable choice of components, to construct a network of resistors and capacitors which will yield the same frequency response as a given dielectric material (64). Consider Figure 37

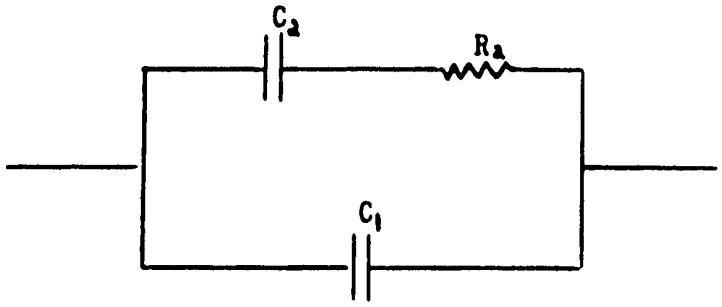

Figure 37

for which:

$$Y^* = \frac{1}{Z^*} = \frac{1}{Z_1^*} + \frac{1}{Z_2^*} = \left[\frac{1}{j\omega C_1}\right]^{-1} + \frac{1}{R_2 + \frac{1}{j\omega C_2}} \qquad (85)$$

Now the time dependence for the voltage of a simple RC circuit may be written:

$$V = V_o\, e^{-t/RC} \qquad (86)$$

thus for the top portion of figure 37 above we have:

$$\tau_2 = R_2 C_2 \tag{87}$$

Substitution of (87) in (85) yields:

$$Y^* = \frac{\omega^2 C_2 \tau_2^2}{1+\omega^2 \tau_2^2} + j\omega C_1 + \frac{j\omega C_2}{1+\omega^2 \tau_2^2} \tag{88}$$

Now introducing:

$$\epsilon^* = \epsilon' - j\epsilon'' \tag{89}$$

we write

$$\begin{aligned} I^* &= j\omega C V^* \\ &= j\omega \epsilon^* C_o V^* \\ &= j\omega C_o (\epsilon' - j\epsilon'') V^* \end{aligned} \tag{90}$$

Whence

$$Y^* = \frac{I^*}{V^*} = \epsilon'' \omega C_o + j \epsilon' \omega C_o \tag{91}$$

Equating real and imaginary parts of (88) and (91) we obtain:

$$\epsilon'' = \frac{C_2}{C_o} \left(\frac{\omega \tau_2}{1+\omega^2 \tau_2^2}\right) \tag{92a}$$

$$\epsilon' = \frac{C_1}{C_o} + \frac{C_2}{C_o}\left(\frac{1}{1+\omega^2\tau_2^2}\right) \qquad (92b)$$

If we now set:

$$\frac{C_1}{C_o} = \epsilon_\infty \quad , \quad \epsilon_o - \epsilon_\infty = \frac{C_2}{C_o}$$

we have from 92a and 92b

$$\epsilon'' = \frac{C_2}{C_o}\left(\frac{\omega\tau_2}{1+\omega^2\tau_2^2}\right) = (\epsilon_o - \epsilon_\infty)\frac{\omega\tau_2}{1+\omega^2\tau_2^2} \qquad (93a)$$

$$\epsilon' = \frac{C_1}{C_o} + \frac{C_2}{C_o}\left(\frac{1}{1+\omega^2\tau_2^2}\right) = \epsilon_\infty + \frac{(\epsilon_o - \epsilon_\infty)}{1+\omega^2\tau_2^2} \qquad (93b)$$

where 93a and 93b will be seen to be identical to Debye's equation. If now there was a certain amount of dc conductance in the sample we should have to introduce a suitable conductance in Figure 38 obtaining:

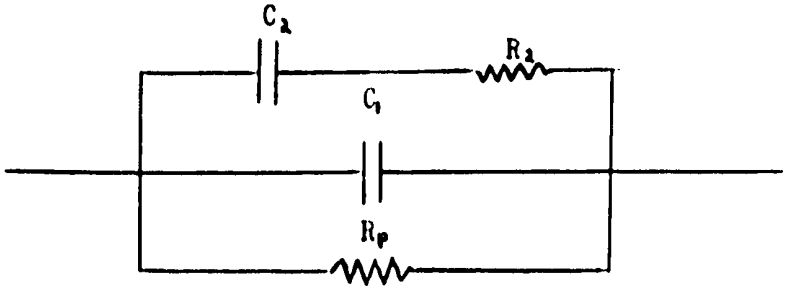

Figure 38

we would now obtain

$$\epsilon'' = \frac{G_p}{\omega C_o} + \frac{C_2}{C_o}\left(\frac{\omega\tau_2}{1+\omega^2\tau_2^2}\right) \qquad (94)$$

Now equation 94 shows that should dc conductance occur, a rise in ϵ'' is to be expected and is thought to be due to the presence of trace ionic impurities. In the present work increases in ϵ'' at low frequency were accordingly ignored. They were observed in all the dispersion runs. A sample result being shown below:

TABLE X

EFFECT OF DC CONDUCTANCE ON ϵ'' IN 100% PMS at -54.75°C

freq.	ϵ'	ϵ''
100 kHz	4.548	1.135
50 kHz	5.157	1.558
10 kHz	7.322	1.189
5 kHz	7.663	.669
2 kHz	7.783	.302
1 kHz	7.839	.195
500 Hz	7.839	.175
100 Hz	7.839	.292

Ignoring the points which indicated a sudden rise in ϵ'' at low frequencies the dispersion data were fitted by a symmetric arc and a skewed arc (equations 64 and 67). The fitting was achieved in the following manner; an I.B.M. 7040 computer was programmed to regard ϵ_0, ϵ_∞, τ_0, α or β as parameters in equations 65 and 68 . Starting with trial estimates of the four parameters their values were systematically altered until a minimum was found in the difference between the calculated and experimental values of ϵ'. Further systematic alteration of the parameters then brought the estimated ϵ' to within two percent of the experimental values. The values of the parameters so obtained were then used to calculate ϵ'' which was compared with the experimental values. Several methods were then used to decide which function had yielded the best fit to the experimental data. These were:

1) Success of the computer operation i.e. the machine was allowed five hundred trial attempts to approximate the experimental data. If this failed the result after five hundred trials was allowed an additional five hundred iterations. Failure on the second attempt was regarded as a failure of the function.

2) Realistic values of parameters i.e. ϵ_0, ϵ_∞, τ_0 cannot have certain values. A negative τ_0 value for instance may be immediately rejected; similarly, an ϵ_∞ value of less than two. ϵ_0 may be closely approximated from the raw data and values differing markedly from such an approximation may be ignored. Davidson and Cole (32,19) both limit their values of β and α to between 0 and 1. Their convention is respected.

3) Best fit, i.e. if conditions 1) and 2) were both satisfied an average error was calculated for the approximations of ϵ' and ϵ'' and

the fit giving the smallest relative error was used. Confusion arose only in cases where $\alpha \doteq 0$ and $\beta \doteq 1$, that is when nearly ideal behaviour was approximated.

4) It will be found that other approximations were used to fit the data, as these are introduced the additional criteria by which they were judged will be also.

(IIIc) Analysis of Dispersion

Using the methods outlined in (IIIb) the 100% data in the dielectric dispersion region were found to be fitted well by the equations of Cole and Cole. The ability of the parameters used to fit the results is shown in Figures 39a to 39d. The parameters used are shown in Table XI below.

TABLE XI

100% PMS	T °C	ϵ_o	ϵ_∞	τ_o	α
	-66.5	8.027	3.778	3.876×10^{-5}	.1077
	-59.4	7.258	3.034	1.009×10^{-5}	.1326
	-54.7	7.835	4.169	5.584×10^{-6}	.0504
	-45.1	7.831	3.262	1.025×10^{-6}	.0689

A plot of $\ln T\tau_o$ vs $1/T^\circ K$ is shown in Figure 40. The linearity of the plot is evident. The result was fitted to a best straight line using a least square computer program. At this time, however, it would be well to recall the point made in the introduction of this work, i.e. that the linearity and correctness of the plot of $\ln \tau_o$ vs T could be improved if $\ln T\tau_o$ vs 1/T was used instead. When this was done the sigma value and hence the linearity of the plot was greatly improved. The resulting

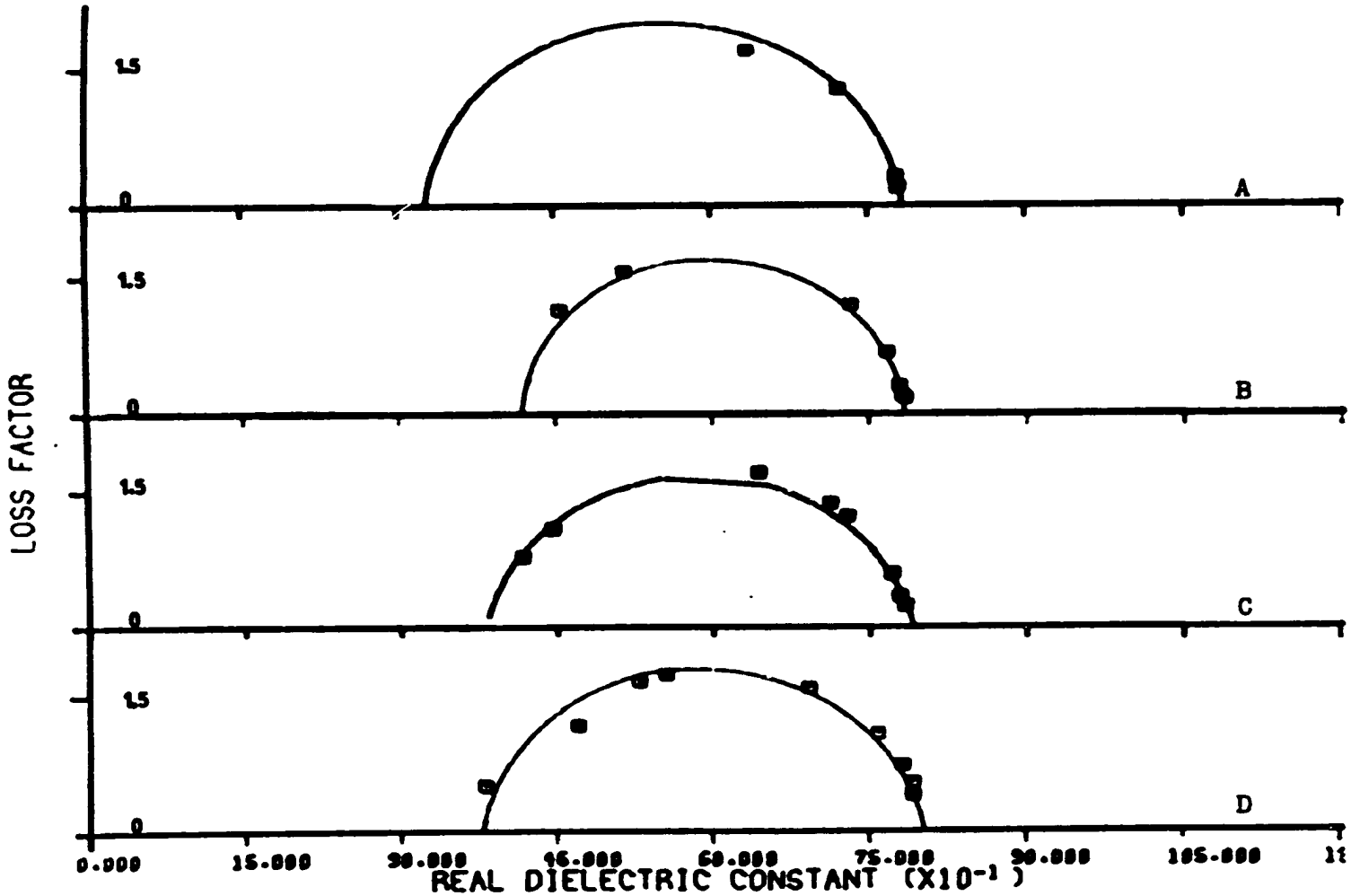

Figure 39

100% PMS A = -45.I C. B = -59.4 C. C = -54.7 C. D = -66.5 C.

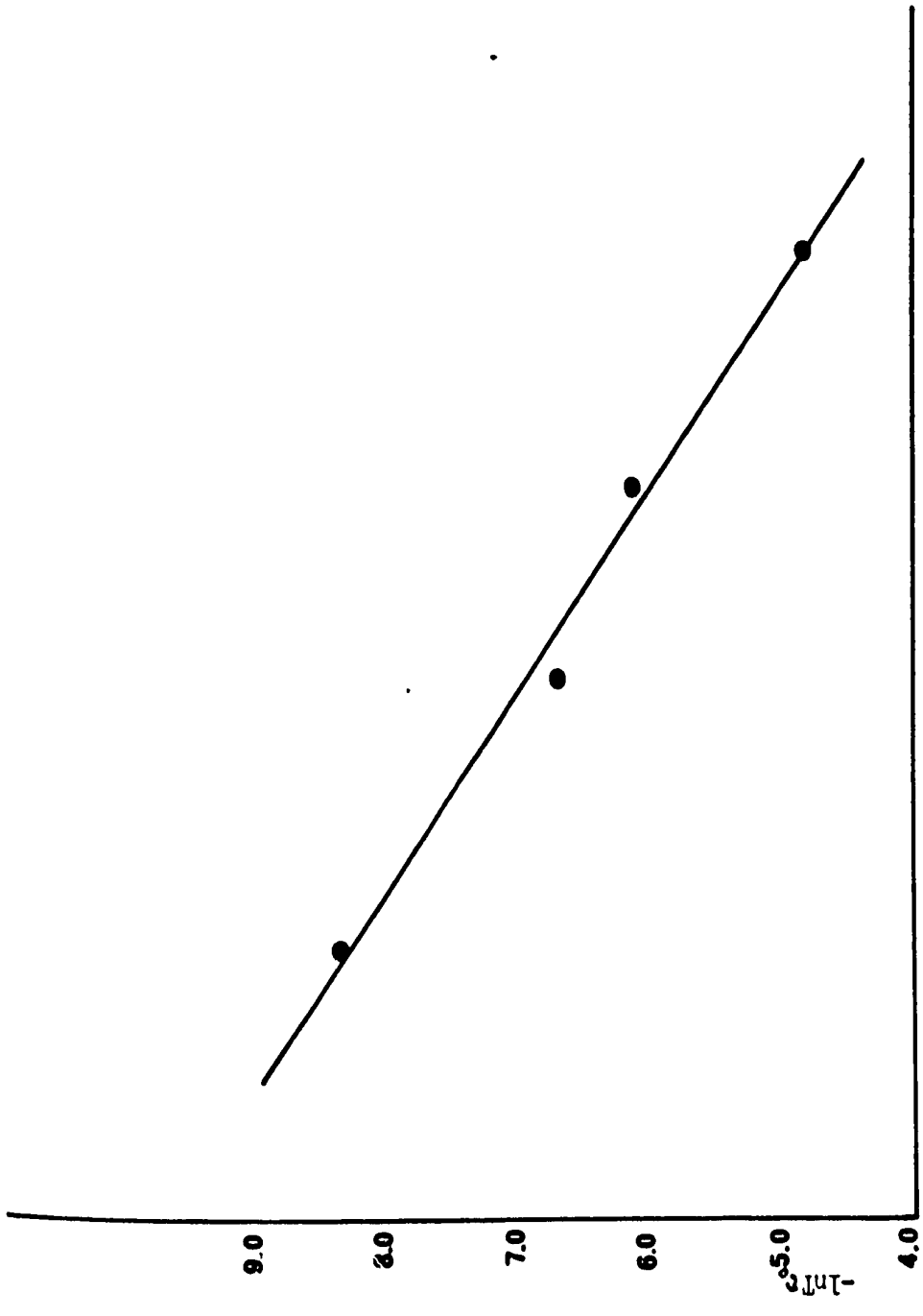

Figure 40

values of the thermodynamic properties thus obtained are recorded in Table XIIbelow.

TABLE XII

100% PMS $\Delta H^{\ddagger}$ = 15290 cal/mole

T(°C)	$\Delta G^{\ddagger}$ (cal/mole)	$\Delta S^{\ddagger}$ (cal/°K/mole)
-66.5	7774	36.36
-59.4	7483	36.51
-54.75	7399	36.12
-45.10	6977	36.44

The $\Delta H^{\ddagger}$ value is in good agreement with previous work. Lydia Reinisch (37) found $\Delta H^{\ddagger}$ = 18 Kcal/mole while Kondo and Motsumoto (68) found $\Delta H^{\ddagger}$ = 13.22 Kcal/mole. It is gratifying to find our value is very nearly the average of these two.

The high value of $\Delta S^{\ddagger}$ is also of interest. Kauzmann(26) has pointed out that such values, common in dielectric work, tend to indicate that a cooperative process involving many molecules is taking place. The implication is that when a molecule enters its rotational transition state, neighboring molecules tend to become disoriented and gain considerable freedom of their own. Thus the rotating molecule would tend to find itself in a gas-like environment. This suggestion leads at once to the conclusion that $\Delta H^{\ddagger}$ should be close to the enthalpy of sublimation. Kauzmann(26) has pointed out that this might be expected to lead to a $\Delta H^{\ddagger}$ of 10-15 Kcal/mole. The enthalpy of sublimation of PMS at -30°C has been estimated based on the results of McCullough and his co-workers (36) and has been found to be about 14 Kcal. This agreement is too good to be ignored and

it seems reasonable to conclude that dipolar orientation in PMS is the result of a cooperative process.

Despite the agreement with previous results, one further point must be noted. Reference to Table XII will show that ϵ_0 and ϵ_∞, while showing the predictable temperature variations, are not as regular as might be hoped. This is almost certainly due to the presence of a second dispersion at higher frequencies which will tend to intrude itself to a greater or lesser degree into the present results and it is due to this unseen presence that the errors are ascribed. Our reason for asserting that there is a second dispersion region is twofold. Firstly, our ϵ_∞ values appear high; secondly, Lydia Reinisch (37) has observed this dispersion. Though, as will be seen later, attempts are made in this work to resolve this region further, we are limited to frequencies less than 100 kHz and this serious limitation prevents a characterization of the second dispersion.

Finally, for reasons which will be outlined in the next two sections, it would appear that it would be unwise to place undue emphasis on the thermodynamic interpretation of these results.

d i) Discussion

Despite the excellent agreement of our results with those of previous workers, two serious questions are raised by them. These are:

1. Since the formulae used, and for that matter any other formulae, would differ from Debye's simple and highly successful formulation, why should such differences arise?
2. Could the results be better represented by different formulae from those used?

Let us address ourselves to the first question. Kauzmann(26) speculates that deviations from Debye's result are due to thermal fluctuations in the local free energy barriers to rotation. Such fluctuations allow distributions of relaxation times to appear. Suitable continuous distributions have been suggested on empirical grounds by several authors (65,80,81). These assume that deviations from Debye behaviour occur as the result of the presence of a continuous spectrum of relaxation times rather than a single relaxation time. Fuoss and Kirkwood (65) have shown that a symmetric arc will result in a distribution which is represented by a function of the form:

$$F(s)ds = \tfrac{1}{2} \cdot \frac{\sin \alpha\pi}{\cosh(1-\alpha)s - \cos\alpha\pi}\, ds \qquad (95)$$

These methods, however, appear as exercises in curve fitting and supply no suitable physical models. These functions have been supplemented by physical models which are capable of explaining a wide range of dielectric dispersion phenomena. These are discussed in the next sections.

d ii) The Glarum Model

A recently proposed model (66) which, though highly simplified, is capably of generating all three dispersion types (i.e. semicircle, symmetric arc, skewed arc) will now be discussed. The argument proposed by Glarum runs as follows: Suppose that the skewed arc results from a selected number of dipoles relaxing at a very rapid rate, the remainder relaxing at a slower rate. Further, let us assume the rapid rate is virtually instantaneous and occurs when a neighbour-lattice site is vacant.* Adopting Glarum's notation, we now write the molecular re-

---

* Thus vacancies are the only type of defect which we consider.

laxation function

$$\phi(t) = [1-P(t)] \exp(-\alpha_o t) \tag{96}$$

where α_o = relaxation frequency in a defect-free region, $P(t)$ is the probability that a defect arises at a molecule for the first time at time t. If the defect is a distance l_o removed from a given molecule, the problem of finding when this defect reaches the molecule is equivalent to the problem of an absorbing wall for which Chandrasekhar (69) has found:

$$\dot{P}(t,l_o) = l/(4\pi D)^{\frac{1}{2}} \; t^{-3/2} \exp(-l_o^2/4Dt) \tag{97}$$

where D is the diffusion coefficient. Averaging over all possible values of l_o yields:

$$\dot{P}(t) = (D/l_o^2)^{\frac{1}{2}}$$

$$\left[(1/\pi t)^{\frac{1}{2}} - (D/l_o^2)^{\frac{1}{2}} \exp(Dt/l_o^2) \operatorname{erfc}(Dt/l_o^2)^{\frac{1}{2}}\right] \tag{98}$$

Differentiation of (96) yields:

$$-\dot{\phi}(t) = \alpha_o \phi(t) + \dot{P}(t) \exp(-\alpha_o t) \tag{99}$$

Substitution of (98) in (99) yields:

$$-\dot{\phi}(t) = \alpha_o \phi(t) + \exp(-\alpha_o t) (D/l_o^2)^{\frac{1}{2}}$$

$$\left\{\left[1/(\pi t)^{\frac{1}{2}}\right] - (D/l_o^2)^{\frac{1}{2}} \exp(Dt/l_o^2) \operatorname{erfc}(Dt/l_o^2)\right\} \tag{100}$$

If we now write

$$a = \alpha l_o^2/D$$

$$a_o = \alpha_o l_o^2/D$$

then Glarum finds the distribution of relaxation frequencies to be

$$F(a) = \pi^{-1}\left[1/(a-a_o)^{\frac{1}{2}}\right] a/(a-a_o+1) \quad \text{for } a > a_o \qquad (101)$$

$$= 0 \qquad a < a_o$$

Three particular cases are said to be of interest here. They are: $a_o \gg 1$ which would correspond to a Debye-type relaxation, $a_o = 1$ corresponding to a skewed arc and $a_o \ll 1$ yielding a symmetric arc.

Taking the Laplace transform of equation (100), Glarum now obtains:

$$L\left[-\dot{\phi}(t)\right] = \frac{1}{1+i\omega/\alpha_o} + \left\{\frac{i\omega/\alpha_o}{1+i\omega/\alpha_o}\left[(1+i\omega/\alpha_o)^{\frac{1}{2}}(a_o)^{\frac{1}{2}}+1\right]^{-1}\right\}$$

$$= (\epsilon^* - \epsilon_\infty)/(\epsilon_o - \epsilon_\infty) \qquad (102)$$

This result will be examined further in the next section.

d iii) Test of Glarum's Defect Diffusion Model

It might be anticipated that Glarum's defect diffusion model is far too simplistic to yield agreement with a real system. It was resolved however to propose a simple means to test this approach and apply it to our work.

The procedure, detailed in Appendix A, was as follows. Equation (102) was separated into real and imaginary parts. This yielded an expression for ϵ' which was then reduced by introduction of new variables in the form of a simple quadratic in a_o. It was then possible to solve for a_o using the values of ϵ_o, ϵ_∞ and τ_o obtained from the symmetric arc which had already been fitted to the 100% PMS data.

The results obtained at three temperatures are shown in Table XIII.

TABLE XIII

T(°C)	a_o	τ_o (sec)	l_o^2/D (sec)
-54.75°	4.16 or 0.56	5.58×10^{-6}	23.2×10^{-6} or 3.12×10^{-6}
-59.4	3.75 or 0.57	1.009×10^{-5}	3.78×10^{-5} 0.57×10^{-5}
-66.5	0.07 or 0.26	3.876×10^{-5}	$.27 \times 10^{-5}$ 1.00×10^{-5}

The first unsatisfactory point to be noted in Table XII is that due to the form of the equation used to obtain a_o we do not obtain a unique answer for a_o. Further, if we consider the a_o terms here to be of order unity, a skewed arc would be expected. On this point note that a skewed arc function is in fact a good fit for these data, the symmetric arc plot being marginally better. The comparison is again unsatisfactory. Finally, one might expect that it would be possible to insert a reasonable value of l_o^2. Once again such a procedure is difficult. Sherwood (48) has shown that values of D for self-diffusion in organic solids may differ by as much as 400% depending on sample history. The fact that the nature of the defect we must use is unspecified, is of little help since a vacancy should move more rapidly than a molecule. Ignoring these facts, we choose (from Sherwood's value for self-diffusion of pivalic acid) $D = 10^{-8}$ cm^2 sec^{-1} to obtain:

TABLE XIII

T(°C)	a_o	τ_o (sec)	l_o^2/D (sec)
-54.75°	4.16 or 0.56	5.58×10^{-6}	23.2×10^{-6} or 3.12×10^{-6}
-59.4	3.75 or 0.57	1.009×10^{-5}	3.78×10^{-5} 0.57×10^{-5}
-66.5	0.07 or 0.26	3.876×10^{-5}	$.27 \times 10^{-5}$ 1.00×10^{-5}

The first unsatisfactory point to be noted in Table XII is that due to the form of the equation used to obtain a_o we do not obtain a unique answer for a_o. Further, if we consider the a_o terms here to be of order unity, a skewed arc would be expected. On this point note that a skewed arc function is in fact a good fit for these data, the symmetric arc plot being marginally better. The comparison is again unsatisfactory. Finally, one might expect that it would be possible to insert a reasonable value of l_o^2. Once again such a procedure is difficult. Sherwood (48) has shown that values of D for self-diffusion in organic solids may differ by as much as 400% depending on sample history. The fact that the nature of the defect we must use is unspecified, is of little help since a vacancy should move more rapidly than a molecule. Ignoring these facts, we choose (from Sherwood's value for self-diffusion of pivalic acid) $D = 10^{-8}$ cm^2 sec^{-1} to obtain:

TABLE XIV

T(°C)	l_o (Å)
-54.75	48 or 18
-59.4	62 or 24
-66.5	17 or 32

This shows at least two interesting features: i) The dimensions of l_o are quite reasonable. ii) The value of l_o should increase with decreasing temperature. This effect would be expected as the defect concentration would tend to fall with temperature. This is not confirmed.

Thus, although our work fails (as expected) to confirm the Glarum defect diffusion model it does show that this type of interpretation is qualitatively capable of explaining the occurrence of the Debye and Davidson plots, and that to some extent our data might be understood on this basis.

Similar analysis of a system for which the physical properties required were well known would be a far better test of this model.

d iv) Conclusions Based on Glarum's Approach

It has been shown that our data must fail to confirm or deny Glarum's theory. That it is in fact naive cannot be doubted nor can it be denied that it is the first model capable of predicting the three basic types of dispersion. This latter success has led Anderson and Ullman (70) to propose a generalized model of their own. In their approach the motion of the

defect as a relaxation mechanism is dropped in favor of a fluctuating environment. The authors point out that many fluctuating physical properties might be expected and select the "free-volume" merely to supply a simple physical concept on which to pin their equations. The conclusions reached are strikingly similar to Glarum's. These are:

1) If the free-volume fluctuations are much slower than the rate of molecular reorientation we shall observe a symmetric arc.

2) Rapid environmental change produces a single relaxation time.

3) For comparable rates of reorientation and environmental fluctuation, the theory predicts a skewed arc type of dispersion.

Since, in a qualitative way at least, we are able to explain the general types of dispersion and the initial results from our system seem to confirm this (i.e. 100% PMS gives a symmetric arc), the temptation now is to conclude that we have an adequate explanation of the system. Further, it would seem that we need only seek a time-dependent fluctuation which might alter the reorientation probabilities of our system in order to fully understand the results. Unhappily, nature is never that simple. Recalling Lydia Reinish's (37) observation that PMS contained a second dispersion region and recalling our remarks on this point in the introduction of this work we must now turn our attention to the possibility of multiple discrete dispersions. This is of vital importance because the success of the symmetric arc and skewed arc representations depend on their being unique and as Davidson (32) has pointed out, there is often doubt as to whether or not given dispersion dataare better fitted by a series of unique dispersions or a skewed arc.

d v) Discrete Relaxations

Fang (71) has concluded that if the Argand diagram is not a semi-circle $g(\tau)$ is a continuous distribution function. One might however question the existence of a truly continuous series of relaxation times, particularly the regular array of a crystalline solid. On the other hand, a Debye function which is actually a Dirac-delta function might also be said to be unrealistic. This latter objection is somewhat reduced if it is suggested that:

$$\frac{1}{\tau_o} = k_o = A \exp [-\Delta H/kT] \qquad (103)$$

It might reasonably be assumed that a number of relaxation times, quite close together, would tend to converge at higher temperatures and yield a Debye function. We shall return to this point later. For the moment it would appear that a discrete sum of Debye functions might be capable of yielding good agreement with data composed of multiple relaxation schemes. We would then have equations of the form:

$$\frac{\epsilon' - \epsilon_\infty}{\epsilon_o - \epsilon_\infty} = \sum_i \frac{A_i}{1 + \omega^2 \tau_i^2} \qquad (104a)$$

$$\frac{\epsilon''}{\epsilon_o - \epsilon_\infty} = \sum_i \frac{A_i \omega \tau_i}{1 + \omega^2 \tau_i^2} \qquad (104b)$$

This approach suffers from the severe difficulty that the number of unknown parameters rapidly becomes so high as to render solution a hopeless task. Thus, for practical reasons we may neglect this technique. Budo (72) has suggested the following simplified approach to the above equations:

$$\frac{\epsilon' - \epsilon_\infty}{\epsilon_o - \epsilon_\infty} = \frac{C_1}{1 + \omega^2 \tau_1^2} + \frac{C_2}{1 + \omega^2 \tau_2^2} \qquad (105a)$$

$$\frac{\epsilon''}{\epsilon_o - \epsilon_\infty} = \frac{C_1 \omega \tau_1}{1 + \omega^2 \tau_1^2} + \frac{C_2 \omega \tau_2}{1 + \omega^2 \tau_2^2} \qquad (105b)$$

This method has distinct advantages. It assumes only two relaxation processes, both obeying Debye's formulation and introduces the condition that $C_1 + C_2 = 1$. The immediate benefits of such an approach are obvious. The number of parameters is reduced to the point where they may be readily amenable to computer analysis and the approach should be useful in certain systems which might be expected to yield two distinct relaxation times. Systems of this type are known i.e. mixtures of an alkyl halide and an alcohol show two dispersion regions ('73). Magee and Walker (74) have carried out an extensive examination of this approach. They have found that the Cole symmetric arc can sometimes be better represented by Budo's equations and that in such cases estimation of $\tau_1 max$ via the Cole arc can lead to serious errors if the ratio τ_1/τ_2 differs significantly from unity.

d vi) Application of Budo's Technique to 100% PMS

The computer program used to fit the symmetric and skewed arc functions to our data was modified to accept equation (105a) using τ_1, τ_2, C_1 and ϵ_∞ as parameters. At most temperatures this program failed to yield a satisfactory convergence but for -54.75^o we obtained :

$$\tau_1 = 6.645 \times 10^{-7} \text{ sec}$$

$$\tau_2 = 4.025 \times 10^{-7} \text{ sec}$$

$$C_1 = 0.333$$

$$\epsilon_\infty = 4.382$$

It must be emphasized that the agreement of the calculated and observed ϵ' values is not as good as it was with the symmetric arc function but a fit is obtained which might be improved with more data. It must be noted however that ϵ_∞ obtained in this way is comparable to the previous value using the symmetric arc (i.e. 4.169), the vital point here being that ambiguity might arise regarding the value of the relaxation time (or times). It might be expected that the symmetric arc might yield a suitable average of the two but this is certainly not the case here and the serious errors outlined by Magee and Walker might well arise.

It seemed desirable at this point to test the range of validity of Budo's method further. This was done in the following way. Synthetic datawere prepared with two relaxation times $\tau_1 = 5.0 \times 10^{-5}$ sec, $\tau_2 = 7.0 \times 10^{-5}$ sec, $\alpha \neq 0$, $\epsilon_0 = 104$, $\epsilon_\infty = 3$. Budo was unable to resolve these times satisfactorily (the computer program failed to converge). This is suspected to be due to the condition that $C_1 + C_2 = 1$. The symmetric arc, however, yielded $\epsilon_0 = 104.1$, $\epsilon_\infty = 3.07$ $\tau_0 = 5.9 \times 10^{-5}$ sec and $\alpha = 0$. It appears, in this case at least that the symmetric arc has admirably fulfilled its task. Note however that the condition for success of the symmetric arc is fulfilled i.e. τ_1/τ_2 does not differ significantly from unity.

d vii) Multiple Dispersions

We have now shown that there exists considerable doubt as to whether or not the symmetric arc functions observed are in fact continuous functions. A further complication arises when we are forced to recognize that a reasonable alternative to the symmetric arc (Budo) can yield τ_0 values very

different from previous results. The question we now ask is: "Does the skewed arc representation suffer from the same difficulty?"

To answer this latter question it is necessary only to refer to Davidson's paper (32) to find instances where a skewed arc might well be fitted to two separate low and high frequency dispersions. Further, Cole and Davidson (31) have fitted the dispersion curve for n-propanol at $-151^{\circ}C$ to a sum of three symmetric arcs.

We must, then, face the fact that unless the entire dispersion range is available, the Cole-Cole and Cole-Davidson functions cannot be regarded as unique. Any physical data acquired from them must need to be regarded with suspicion.

d viii) Brot and Multiple Dispersion Regions

We have already pointed out that Budo's methods employs two constants, the sum of which is set equal to unity. This is an illustration of what Brot (75) refers to as the "classical technique". It requires that if two or more arcs superimposed then:

$$\epsilon_{o_{HF}} = \epsilon_{\infty_{LF}}$$

Where $\epsilon_{o_{HF}}$ is the static dielectric constant for the high frequency dispersion and $\epsilon_{\infty_{LF}}$ is the high frequency (at infinite frequency) dielectric constant of the low frequency dispersion. Figure 58 shows such a condition:

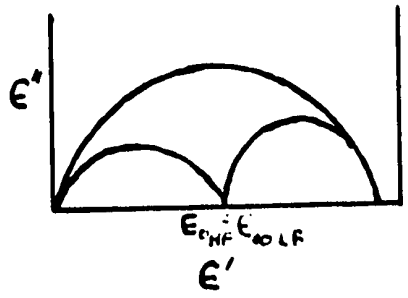

Figure 58

Brot has found that this condition is not met in some of his own work on a series of normal, primary alcohols (C_7-C_{10}). Brot begins his analysis of the problem by writing his dispersion equations as a simple sum of Debye-type relaxations i.e.

$$\epsilon' = \epsilon_\infty + \sum_i' \frac{A_i}{1 + \lambda^2_{ci}/\lambda^2} \tag{106a}$$

$$\epsilon'' = \sum_i' \frac{A_i \lambda_{ci}/\lambda}{1 + \lambda^2_{ci}/\lambda^2} \tag{106b}$$

where $\sum_i' A_i = \epsilon_o - \epsilon_\infty$,

λ_{ci} = wavelength corresponding to the maximum absorption for the discrete relaxation process i,

λ = wavelength of the measuring signal.

Brot now obtains

$$\frac{d\,\epsilon'}{d\left(\frac{\epsilon''}{\lambda}\right)} = -\frac{\frac{d\epsilon'}{d(1/\lambda^2)}}{\frac{d(\epsilon''/\lambda)}{d(1/\lambda^2)}} = \frac{\sum_i' -A_i \left[\frac{\lambda_{ci}^2}{(1+\lambda_{ci}^2/\lambda^2)^2}\right]}{\sum_i' \frac{A_i}{\lambda_{ci}} \left[\frac{\lambda^2_{ci}}{(1+\frac{\lambda^2_{ci}}{\lambda^2})^2}\right]} \tag{107}$$

He obtains a curve of negative slope of which the concavity is always turned upwards as long as we assume the various values of A_i are positive. Brot has found, in the case of the alcohols he studied, that the slope changes around λ = 50 cm. This, he believes, implies that some of the A_i are negative and that the failure of classical methods arises from lack of recognition of the fact that two separate relaxation processes may in fact be cooperative. If we consider two separate relaxation processes which both

contribute to a single, resolvable dispersion region we cannot overlook the possibility that cooperation between the two relaxations will give rise not to a simple sum of the two but to some function in which cross-terms will appear.

Brot has shown, using an approach he credits to Frohlich, that such cross terms may arise and that they may be negative.

It appears evident that Budo's approach must be used with grave reservations. Further ambiguity will arise in almost every resolvable dispersion due to the multiplicity of functions capable of representing such a dispersion.

These things being noted let us turn our attention to Hoffman's method which appears to allow for cooperative effects using a physical model particularly well suited to our solid system.

d ix) Hoffman's Method

Confronted with the problem of multiple relaxation times required to describe certain dispersions Hoffman (76,77,78,79) has advanced a series of papers containing a theory based on the number of positions available to a dipole in a crystal and the height of the energy barriers between positions. This distribution of barrier heights leads either to a Debye-type single relaxation time or a number of discrete relaxation processes. In the last of these papers the author closely approximates the dielectric loss observed for the dispersion resulting from 16-hentriacontanone in urea clathrates.

We shall now examine Hoffman's two-position model.

Consider two non-equivalent sites 180° apart. The transition probability for the elementary process by which a dipole moves from site 1 to

the adjacent site 2 is:

$$k = A \exp(-(W + V)/kT) \tag{108}$$

where A is a constant and W + V is the barrier height between site 1 and site 2. Similarly

$$k' = A\exp(-W/kT) \tag{109}$$

where k' is the transition probability for a jump between site 2 and site 1 while W is the barrier height between site 2 and site 1. Schematically we have

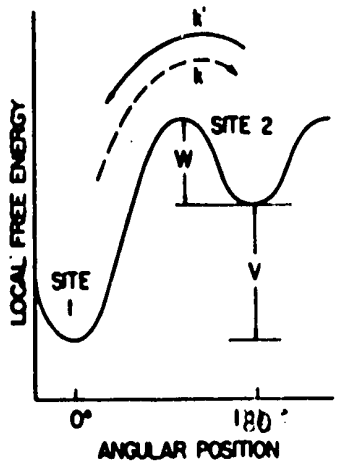

It is possible now to write the net rate at which dipoles enter a given site. We have:

$$\begin{aligned} dN_1/dt &= -2kN_1 + 2k'N_2 \\ dN_2/dt &= -2k'N_2 + 2kN_1 \end{aligned} \tag{110}$$

A set of differential equations of this type have general solutions of the form:

$$N_i = \sum_{\beta=1}^{\Omega} C_{i\beta} \exp\left[-f_{(\beta)}(k)t\right] \quad i = 1,2 \ldots \Omega \tag{111}$$

where Ω is the number of available sites. The functions $\psi_\beta = \exp\left[-f_{(\beta)}(k)t\right]$

are referred to as decay functions or modes of decay and are obtained as eigenfunctions of the operator D = d/dt corresponding to the eigenvalues $-f_{(\beta)}(k)$. These will now be obtained for the two-position model. The characteristic determinant for equation (11) may be written:

$$\begin{vmatrix} (D + 2k) & -2k' \\ -2k & (D + 2k') \end{vmatrix} = 0 \tag{112}$$

whence $D = 0; -2(k + k')$

Here the root zero leads to equilibrium time - independent solutions and we write

$$\begin{aligned} N_1 &= C_{11} + C_{12}\psi_2 \\ N_2 &= C_{21} + C_{22}\psi_2 \end{aligned} \tag{113}$$

where C_{11} and C_{21} are the equilibrium number of dipoles on sites 1 and 2.

Substitution of $\psi_2 = \exp(-2kt-2k't)$ in equation 113 shows:

$$C_{12} = -C_{22} \tag{114}$$

which indicates that decay of polarization is achieved by a flow of dipoles from site 2 to 1. It then follows:

$$P(t) = P_2 \exp\left[-2(k + k')\right] t \tag{115}$$

and a single relaxation time:

$$\tau_2 = 1/2\ (K + k') \tag{116}$$

is observed.

For a three position model we have:

$$\begin{aligned} dN_1/dt &= -2kN_1 + k'N_2 + k'N_3 \\ dN_2/dt &= kN_1 - 2k'N_2 + k'N_3 \\ dN_3/dt &= kN_1 + k'N_2 - 2k'N_3 \end{aligned} \tag{117}$$

with roots D = 0; $-3k'$; $-(2k + k')$. Here, by considering two of the sites to be equivalent we have obtained two decay times. Obviously the more numerous the sites, the more complex the analysis becomes. As already mentioned Hoffman(79) has applied the approach to various urea clathrates and the results are shown in Figures 47[a] to 48[a].

In each case the shape of the potential energy vs orientation diagrams have been calculated from exact X-ray data on the shape of the clathrate cage. The small central potential well is neglected as being statistically unimportant. It is perhaps of interest to note that the 6-12 potential calculations give the best fit to dielectric data.

It is now clear that the present system might be used to test Hoffman's suggestions. If the observed dispersion is altered in such a way that further discrete relaxation regions appear during the systematic addition of PMO to PMS then it might be inferred that the inclusion of PMO in the PMS lattice changes the potential barriers to rotation of PMS in such a way that the emergence of further relaxation times becomes possible.

d x) Summary of 100% PMS Data

This section has been longer than anticipated. Before continuing then let us rapidly review the results so far considered and their implications.

a) The high temperature phase (labelled I in Figure 25) seems to obey Onsager's equation and hence presents itself as a "freely rotating phase". The absence of dielectric dispersion is, of course, a consequence of the limited frequency range used and further examination of this very promising region must be abandoned.

b) The second phase, (labelled II in Figure 25) yields dielectric dispersion data which has been represented by a symmetric arc. The principal

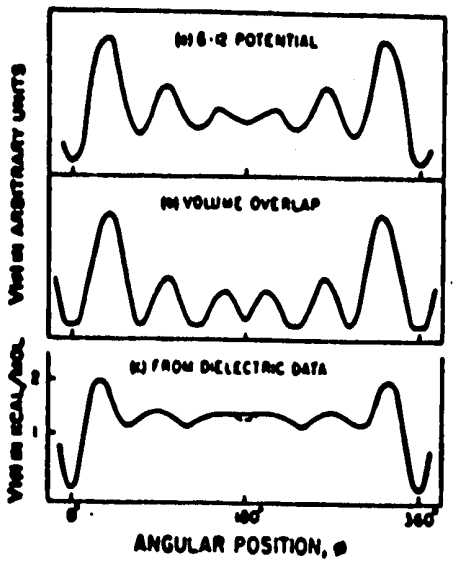

Potential energy as a function of angular position for 12-bromotricosane in urea.

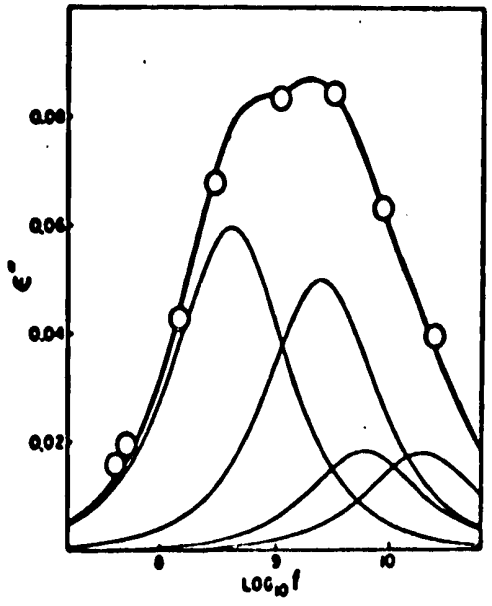

Experimental and calculated dielectric loss factor at 293° K for 12-bromotricosane in urea.
Circles represent values obtained by Meakins.
Light solid lines represent the four component Debye curves.
Heavy solid line represents the resultant dielectric loss factor.

Figure 47 [a]

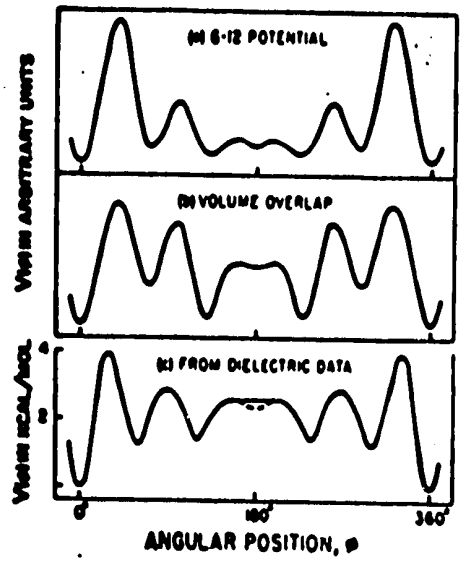

Potential energy as a function of angular position for 16-hentriacontanone in urea.

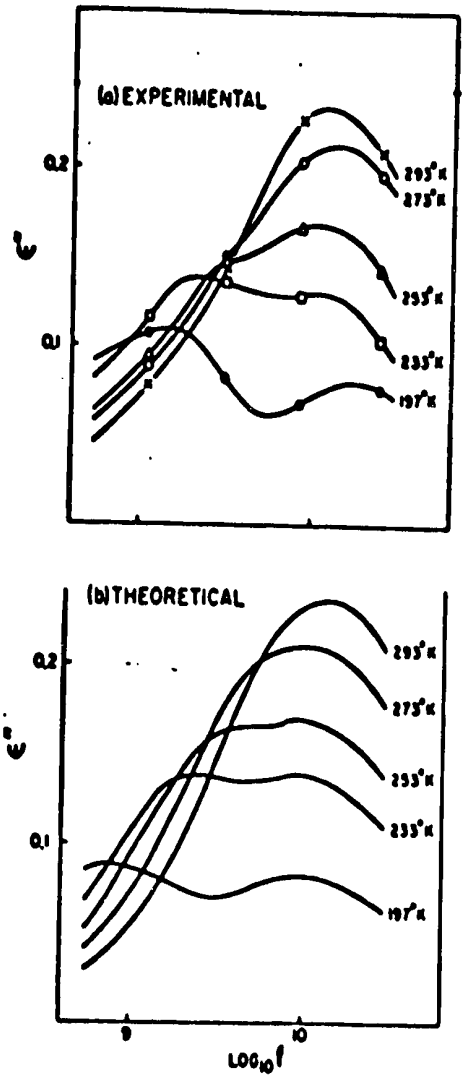

Comparison of experimental and theoretical dielectric loss factor of 16-hentriacontanone in urea at various temperatures. Experimental curves are those published by Meakins.

Figure 48[a]

relaxation time, yielded by this function, has been used to obtainthermodynamic data from this region. The implications of this data have been discussed.

c) Several models have been applied to this region. While this approach has been inconclusive, several lines of reasoning are suggested. First the Glarum and related models appear to be adequate as a skewed or symmetric arc function fits the data.

Second, Brot's discussion, together with Budo's approach suggest that unless sufficient data are available to suggest that the Cole-Cole or Cole-Davidson functions are unique then the relaxation time yielded by these functions may be of little physical significance.

Third, Hoffman's interpretation, being based on a crystalline model, seems best suited to our system. This model does, in fact, seem to be one which might be qualitatively verified by our results.

Fourth, it would seem wise to attempt to fit the observed dispersions with empirical functions of our own. Some effort will be made to do this.

KIII; 90% PMS

a) High Temperature Region*

In this region we confine ourselves to testing equation of Reynolds and Hough (61). The principal difficulty lies in obtaining a reasonable value for the dielectric constant of PMO which is liquid in this region. The equation was tested at $-33^{\circ}C$ using the measured value of ϵ_o for PMS and a value for PMO obtained by extrapolation of the value of ϵ_o for the solid to this temperature. We find using:

---

* i.e. Region marked I in Figure 25.

$$\epsilon_{PMO} \text{ at } -33^{\circ}C = 5.3$$

$$\epsilon_{PMS} \text{ at } -33^{\circ}C = 8.1$$

$$\epsilon_{calc.} = 7.8$$

$$\epsilon_{obs.} = 8.0$$

that the agreement is good but not perfect. But good agreement is to be expected since ϵ_{PMO} and ϵ_{PMS} are not very different. Further, the assumptions we make, though reasonable, are questionable* and sufficient flexibility remains to allow us to obtain equally good agreement at all concentrations studied. We must now acknowledge the fact that we shall not obtain any further information from this line of investigation and it will therefore be discontinued.

b i) 90% PMS Dispersion

As expected, the intermediate phase (marked II in Figure 25) at this concentration showed dielectric dispersion, the pertinent results being listed in Table XV below.

---

* We have assumed extropolation of PMO solid values to the desired temperature is valid, that our cell yields perfect results and the $x_1 f_1$ and $x_2 f_2$ of equation (83) are equal to the mole fractions of the respective components. If we had selected PMO (ϵ) equal to the highest true solid value, we would have obtained $\epsilon_{PMO} = 6.3$, $\epsilon_{PMS} = 8.1$ with $\epsilon_{calc} = 8.0$

TABLE XV

T(°C)	ϵ_∞	ϵ_0	(τ_0) (sec)	α	β
-72.2	4.223	7.947	0.4696×10^{-4}	0.3422	
-67.1	3.989	7.455	0.4472×10^{-4}		0.3845
-61.4	4.323	7.491	0.1518×10^{-4}		0.4400
-53.8	4.309	7.896	0.1261×10^{-5}	0.2280	
-49.2	4.957	8.420	0.7798×10^{-6}	0.1006	
-44.3	5.075	8.381	0.3008×10^{-6}	0.0977	

The dispersion curves obtained are shown in Figures 41 to 42. A plot of $\ln\tau_0$ vs $1/T$ is shown in Figure 43.

Note in Table XIV that the following expected trends occur:

1) The low temperature preference for a Cole-Davidson skewed arc plot is replaced at higher temperatures by a Cole-Cole symmetric arc plot. This appears to occur because as the relaxation time (or times) become shorter they move out of our frequency range and hence the single relaxation we can observe becomes dominant. Simply stated, at higher temperatures there is no need to favor higher frequency data (as does the Cole-Davidson function) in order to fit the measured data.

2) The values of the distribution parameters approach Debye behavior (i.e. $\alpha \to 0$, $\beta \to 1$). Such an effect would be predicted by Hoffman as the relaxation times would tend to converge at higher temperatues.

Table X V shows another curious effect: both ϵ_0 and ϵ_∞ appear to increase with increasing temperature. This is in contrast to the expected result, since the density is decreasing; further, it is not consistent with the observed trend in our 100% sample. Two explanations are now offered:

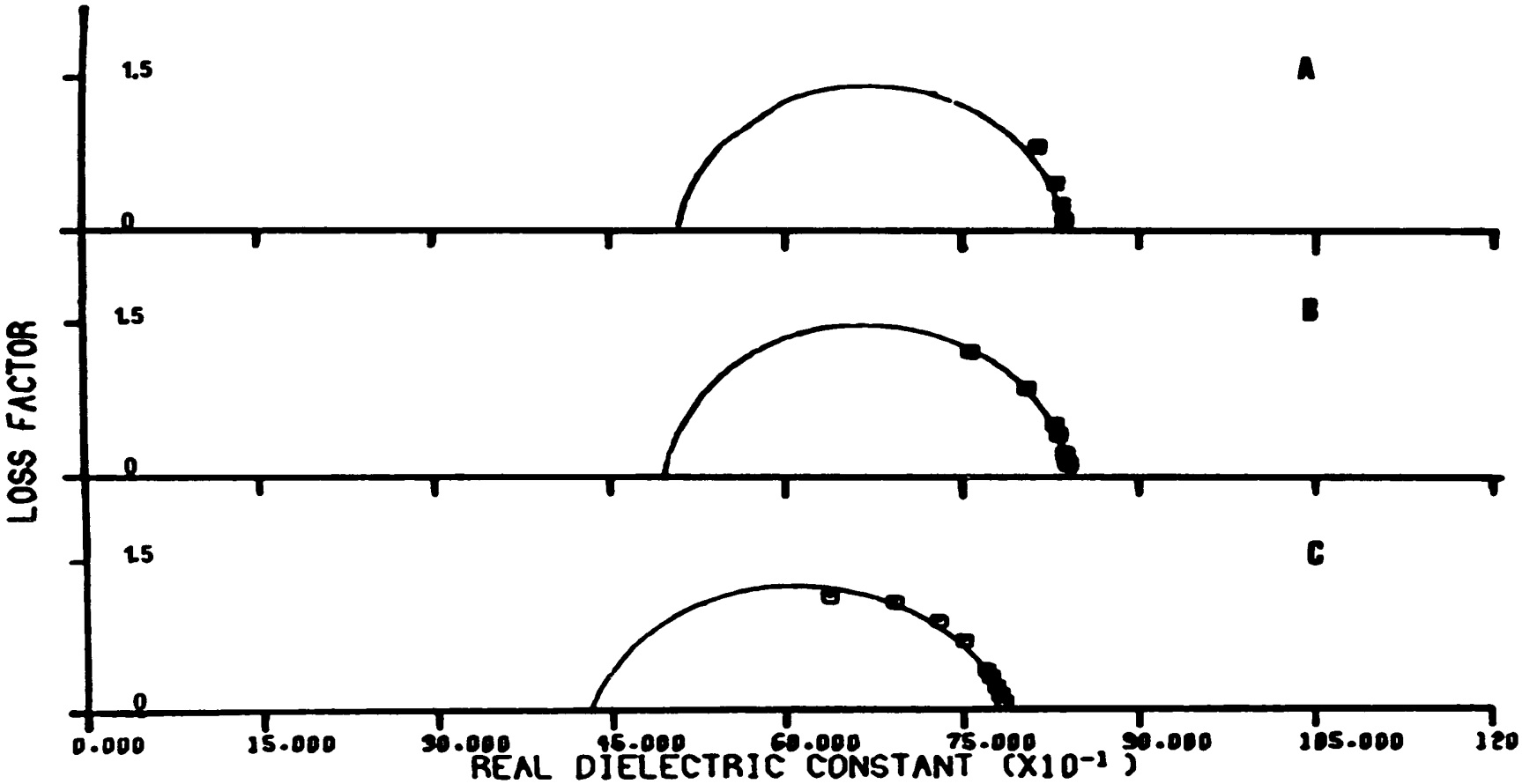

FIGURE 41

90% PMS A = -44.3°C B = -49.2°C C = -53.8°C

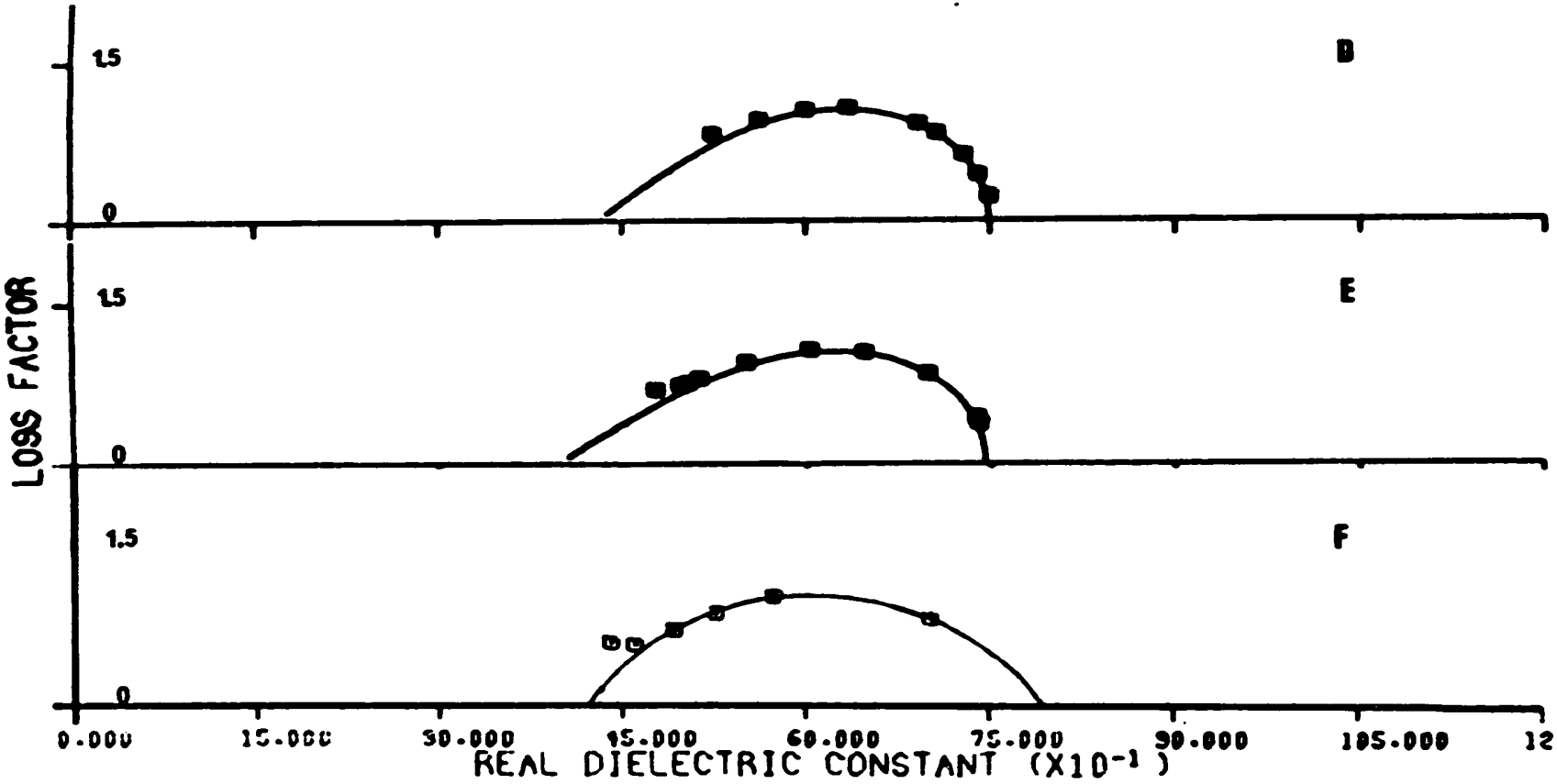

FIGURE 42

90% PMS D = -61.4°C E = -67.1°C F = -72.2°C

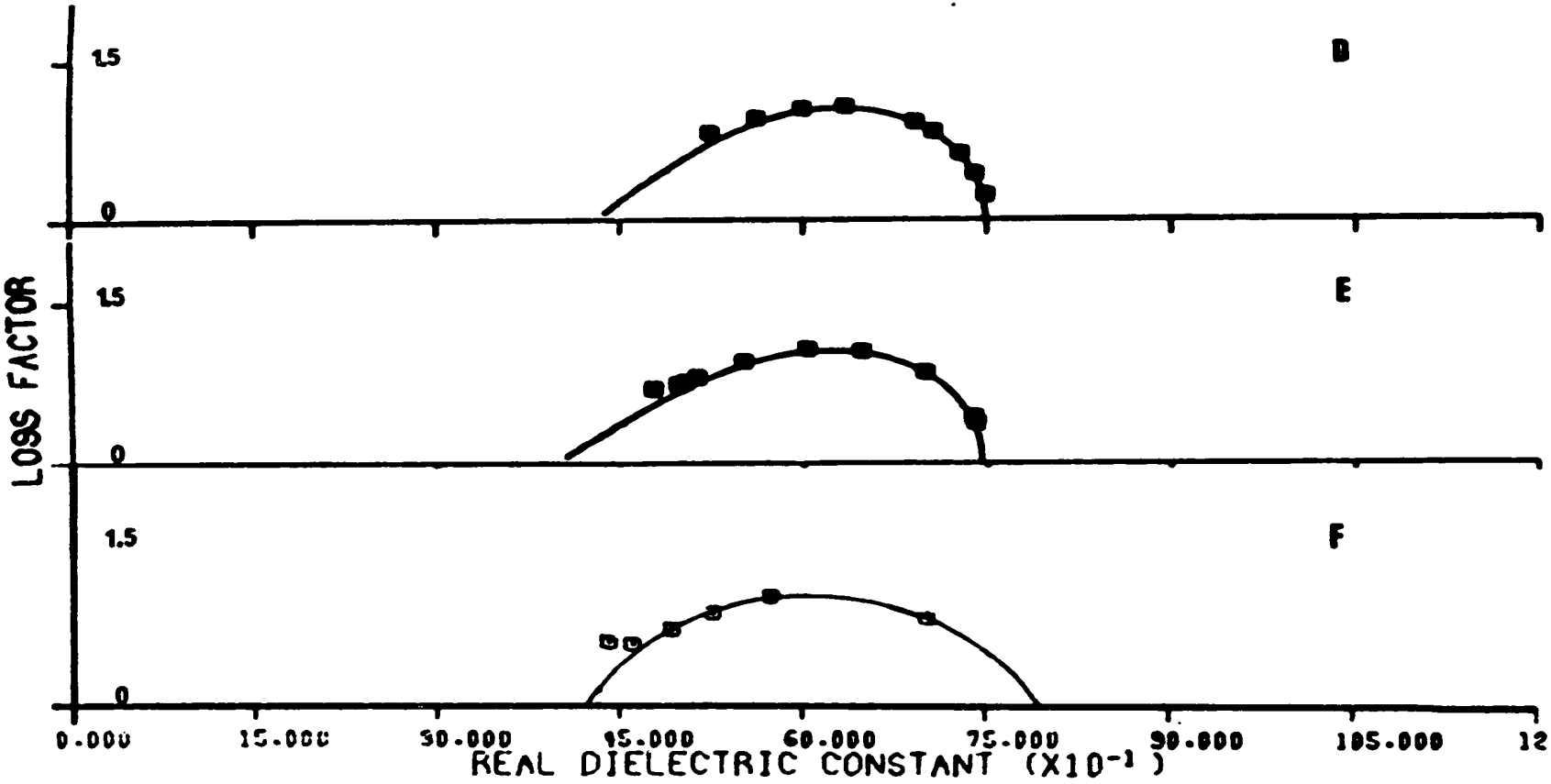

FIGURE 42

90% PMS D = -61.4°C E = -67.1°C F = -72.2°C

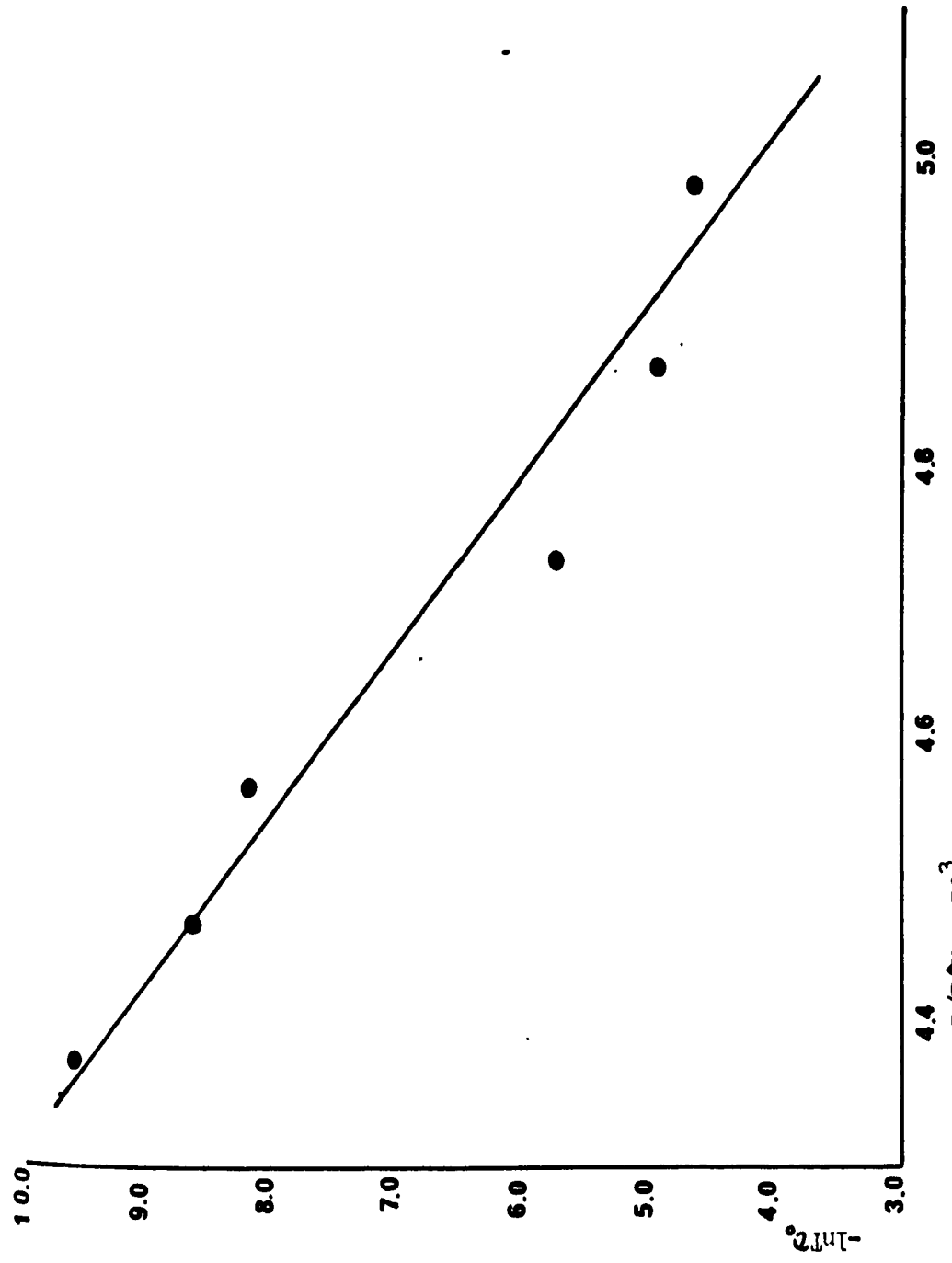

Figure 43

First the compressibility of the sample is lower and therefore the modest pressure in our cell is not yielding the desired result. Second, the bi-modal nature of the true distribution is adversely affecting the ability of our two functions to yield a meaningful fit. Both these conclusions will be seen to be supported by our subsequent work.

b ii) 90% PMS Thermodynamic Data.*

An analysis of the relaxation times such as that used on 100% PMS yields the following results: $\Delta H^{\ddagger}$ = 17.8 Kcal/mole, $\Delta S^{\ddagger}$= 50 e.u.

One is sorely tempted to draw immediate conclusions from these values. They are in qualitative agreement with the 100% PMS data but yield $\Delta H^{\ddagger}$ somewhat higher. It would seem logical to suggest that the presence of PMO has increased the barrier height to rotation. This conclusion is not however consistent with the observed lowering of the temperature at which rotation ceases.

In the previous section much was made of the fact that when multiple relaxation processes occur ambiguity must arise concerning the true value of τ_o. Examination of figures 41 to 42 will show that our dispersion is almost certainly bimodal - a fact which our computer programs must ignore. Further deviations from the Cole-Cole symmetric arc are slight and can readily be accomodated. When the Cole-Cole arc fails the minor adjustments required to fit the data points are seen to arise if a Cole-Davidson function is used. Thus the Cole-Cole and Cole-Davidson functions, while fitting the data to the required degree of exactness (± 2%) do not represent the real situation. Hence the τ_o values we have used to obtain thermodynamic data cannot be viewed with confidence and further discussion of these results is deemed to be unwise.

---

* See figure 43.

b iii) 90% PMS, Theoretical Examination of Dispersion

We have already advanced a number of theories which are capable of explaining symmetric arc and skewed arc behavior. These theories could not be readily verified by our 100% data and appear to contain inaccessible terms (note Glarum's model with its diffusion coefficients) for which a wide range of values may be selected. Great stress must now be laid on the evident bimodal nature of our distributions which would require rigorous separation before any of these theories might be meaningfully tested.

In the event there was reason to suspect that two distinct relaxation processes were at work such as independent relaxation of PMS and PMO, then resolution by Budo's methods may be attempted. There is no reason however to assume that this is the case, indeed the fact that a solid solution is formed and that the relaxation appears to be cooperative argue strongly against such a possibility.

One theory, however, seems to be capable of explaining our observations This is Hoffman's model. Introduction of a PMO molecule in the shell of nearest neighbors of a PMS molecule must alter the shape and number of energy barriers encountered by the PMS during rotation. It would be expected that the shape of the resulting dispersion curve must now become more complex. Since this is what we are in fact observing it is difficult to escape the conclusion that our results are beginning to supply a verification of this theory.

b iv) 90% PMS, Attempt at Fitting Observed Multiple Dispersions

Brot has shown that "classical analysis" of dispersion curves may often

be in error. It is also evident that Budo's method being classical in nature also ignores the possibility of co-operative effects. We have accordingly attempted to generate a set of highly generalized functions by combining the observed empirical relations of Cole and Cole and that derived by Cole and Davidson in the following way:

$$\epsilon' - \epsilon_\infty = \frac{C_1(\epsilon_o - \epsilon_\infty)\left[1 + (\omega\tau_1)^{(1-\alpha_1)} \sin \tfrac{1}{2}\alpha_1\pi\right]}{1 + 2(\omega\tau_1)^{(1-\alpha_1)} \sin \tfrac{1}{2}\alpha_1\pi + (\omega\tau_1)^{2(1-\alpha_1)}}$$

$$+ \frac{C_2(\epsilon_o - \epsilon_\infty)\left[1 + (\omega\tau_2)^{(1-\alpha_2)} \sin \tfrac{1}{2}\alpha_2\pi\right]}{1 + 2(\omega\tau_2)^{(1-\alpha_2)} \sin \tfrac{1}{2}\alpha_2\pi + (\omega\tau_2)^{2(1-\alpha_2)}} \qquad (118)$$

$$\epsilon' - \epsilon_\infty = \frac{C_1(\epsilon_o - \epsilon_\infty)\left[1 + (\omega\tau_1)^{(1-\alpha_1)} \sin \tfrac{1}{2}\alpha_1\pi\right]}{1 + 2(\omega\tau_1)^{(1-\alpha_1)} \sin \tfrac{1}{2}\alpha_1\pi + (\quad)^{2(1-\alpha_1)}}$$

$$+ C_2(\epsilon_o - \epsilon_\infty)\left[\left(\cos(\tan^{-1}\omega\tau_2)\right)^{\beta}\left(\cos\beta(\tan^{-1}\omega\tau_2)\right)\right] \qquad (119)$$

$$\epsilon' - \epsilon_\infty = C_1(\epsilon_o - \epsilon_\infty)\left[\left(\cos(\tan^{-1}\omega\tau_1)\right)^{\beta_1}\left(\cos\beta_1(\tan^{-1}\omega\tau_1)\right)\right]$$

$$+ C_2(\epsilon_o - \epsilon_\infty)\left[\left(\cos(\tan^{-1}\omega\tau_2)\right)^{\beta_2}\left(\cos\beta_2(\tan^{-1}\omega\tau_2)\right)\right] \qquad (120)$$

This approach can, of course, be criticized and strongly criticized. It has been said, with justification, that if a sufficient number of parameters are used in any equation, virtually any function might be approximated. We shall however apply these equations to our 90% PMS data and discuss the results.

We employed the same computer methods here as were used to fit the Cole-Cole and Cole-Davidson functions. This program was expanded to estimate six parameters. These six were chosen to be τ_1, τ_2, α_1, α_2 (or β_1, β_2 or α_1, β_2) C_1 and C_2. The restriction on C_1 and C_2 (i.e. $C_1 + C_2 = 1$) was relaxed. ϵ_∞ was set equal to the low temperature dielectric constant and was assumed to be 2.35. ϵ_o was set equal to the value obtained at the lowest frequency used.

The results, when applied to 90% PMS data yielded the following successful fits: For T = -67.1°C (fitted best by the sum of a Cole-Cole and a Cole-Davidson function)

$T_1 = 1.085 \times 10^{-2}$

$T_2 = 2.655 \times 10^{-5}$

$C_1 = 1.797$

$C_2 = .575$

$\alpha = .7228$

$\beta = .1871$

For T = -61.4°C (fitted best by the sum of two Cole-Cole functions)

$\tau_1 = 7.890 \times 10^{-2}$

$\tau_2 = 1.499 \times 10^{-6}$

$C_1 = .7741$

$C_2 = .9535$

$\alpha_1 = .7463$

$\alpha_2 = .4475$

For T = -49.2°C (best fit from the sum of two Cole-Cole functions)

$\tau_1 = 5.762 \times 10^{-6}$

$\tau_2 = 1.212 \times 10^{-19}$

$C_1 = .5604$

$C_2 = .8194$

$\alpha_1 = .8348$

$\alpha_2 = .9559$

It is very easy to attack this approach. Note, for instance, that in no case does $C_1 + C_2 = 1$. This latter condition is required if the low frequency limits of equations 118 to 120 are to be valid. Note further that it is difficult to supply a meaningful physical interpretation of the results and that even if this were not the case there is every reason to believe that the curves obtained in this way might be further reduced. Such obviously erroneous behavior is sufficient to preclude further use of these equations.

Before closing note however that at low temperatures the Cole-Davidson and Cole-Cole fits must be combined while at higher temperatures two Cole-Cole arcs supply a fit. Such

behavior is again consistent with Hoffman's theory which predicts that a distribution of barrier heights such as those he proposes will tend to converge with rising temperature. This would allow the antisymmetric Cole-Davidson plot to become a more symmetric Cole-Cole arc. Also $C_1 + C_2 = 1$ as T increases.

Further the fact that $C_1 + C_2 \neq 1$ would imply one or both of the following:

1) More than two relaxation times are present.

2) There is overlap of relaxation regions leading to behavior such as that predicted by Brot (i.e. some Ai in equation 86 may be negative).

The final blow (if one more is indeed necessary) is dealt to this approach by the severe experimental limitations which do not permit measurement beyond 100 KHz. This renders selection of ϵ_∞ difficult and one blithely assumes that no complications occur between the last measured value of ϵ' and the assumed value of ϵ_∞.

Regretfully then, it is concluded that this approach, in its present form is a waste of computer time.

K. (IV) 80% PMS

a i) High Temperature Region

Little can be said of this region except that it shows no evidence of phase separation.

K(IV) aii) 80% PMS Dispersion Data

The dispersion region yielded results plotted in Figures 44-46 together with the curve generated by the fitted parameters. These parameters were found to be:

Table XVI

T(°C)	τ_D(sec)	ϵ_o	ϵ_∞	α	β
-79.4	0.6575×10^{-3}	7.393	3.599		0.2245
-73.1	0.8418×10^{-4}	7.206	4.292		0.2973
-69.5	0.5203×10^{-4}	7.347	4.259		0.2983
-65.2	0.1486×10^{-4}	7.299	5.369		0.6646
-58.0	0.1548×10^{-5}	7.375	4.604	0.3026	
-50.2	0.5990×10^{-6}	7.214	4.910	0.1416	

We note at once:

1) There is no systematic variation of ϵ_o or ϵ_∞.

2) A low temperature preference for a Cole-Davidson function gives way to a higher temperature Cole-Cole arc, further $\beta \to 1$, and $\alpha \to 0$ as the temperature increases.

Reference to figures 44 to 45 will show that the first of these observations is due to the same factors mentioned in section K(III)bii and biii.

The second arises from one or both of the following causes:

First the points due to higher frequency processes gradually move far outside our frequency range, we thus find ourselves looking at the beginning of an isolated,

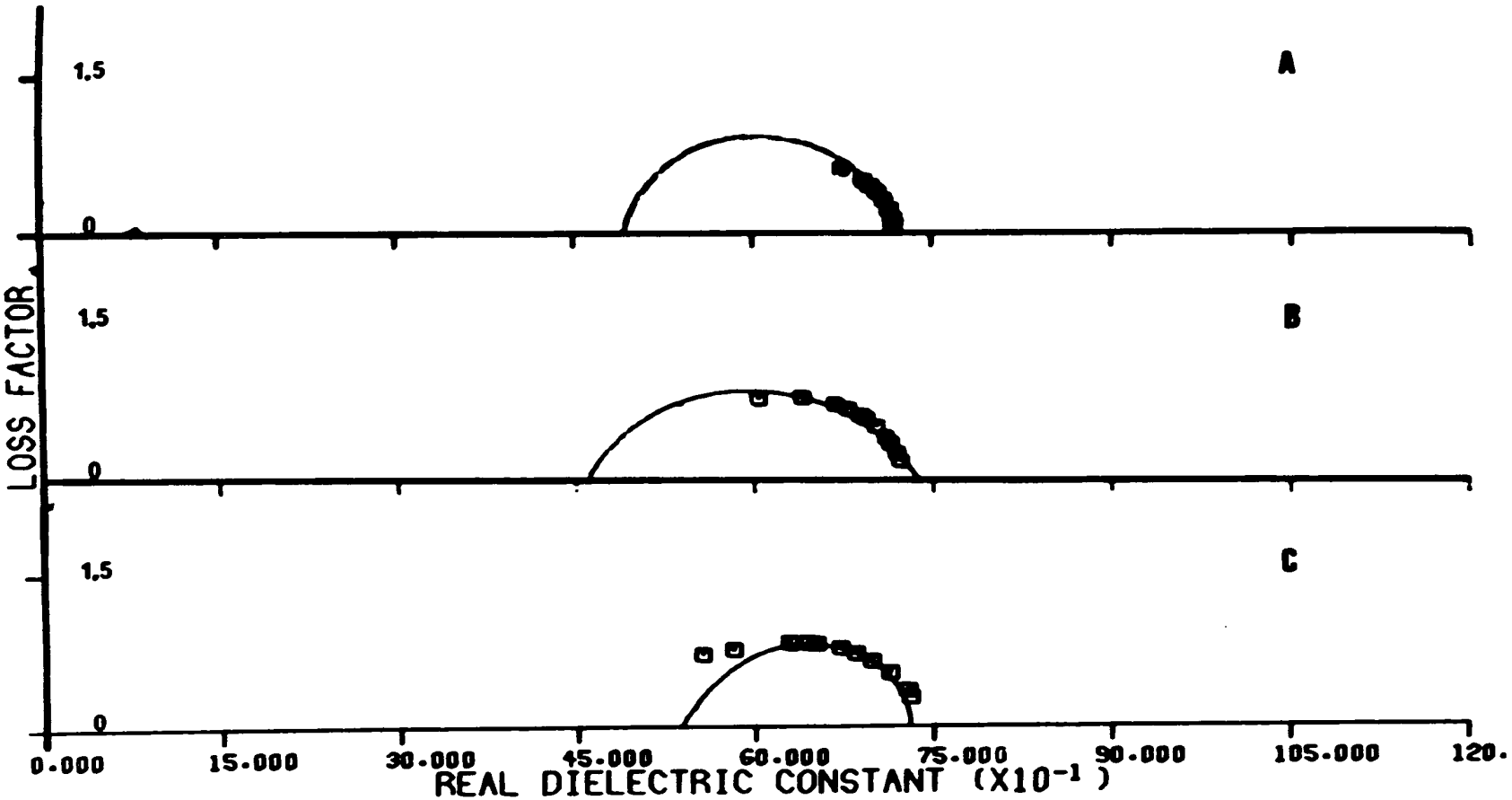

FIGURE 44

80% PMS A = -50.2°C B = -58.0°C C = -65.2°C

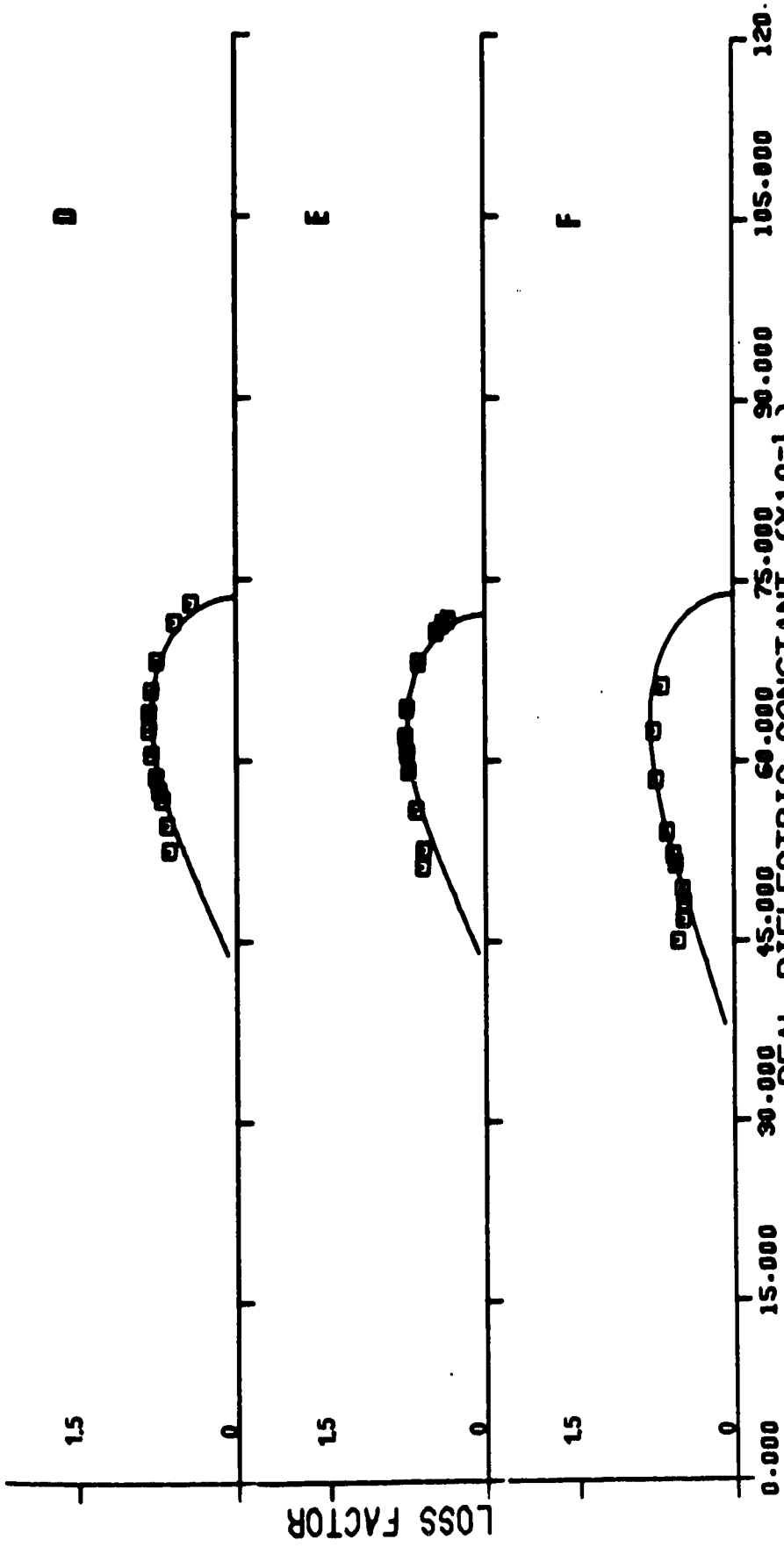

FIGURE 45

805 P:S D = -69.5°C E = -73.1°C F = -79.4°C

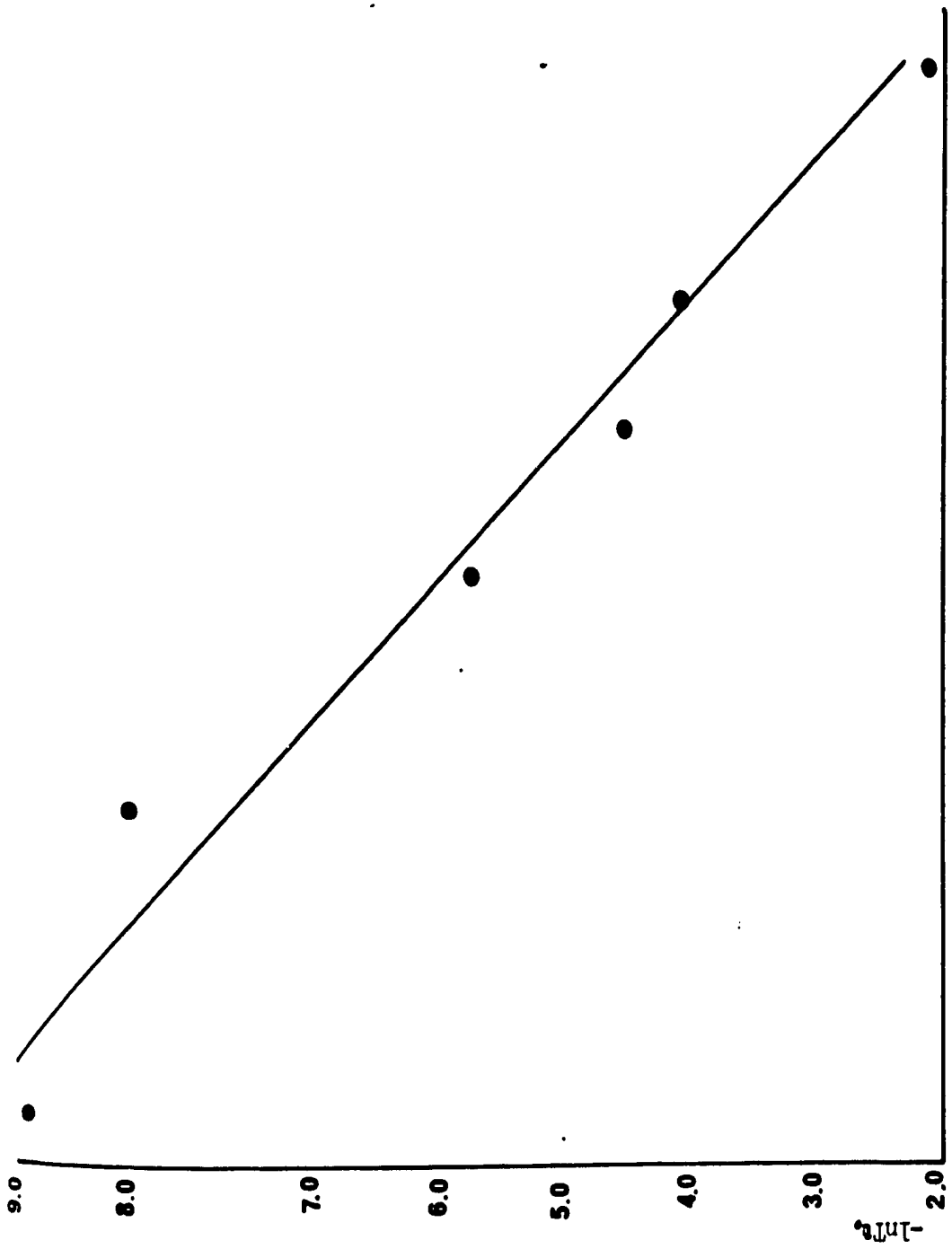

Figure 46

almost ideal region.

Second, at the risk of repetition, this effect would be expected from Hoffman's theory.

a iii) 80% PMS Thermodynamic Data

The evidence so far accumulated must lead to the strongest possible suspicion that neither the Cole-Cole nor the Cole-Davidson plots are capable of yielding reliable relaxation times for the data we are now observing. We shall continue to quote the results obtained (see Figure 46) from it but stress most strongly that its meaning is minimal. We do obtain for 80% PMS

$$\Delta H^{\ddagger} = 20.8 \text{ Kcal/mole}$$

$$\Delta S^{\ddagger} = 64 \text{ e.u./mole}$$

a iv) 80% PMS Theoretical Interpretation of Results

Reference to Figures 47^b to 48^b clearly shows that the dispersion region is becoming less and less well defined. We have suggested that this is due to the systematic alteration of barrier heights observed in Hoffman's single axis multi-position rotator model as the result of addition of PMO to the nearest neighbor shell of any given PMS rotator.

If we consider (for simplicity) that each PMS molecule is surrounded by ten nearest neighbors, then in 90% PMS we shall have introduced one new relaxation process. Moving to 80% PMS will not however yield two new processes since the random positioning of a second PMO in a nearest neighbor shell may now lead to more than one further relaxation. It

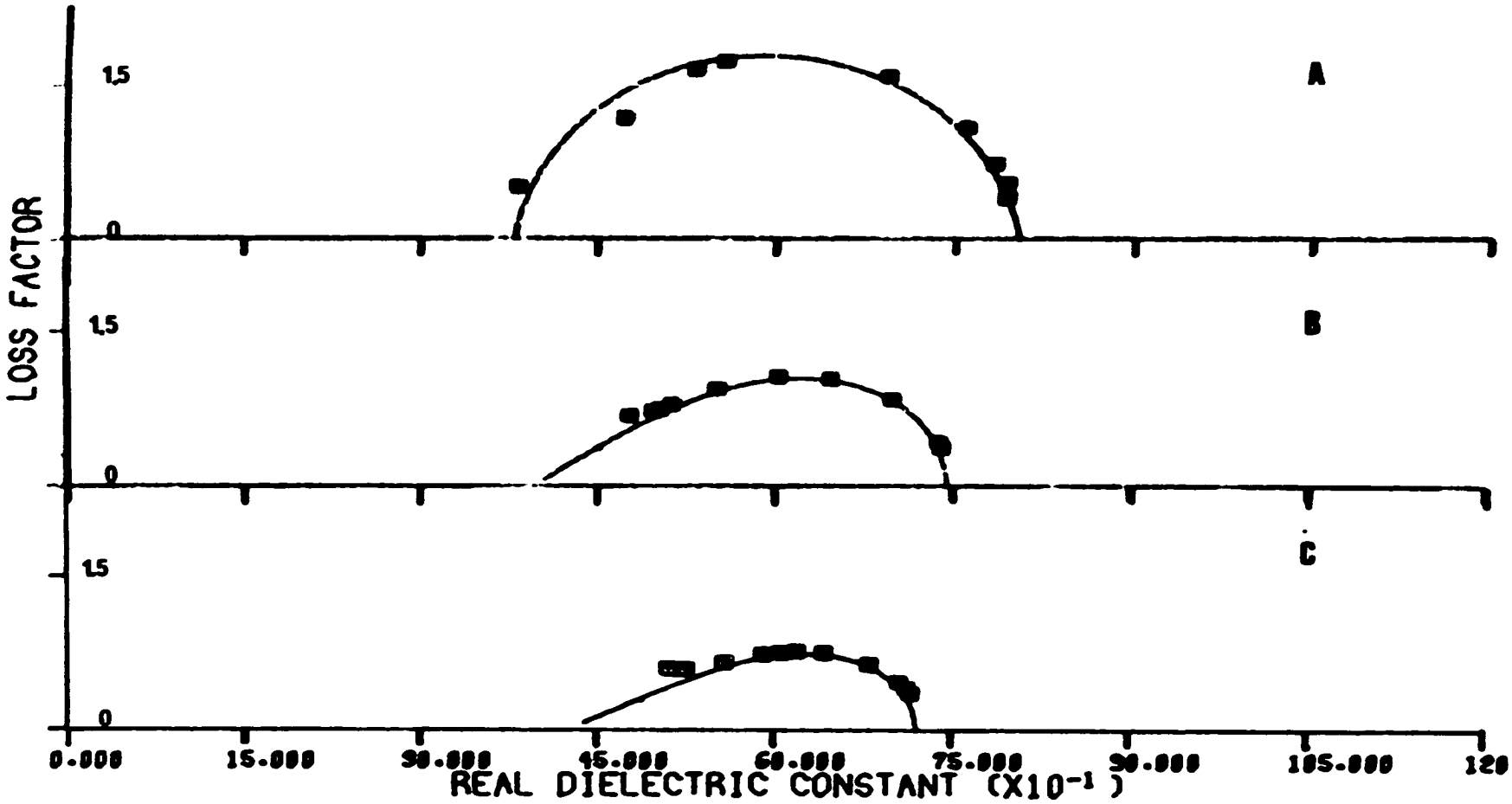

FIGURE 47[b]

A = 100% PMS −66.5°C B = 90% PMS −67.1°C C = 80% PMS −73.1°C

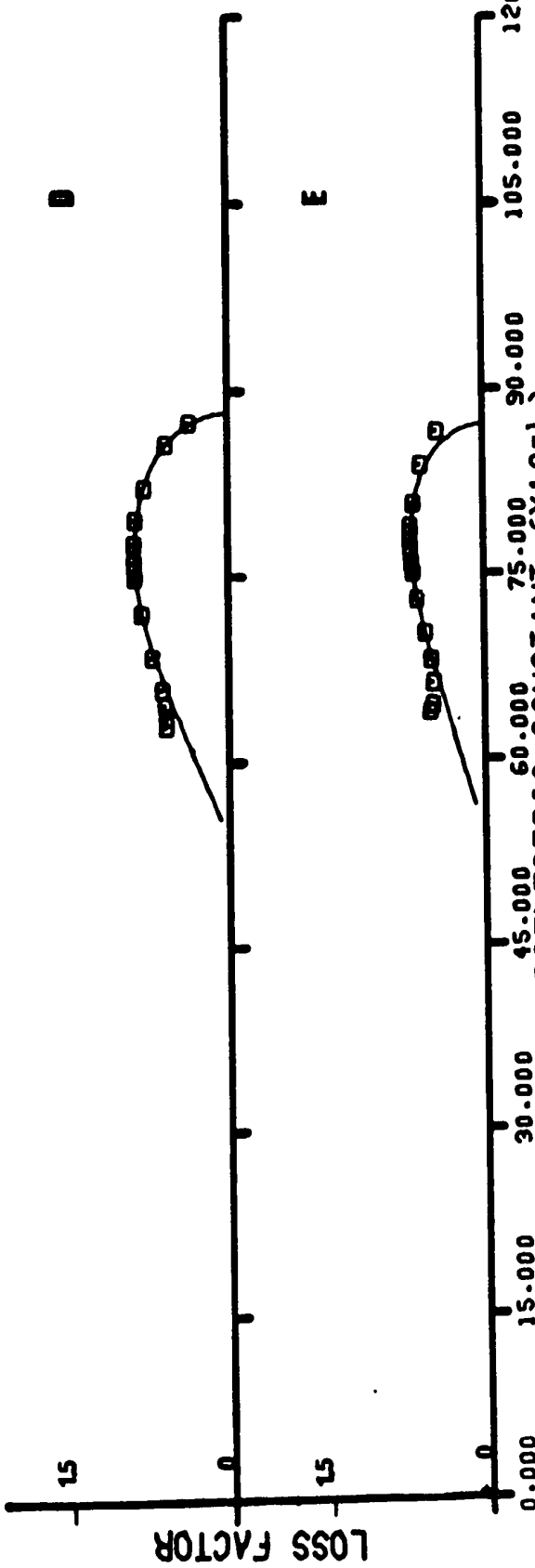

FIGURE 48[b]

D = 67.5% PMS -73.4°C E = 60% PMS -79.1°C

is reasonable to assume that two neighboring PMO molecules would have a different effect than two remote from each other, i.e. the arrangement:

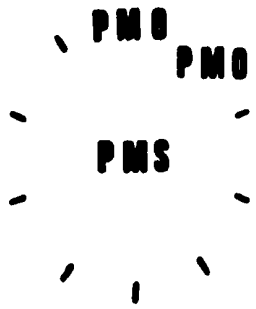

will yield a relaxation spectrum different from

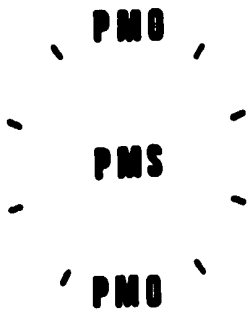

Both will occur with approximately the same probability as will the other possible arrangements. We should then observe further deterioration* of any discrete dispersions with increasing PMO concentration. This is in fact observed and in order to illustrate this the reader is referred to figures 47[b] to 48[b] which show this effect in the concentration range 100% PMS to 60% PMS.

---

* By deterioration of the dispersion we mean the increasing inability of the symmetric or skewed arc to fit the dispersion in a meaningful way.

a v) 80% PMS Further Attempts to Fit Dispersion

In view of the conclusions of a iii, our limited frequency range and our failure to obtain really meaningful data from equations 118 to 120, these attempts have been abandoned.

K(v) 70%, 67.5% and 50% PMS Dispersion Region

The dispersion data is presented below and in Figures 49 to 54. Thermodynamic data are quoted without further comment since τ_o is no longer regarded as being meaningful. It is interesting to note however that plots of $\ln T\tau_o$ vs $1/T$ (see Figures 55 to 57) remain reasonably linear. One concludes that some sort of average τ_c is generated by our approach.

TABLE XVII

70% PMS $\Delta H^* = 18.5$ Kcal $\Delta S^* = 52.$ e.u./mole

T(°C)	τ_o(sec)	ϵ_o	ϵ_∞	α	β
-79.2	0.5409×10^{-3}	8.455	4.720		0.2943
-74.9	0.1590×10^{-3}	8.528	5.183	0.3466	
-70.5	0.6515×10^{-4}	8.557	5.331		0.3275
-67.2	0.1256×10^{-4}	8.662	6.235	0.2347	
-60.5	0.2252×10^{-5}	8.525	4.666	0.1442	
-55.3	0.1327×10^{-5}	8.437	6.770	0.2667	

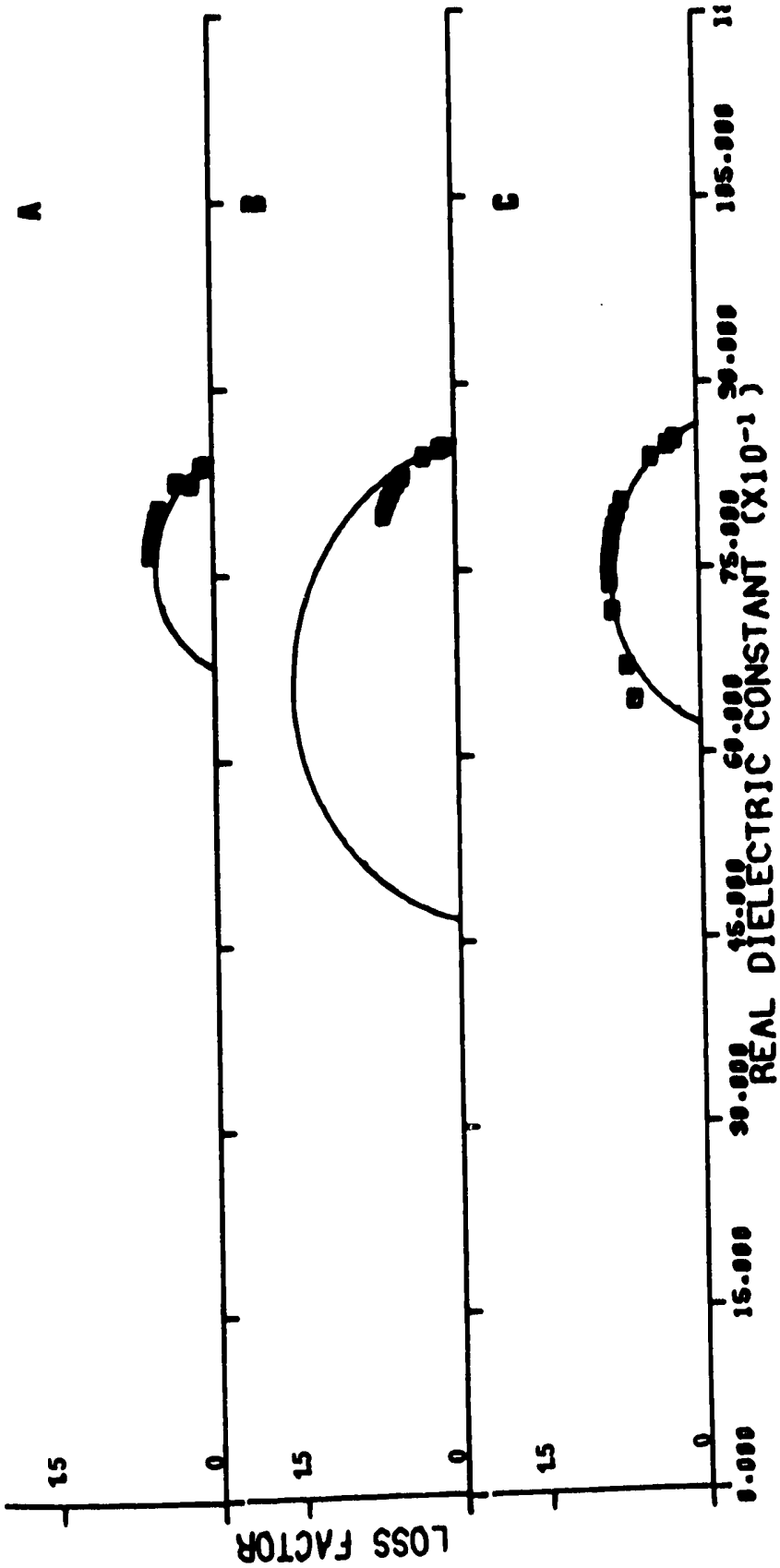

FIGURE 49

70% PMS A = -55.3°C B = -60.5°C C = -67.3°C

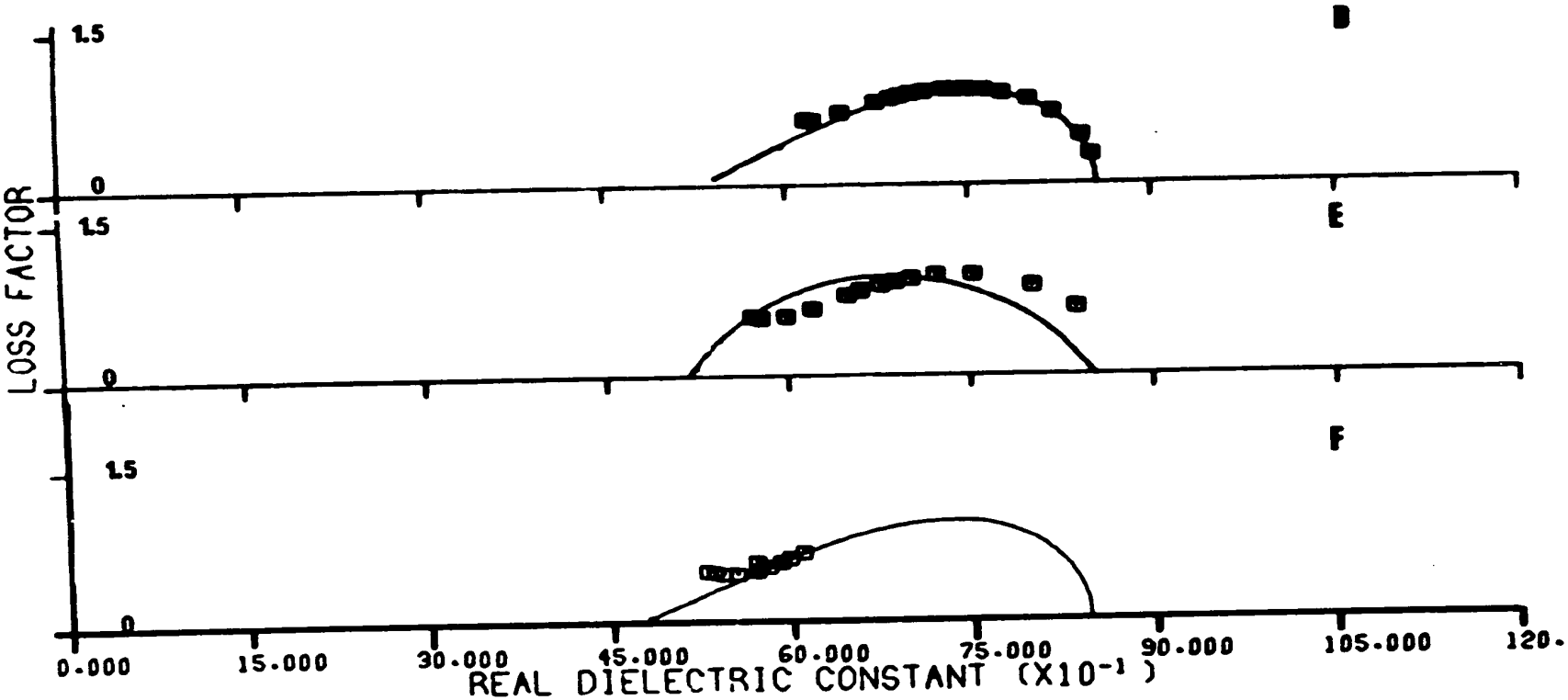

FIGURE 50

70% PMS D = -70.5°C E = -74.9°C F = -79.2°C

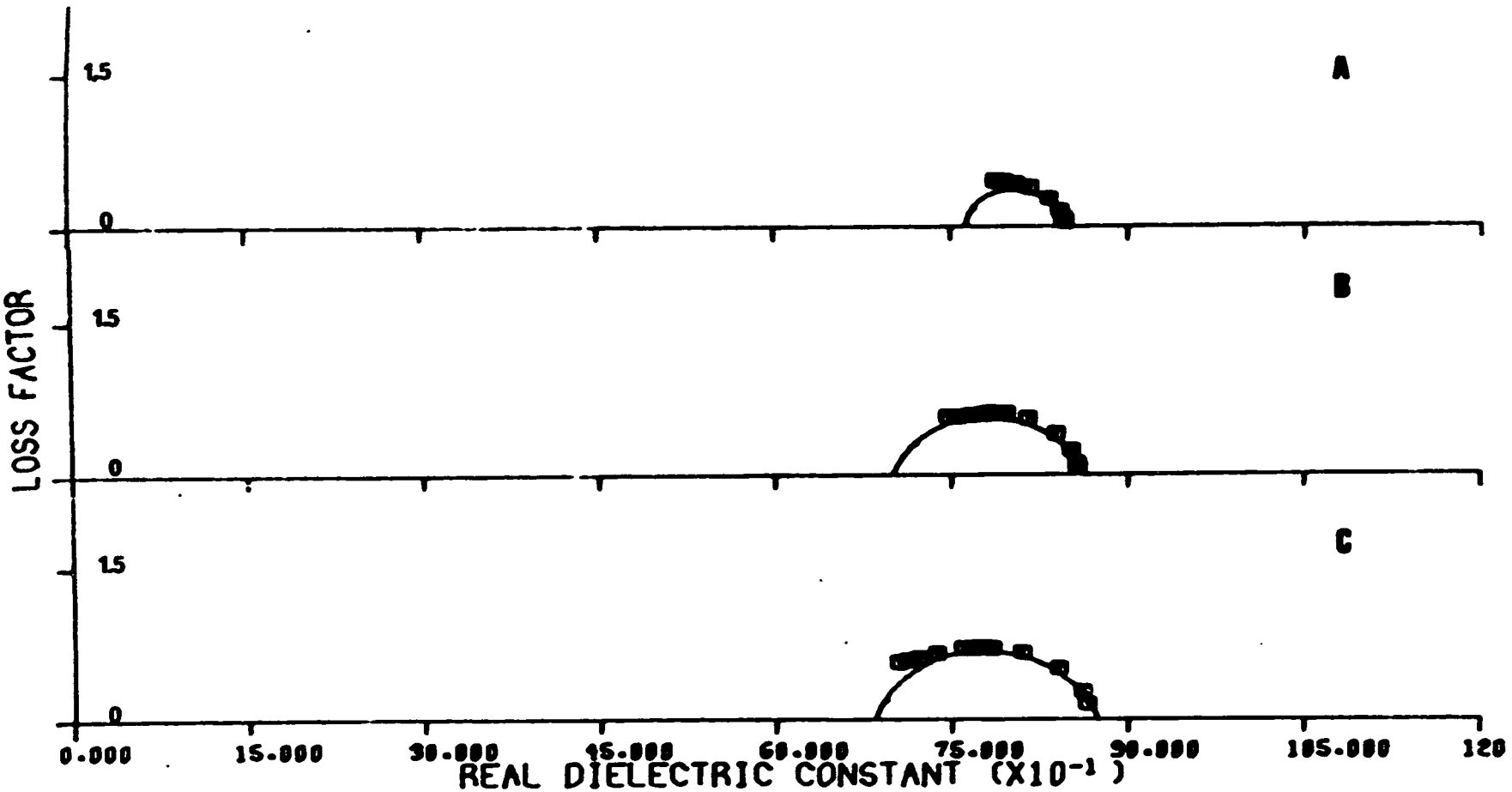

FIGURE 51

67.5% PMS A = -56.3°C B = -61.2°C C = -66.2°C

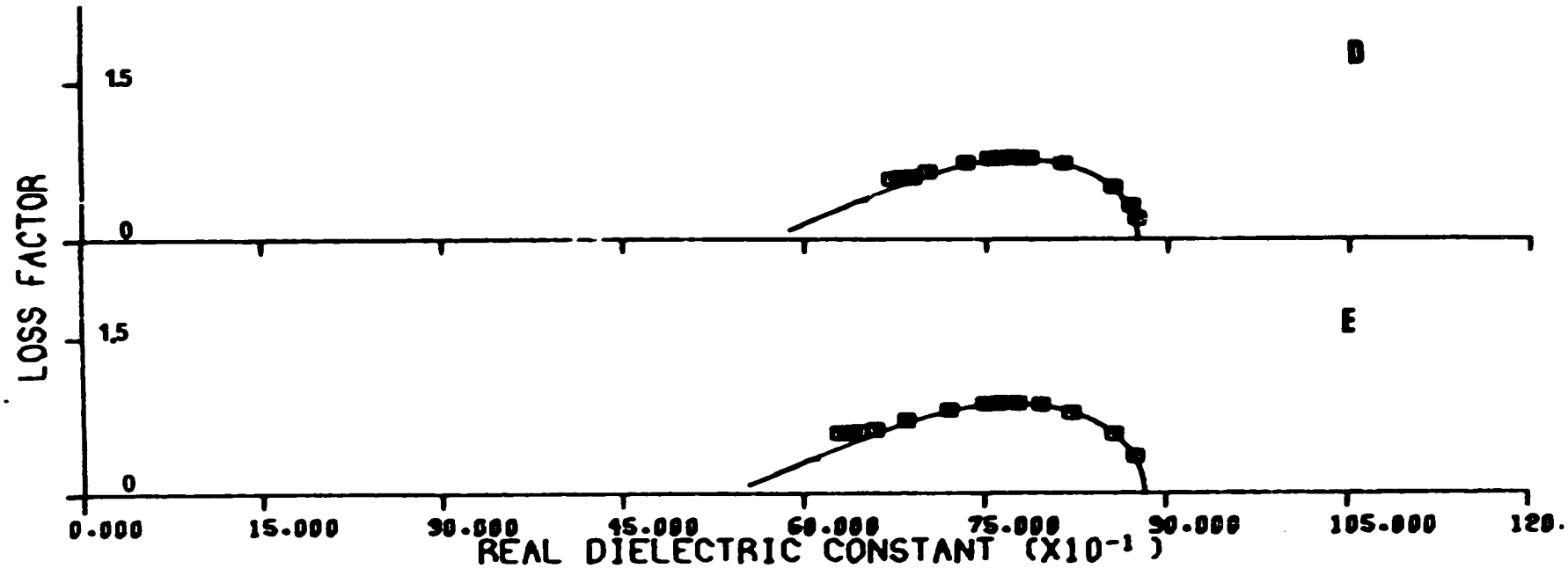

FIGURE 52

67.5% PUS D = -69.5°C E = -73.4°C

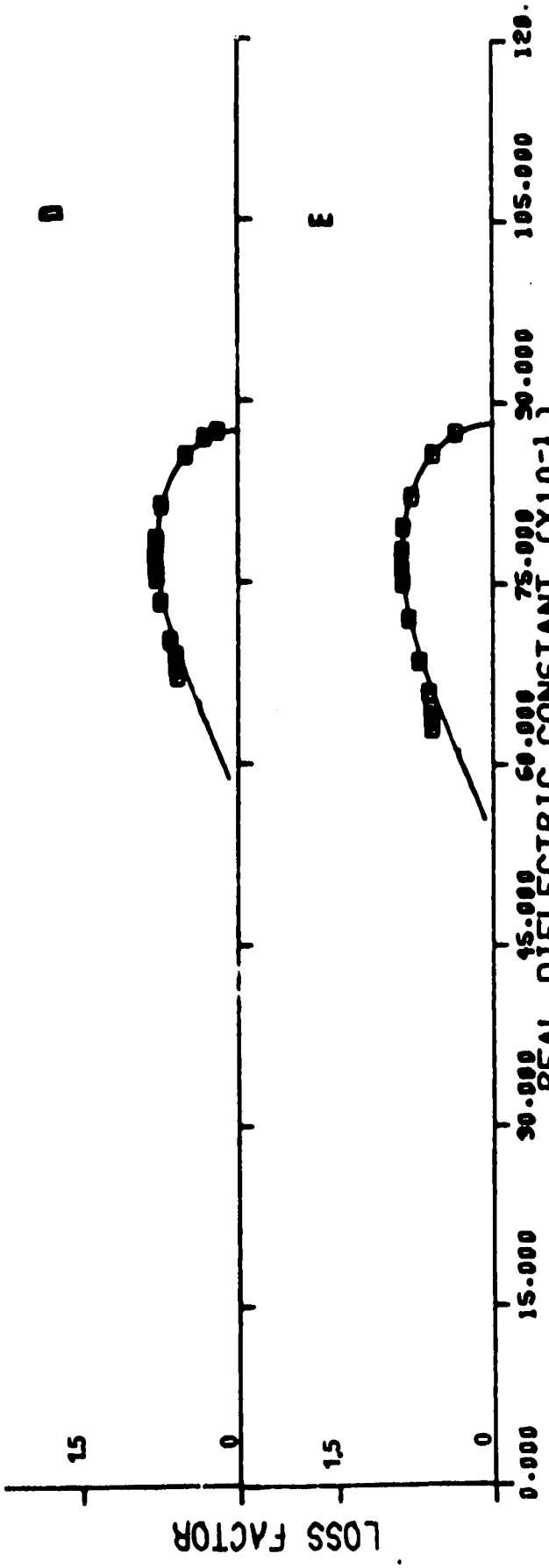

FIGURE 52

87.5% PVS D = -69.5°C E = -73.4°C

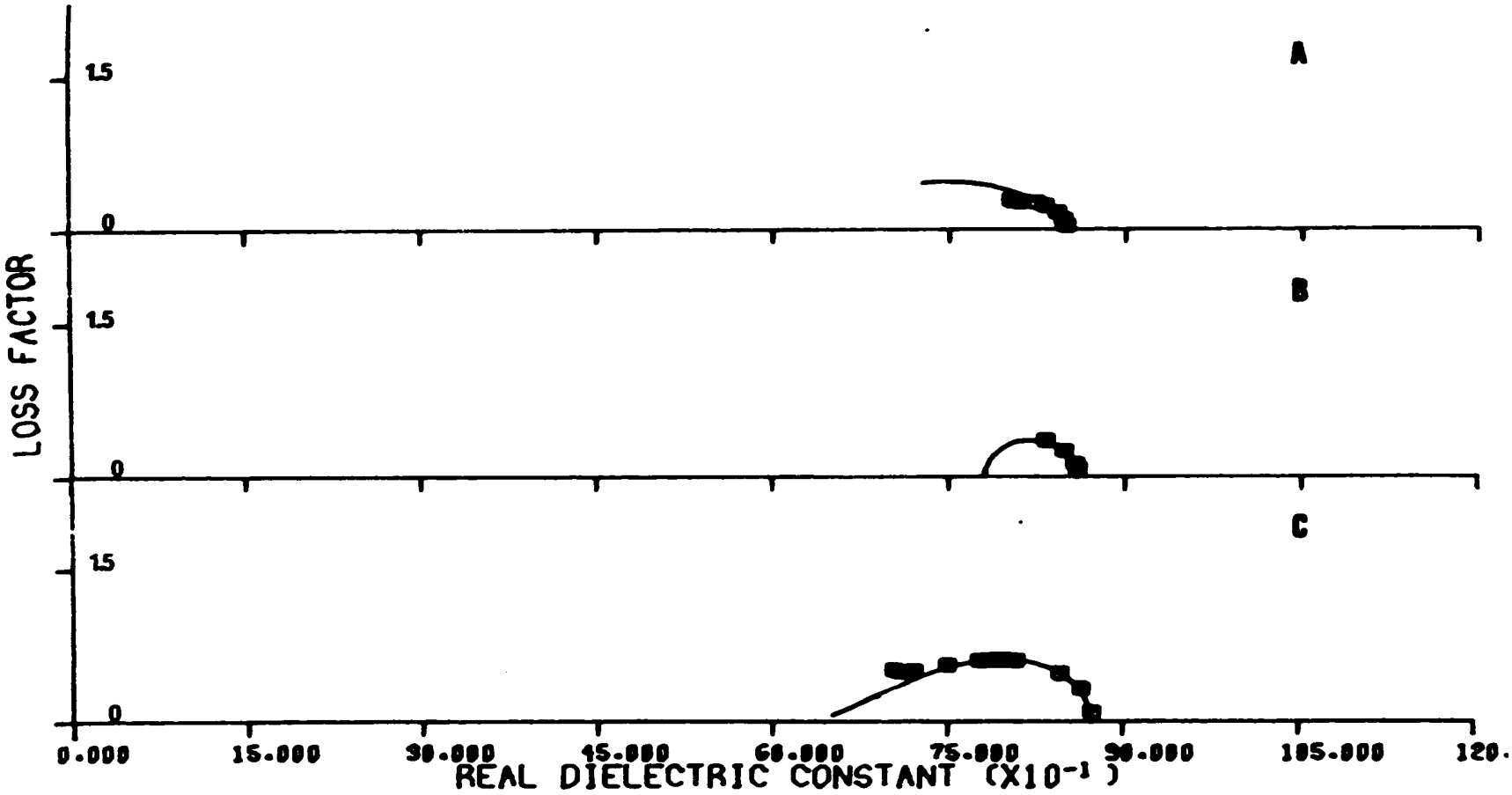

FIGURE 53

60% PMS A = -59.5°C B = -65.7°C C = -72.2°C

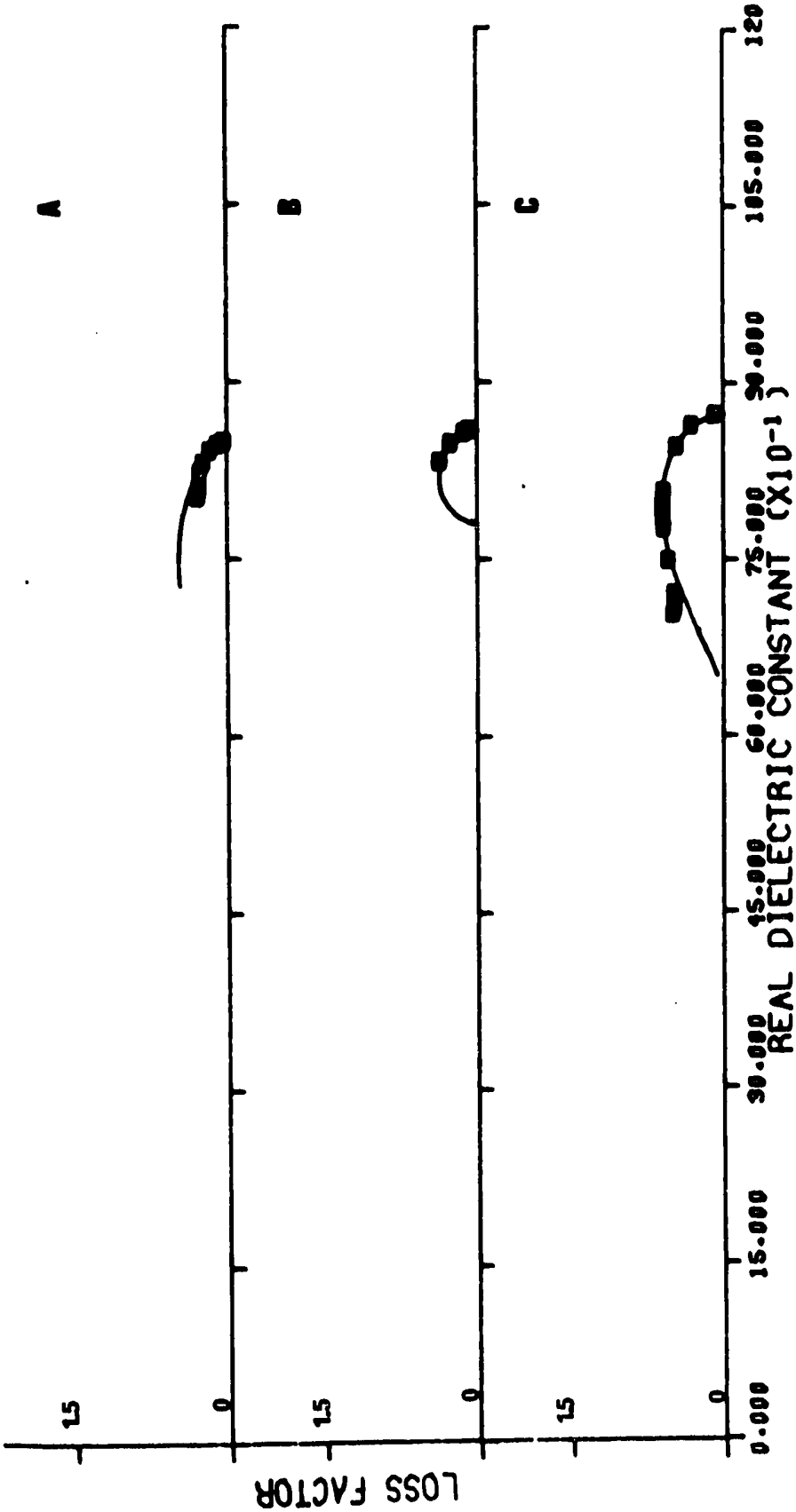

FIGURE 53

60% PBS A = -59.5°C B = -65.7°C C = -72.2°C

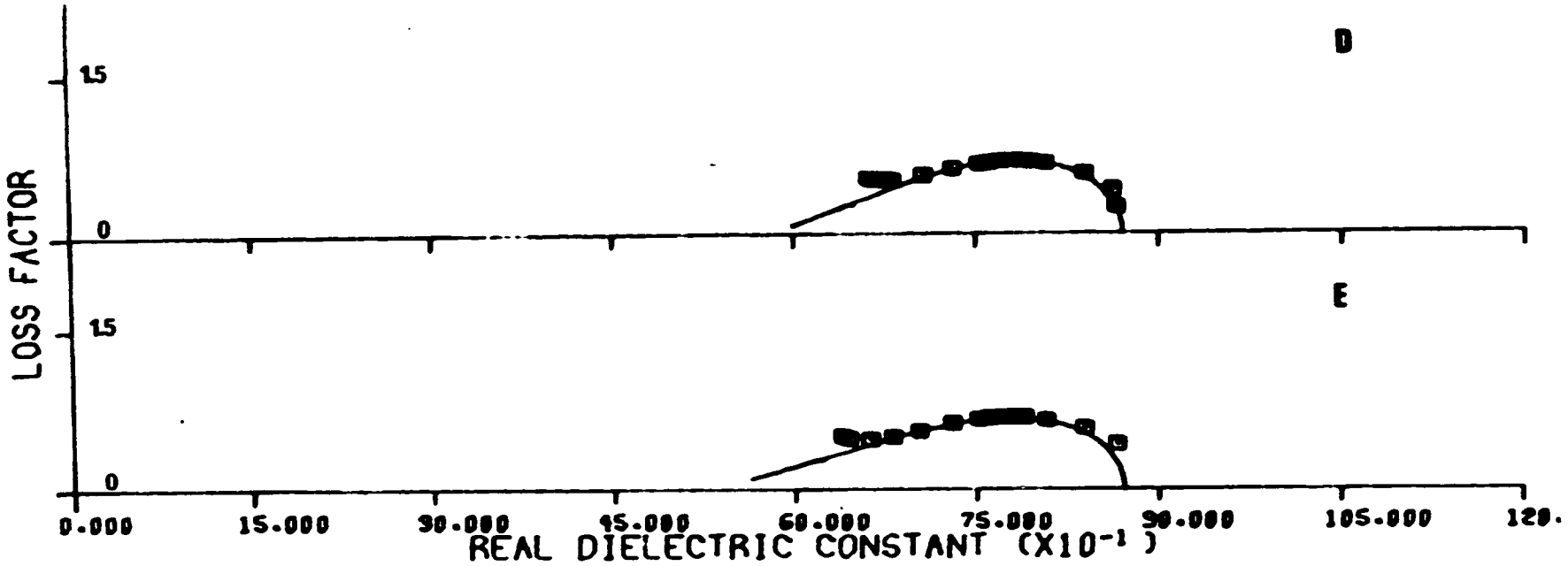

FIGURE 14.

LOT PHS D = -78.8°C E = -79.1°C

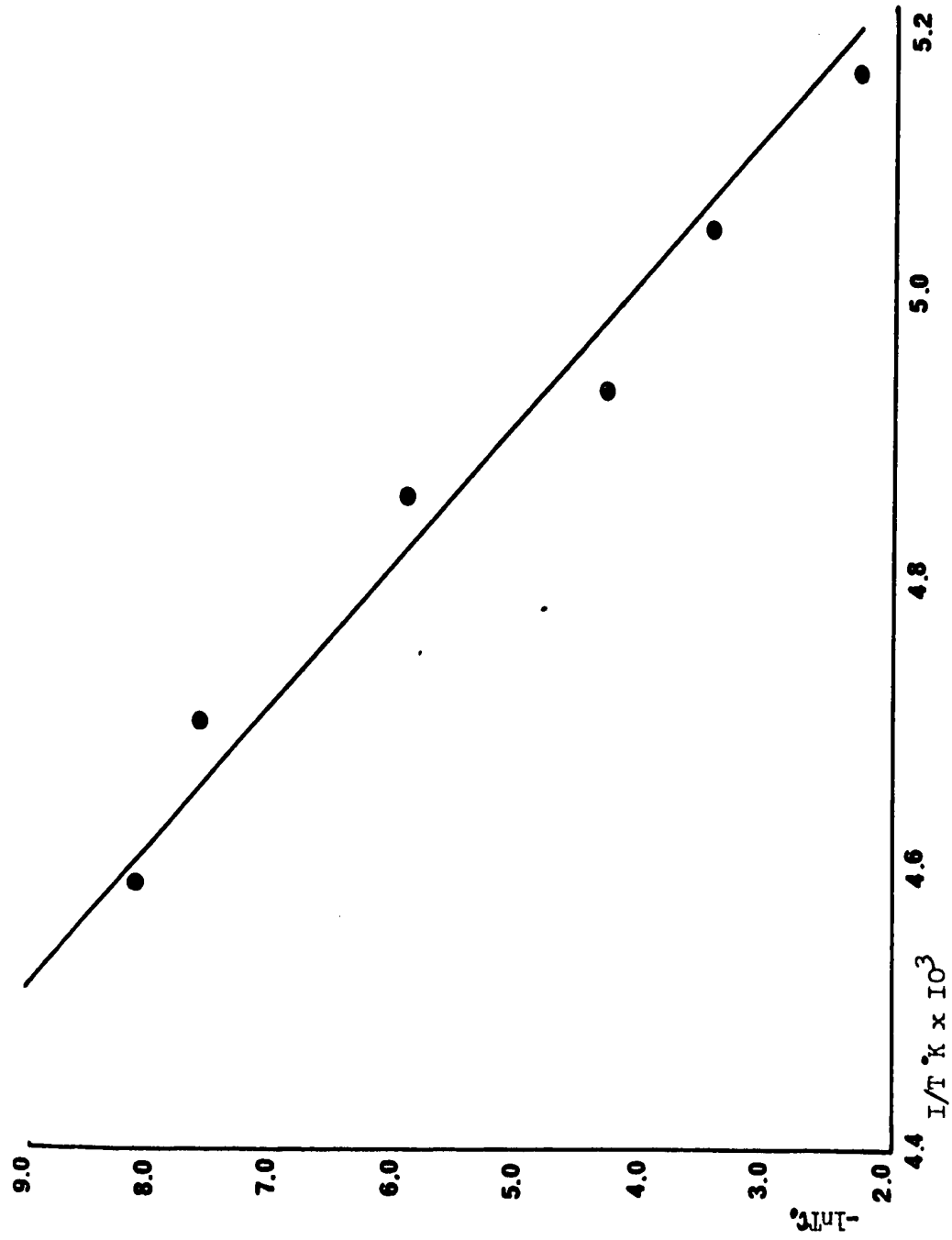

Figure 55

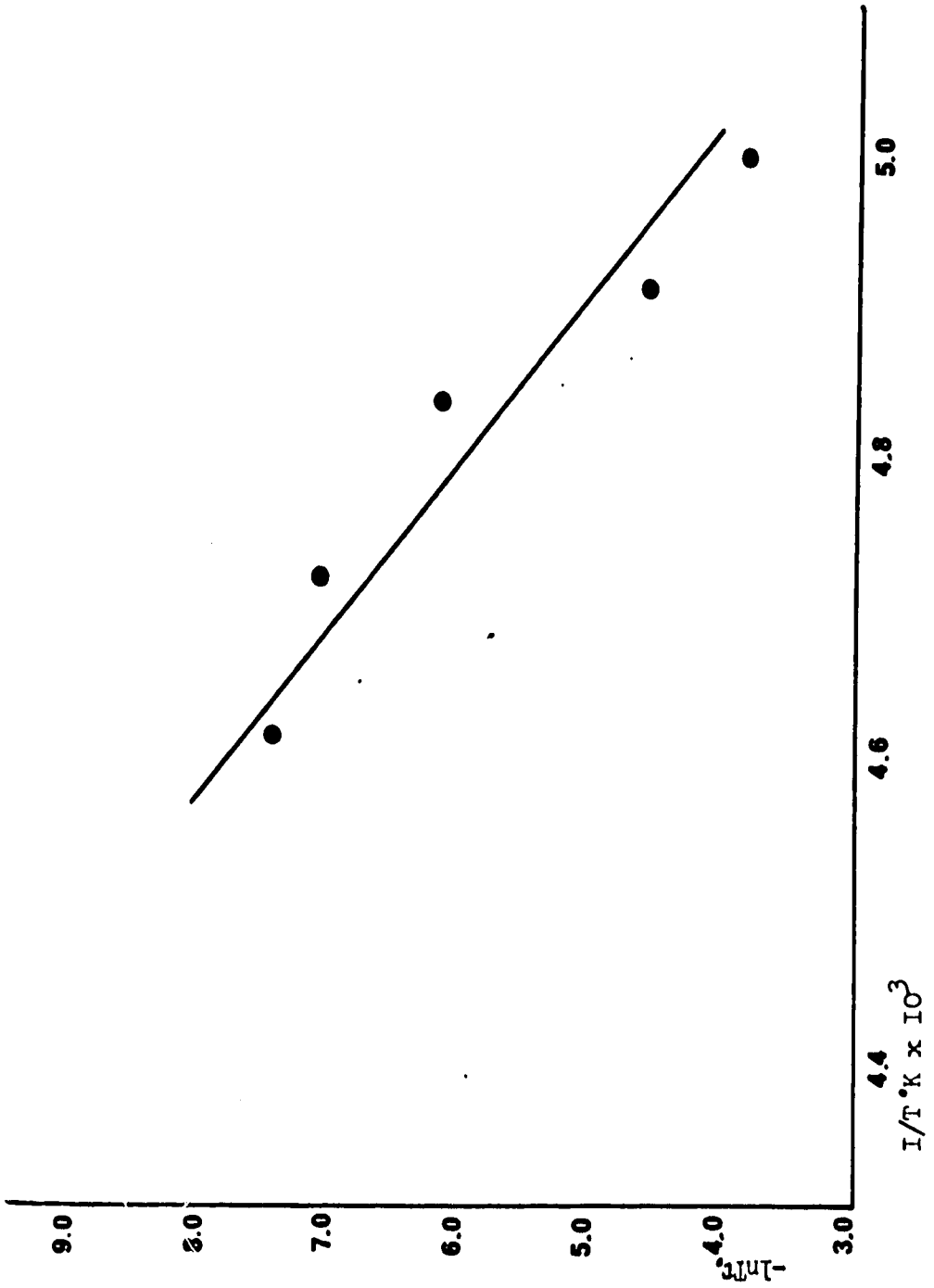

Figure 56

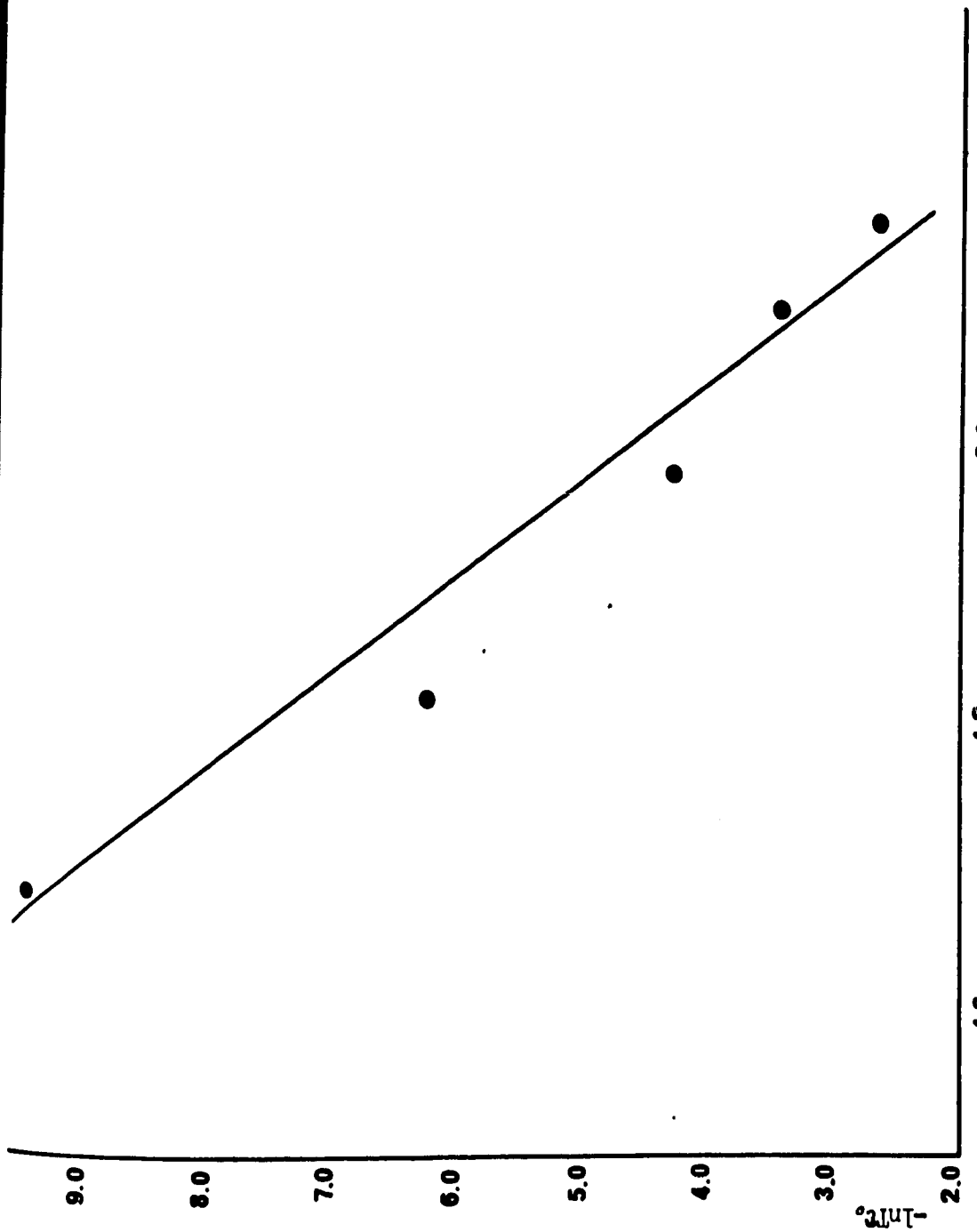

Figure 57

TABLE XVIII

67.5% PMS $\Delta H^{\ddagger}$ = 19.5 Kcal/mole $\Delta S^{\ddagger}$ = 58 e.u./mole

T(°C)	τ_o(sec)	ϵ_o	ϵ_∞	α	β
-73.4	0.10604×10^{-3}	8.820	5.414		0.2900
-69.5	0.5089×10^{-4}	8.748	5.731		0.2907
-66.2	0.9083×10^{-5}	8.746	6.847	0.2054	
-61.2	0.3720×10^{-5}	8.637	7.003	0.2317	
-56.3	0.2648×10^{-5}	8.469	7.628	0.0852	

TABLE XIX

60% PMS $\Delta H^{\ddagger}$ = 27.8 Kcal/mole $\Delta S^{\ddagger}$ = 100 e.u./mole

T (°C)	τ_o (sec)	ϵ_o	ϵ_∞	α	β
-79.1	0.3566×10^{-3}	8.715	5.386		0.2098
-76.8	0.1579×10^{-3}	8.702	5.854		0.2602
-72.2	0.6686×10^{-4}	8.729	6.438		0.3149
-65.7	0.9108×10^{-5}	9.108	8.557		0.4991
-59.9	0.3326×10^{-6}	8.564	6.456	0.4620	

Perhaps the first point to be noted here is the agreement between the 70% PMS results and the 67.5% PMS. This observation is gratifying because it lends confidence to our experimental data.

The second point of interest is the very high value obtained for ϵ_∞. Clearly it is unrealistic. It is possible, but unlikely, that the function is now fitting a small low frequency dispersion. If we accept that this interpretation is incorrect we are led to the conclusion that our initial function has

failed. Since this march to failure was predicted after studying the 90% PMS and 100% PMS dispersion regions, we can only call this failure satisfying.

Reference to figures 47 to 48 will show that the shape of the experimental curve is deteriorating. This is the reason for the gradual ascendence of the Cole-Davidson plot over the Cole-Cole representation.

We have already drawn attention to the linearity of a plot of $\ln T\tau_s$ vs 1/T. This appears to be the result of the ability of our two empirical equations to yield some sort "average" relaxation times. We have already shown that there is every reason to believe that this average does not yield physically meaningful data. Once more Hoffman's results yield a qualitative model which suits this system well.

Mention was made in the introduction to this work of the relation drawn between viscosity and the relaxation time by Debye. It is evident that an attempt to co-relate these properties is meaningless in our system.

K(VI) 50% PMS to 100% PMO A General Discussion

This region has already been discussed as that which lies furthest beyond the probing abilities of our instrumentation. The following observations wrung from a region of low temperature and dubious equilibrium have been made:

First, in 50% PMS a dispersion region is still visible. It is however weak and non-reproducible. This latter problem

has been growing with addition of PMO since 80% PMS. Note for instance that in 70% PMS the dispersion at -51.1°C is fitted by a Cole-Davidson function while the three temperatures below are Cole-Cole fits. Similarly in 60% PMS ϵ_o and ϵ_∞ at -65.7°C appear to be much in error.

Second, a tendency for values of ϵ' and ϵ'' to be abnormally high when a given temperature is first reached has been observed at all concentrations. The time required to reach equilibrium (after ϵ' and ϵ'' have declined from these high values) has become rather long in this region. A typical result is advanced here because it is most instructive.

40% PMS showed dispersion beginning at -139.5°C on warming from liquid nitrogen temperature thus:

T = -139.5°C

freq. (kHz)	ϵ'	ϵ''
100	5.102	.6122
80	5.202	.6097
60	5.301	.6089
40	5.445	.6141
20	5.680	.6121
10	5.943	.6229
5	6.202	.6288
1	6.884	.6092
0.5	7.177	.5659

T = -132.8

freq. (kHz)	ϵ'	ϵ''
100	6.529	.6714
80	6.616	.6665
60	6.740	.6582
40	6.877	.6386
20	7.142	.5660
10	7.376	.5227
5	7.606	.4755
1	8.038	.3714
0.5	8.190	.3262

These high values were suspicious and some drift was evident. The sample was stored overnight in dry ice and the next day the temperature was slowly lowered to -140°C and held for 3 hrs. Measurements of the dielectric constant were then made with the following results:

T = -140°C

freq. (kHz)	ϵ'	ϵ''
100	3.429	.1777
80	3.450	.1777
40	3.528	.1793
10	3.686	.1847
5	3.768	.1886
1	3.966	.1965
0.5	4.050	.1886

It is immediately evident that the first two series here do not represent an equilibrium situation. The following theory is advanced. Sherwood (48) has shown that the number of defects is a function of the thermal history of organic solids. Thus his diffusion rates were found to depend markedly on thermal history. Now if we assume, as did Glarum, that dipole orientation takes place more easily in the region near a defect and further assume that rapid cooling insures a high non-equilibrium defect concentration then the high values of ϵ' and ϵ'' may be blamed on high defect concentration. If we now further postulate that the fall with time of ϵ' and ϵ'' observed at constant temperature is due to the elimination of defects (possibly by diffusion) then we are able both to rationalize our results and support Glarum's model. We do not propose to develop this topic further but study of the rate of attainment of equilibrium in systems of this nature seems to have some promise.

Finally, for this total region (50% PMO - 100% PMO) no further conclusions other than those already mentioned in other parts of this work may be advanced.

CHAPTER IV

Conclusions

First, the physical tests to which the system was subjected show that a continuous series of liquid and solid solutions is formed by the two pure components. On the basis of studies of the solid solutions formed it is evident that, while complete characterization of the solid phases is impossible, three regions may be defined. These are: a high temperature region, an intermediate region and an ill-defined low temperature region*. The intermediate region has been found to be suitable for study of the dielectric dispersion phenomenon.

Second, attempts to fit the dielectric dispersion observed by Cole-Cole and/or Cole-Davidson functions have met with qualified success. This success is qualified because, as our previous discussion has shown, the functions mentioned can be accepted only if very complete dispersion data are available (i.e. ϵ' and ϵ'' values are available over such a frequency range as to define the entire function) and there is no reason

---

* Labelled phases I, II and III in figure 25.

to believe various composite functions (e.g. Budo's) would serve as well or better to define the relaxation processes involved. Since we have reason to believe secondary processes are important we have paid only lip service to these functions.

Third, notwithstanding the observations just made, attempts have been made to test Glarum's defect diffusion model. This theory explains the existence of symmetric and skewed arc behavior on the basis of defect mobility. The results fail to indicate whether or not such an approach is valid in this system, indeed it appears to be inappropriate. There are indications however that this approach, or a conceptually equivalent one such as Ullman's (70), might be applied with much success to a system for which a Cole-Cole or Cole-Davidson arc may be regarded as an adequate representation.

Fourth, Hoffman's single axis, multiposition rotator in a crystalline field appears to be admirably suited to our observed dispersion. This method has been applied to a number of solids with some success. The true test of a theory however lies in its ability to make accurate predictions. Such predictions have been made and verified only in the case of urea clathrates (79) by Hoffman. We have pointed out that the systematic variation of our system resulting from the addition of PMO to a PMS lattice should yield results predictable by Hoffman's method. Thus we predict that our dispersion region will become more complex and ill-defined with addition of PMO.

This effect is observed. Our work may, then, be regarded as a verification of this approach.

Finally, it appears that we are severely limited by our system and equipment. Work must be carried out in a very limited region of temperature, concentration and frequency, the last of these being most damning. Though the success of our methods is evident, it is not unqualified. Completely satisfactory confirmation of our speculations must then rest in a frustrating limbo of experimental uncertainty just beyong our eager grasp.

REFERENCES

I. Faraday, M., Experimental Researches p. I699 (I838).

2. Clausius, R., Die Mechanische Warmetheorie II p. 62 Braunschweig I879.

3. Mosotti ,D.F., Men. Math. Fis. Modena I4, II (I850) 49.

4. Smyth, C.P. Dielectric Behavior and Structure, McGraw-Hill, (a) P. 5 (b) p. 63 (c) Chapter 5.

5. Lorentz, H.A., "Theory of Electrons", Neubner Verlagsgesellschaft, Leipzig, I909, 306, note 55.

6. C.P. Smyth and W.N. Stoops, J. Am. Chem. Soc. 50, I883 (I928).

7. C.P. Smyth and W.N. Stoops, J. Am. Chem. Soc. 5I, 33I2 (I929).

8. K.B. McAlpine and C.P. Smyth, J. Am. Chem. Soc. 55, 453 (I933).

9. R.K. Chan and H.A.M. Chew, Can. J. Chem. 47, 2249, (I969).

I0. C.P. Smyth and S.O. Morgan, J. Am. Chem. Soc. 50, I547 (I928).

II. C.P. Smyth and K.B. McAlpine, J. Chem. Phys., 2, 499 (I934).

I2. P. Debye, Polar Molecules, Dover Publications, Copyright, The Chemical Catalog Company (I929), (a) p. 27 (b) p. 77.

I3. Langevin, P.J. phys. 4 4, 698 (I905); Ann chim. et phys. (8) 5, 70 (I905).

I4. Onsager, L., J. Am. Chem. Soc., 58 I486, (I936).

I5. Böttcher, C.J.F., Theory of Electric Polarization, Elsevier Publishing Company (I952), (a) Chapters III and VI (b) p. 255.

I6. Davies, "Some Electrical and Optical Aspects of Molecular Behavior", Pergamon Press (I965), (a) p. 76 (b) p. 86.

I7. J.G. Kirkwood, J. Chem. Phys., I, 9II (I939); Ann. N.Y. Acad. Sci., 40, 3I5 (I940); Trans. Faraday Soc. 42A, 7 (I946).

I8. Gerald Oster and John G. Kirkwood, J. Chem. Phys., II, I75 (I943).

I9. J.W. Smith, Electric Dipole Moments, Butterworths Scientific Publications (I955), (a) p. I5 (b) p. I27.

20. J.C. Maxwell, Treatise on Electricity, Oxford, London, I88I, Vol. II.

2I. L.V. Lorentz, Ann. Physik II, 70 (I880).

22. H.A. Lorentz, Ann. Phys. Lpz. 9, 64I, (I880).

23. J.P. Poley, Appl. Sci. Res. (The Hague) 4B, 337 (I955).

24. S.K. Garg and C.P. Smyth, J. Chem. Phys. 42, I397 (I965).

25. E. Whalley, Advances in High Pressure Research vol. I, Academic Press (I966).

26. Kauzmann, Walter, Rev. Med. Phys. I4, I2, (I942).

27. A. Einstein, Ann. d. Physik I7, 549 (I905).

28. R. Cole, J. Chem. Phys. 6, 385 (I938).

29. R. Cole and K. Cole, J. Chem. Phys. 9, 34I (I94I).

30. A.J. Van Eick and J.P. Poley, Appel. Sci. Res. (The Hague) 6B, 359 (I957).

3I. D.W. Davidson and R.H. Cole, J. Chem. Phys. 19, 1484 (1951).

32. D.W. Davidson, Can. J. Chem. 39, 571 (1961).

33. R.H. Cole and D.W. Davidson, J. Chem. Phys., 20, 1389 (1952).

34. H. Eyring, J. Chem. Phys. 3, 107 (1935).

35. J.P. Poley, Appl. Sci. Res. (The Hague) 4B, 337 (1955).

36. J.P. McCullough et al, J.A.C.S. 76, 2661 (1953).

37. Lydia Reinisch, Comptes Rendu, 242, 2915 (1956)

38. J.S. Allen and Harold Hibbert, J.A.C.S. 56, 1398,(1934).

39. E.A. Moelwyn-Huges and P.L. Thorpe Royal Soc. Lond. Proc. 277, 423, (1964).

40. A. Weissler, J.A.C.S. 71, 419, (1949).

41. Handbook of Chemistry and Physics, The Chemical Rubber Publishing Company. (1965-1966)

42. E.A. Guggenheim, Trans. Faraday Soc. 45, 714, (1949).

43. J.N. Smith, Trans. Faraday Soc. 46, 394 (1950).

44. J.A. McMillan and S.C. Los, J. Chem. Phys, 42, 160 (1965).

45. A.R. Ubbelohde, Melting and Crystal Structure, Clarendon Press: Oxford (1965), p. 108.

46. R.P. Auty and R. H. Cole, J. Chem. Phys. 20, 1309 (1952).

47. N.L. Brown and R.H. Cole, J. Chem. Phys. 21, 1920 (1953).

48. J.N. Sherwood, J. Phys. Chem. Solids 283, Suppl. I, 839 (1967).

49. J.G. Aston, J. Szasz and H.L. Finke, J. Am. Chem. Soc. 65, 1135 (1943).

50. Narasimhan, J.P.T., J. Indian Inst. Sci., A37, 30, (1955).

51. C.P. Smyth, E.W. Engel and E.B. Wilsnn Jr., J.A.C.S. 51, 1736 (1929).

52. Tables of Experimental Dipole Moments, McClellan A.L., W.H. Freemand and Co. (1963) (a) p. 148 (b) 149.

53. V.M. Rao and R. Kewly, Can. J. Chem. 47, 1289 (1969).

54. J. Timmermans, J. Chim.Phys, 35, 332 (1938).

55. J. Timmermans, J. Phys. Chem. Solids, 18, 1,(1961).

56. L. Pauling, Phys. Rev, 36, 430 (1930).

57. John G. Aston, H. Segall, N. Tuschillo, J. Chem. Phys, 24, 1061 (1956).

58. A.H. White and W.S. Bishop, J. Am. Chem. Soc, 62, 8 (1940).

59. Hideaki Chihara, Masako Otsuru and Syuzo Seki, Bull. Chem. Soc. Japan, 39, 2145 (1966).

60. W.P. Conner and C.P. Smyth, J. Am. Chem. Soc, 63, 3424 (I94I).

6I. J.A. Reynolds and J.M. Hough, Royal Soc. Proc. 70-B, 769 (I957).

62. P.W. Bridgman, Collected Experimental Papers, Harvard University Press

63. William L. Clayton, Ph.D. Thesis, U.W.O.

64. Arthur R. Von Hippel, Dielectrics and Waves, John Wiley & Sons p. 228.

65. R. Fuoss and J.G. Kirkwood, J. Am. Chem. Soc, 63, 385 (I94I).

66. Sivert H. Glarum, J. Chem. Phys, 33, 639 (I960).

67. Seiichi Kondo, Bull. Chem. Soc. Japan 29, 999 (I956).

68. S. Kondo and M. Matsumoto, Bull. Chem. Soc. Japan, 3I, 3I9 (I958).

69. Chandasekhar, S. Rev. Modern Phys. I5, I (I943).

70. J.E. Anderson and Robert Ullman, J. Chem. Phys. 47, 2I78 (I967).

7I. P.H. Fang. J. Chem. Phys. 42, 34II (I965).

72. A. Budo, Physik Z. 39, 706 (I938).

73. Adolf. Schmallamach, Trans. Faraday Soc. 42, I80 (I946).

74. M. D. Magee and S. Walker, J. Chem. Phys. 50, 2580 (I969).

75. C. Brot, J. Chim. Phys. 53, 45I (I956).

76. John D. Hoffman and Heinz G. Pfeiffer, J. Chem. Phys. 22, I32 (I954).

77. John D. Hoffman, J. Chem. Phys. 23, I33I (I955).

78. John D. Hoffman and Benjamin M. Axilrod, Journal of Research of the National Bureau of Standards 54, 357 (I955).

79. John D. Hoffman, Arch. Sci. (Geneva) Fac. Spec. I2, 36 (I959).

80. Wagner, Ann. Physik 40, 8I7 (I9I3).

8I. Yager, Physics, 7, 434 (I936).

82. I. Prigogine and R. Defay, Longmans Green and Co., page 368 (1954) Chemical Thermodynamics

Appendix A

1. Separation of variables.

Blaunn's equation reads:

$$\frac{\epsilon^* - \epsilon_\infty}{\epsilon_0 - \epsilon_\infty} = \frac{1}{1 + i\omega/\alpha_0} + \left[\frac{i\omega\alpha_0}{1+i\omega/\alpha_0}\right]\left[1 + q_0^{1/2}(1+i\omega/\alpha_0)^{1/2}\right]^{-1}$$

Let $\frac{1}{1+i\omega/\alpha_0} = R e^{i\phi}$

then $1 + i\omega/\alpha_0 = \frac{1}{R} e^{-i\phi} = \frac{1}{R}(\cos\phi - i\sin\phi)$

whence $\left[1 + \left(\frac{\omega}{\alpha_0}\right)^2\right] = \frac{1}{R^2}$

and $-\tan\phi = \left(\frac{\omega}{\alpha_0}\right)$

$\therefore \quad \phi = -\tan^{-1}\left(\frac{\omega}{\alpha_0}\right)$

Thus: $\frac{\epsilon^* - \epsilon_\infty}{\epsilon_0 - \epsilon_\infty} = R e^{i\phi} + \left\{ R e^{i\phi}\left[\frac{1}{R} e^{-i\phi} - 1\right]\left[\frac{1}{1 + \frac{q_0^{1/2}}{R^{1/2}} e^{-i\phi/2}}\right]\right\}$

$= R e^{i\phi} + \left\{ (1 - R e^{i\phi})\left[\frac{1 + (q_0^{1/2}/R^{1/2})(e^{i\phi/2})}{(1 + (q_0^{1/2}/R^{1/2})(e^{-i\phi/2}))(1 + (q_0^{1/2}/R^{1/2})(e^{i\phi/2}))}\right]\right\}$

$= R e^{i\phi} + \left\{ (1 - R e^{i\phi})\left[\frac{1 + (q_0^{1/2}/R^{1/2})(e^{i\phi/2})}{(1 + q_0/R + (q_0^{1/2}/R^{1/2})(e^{i\phi/2} + e^{-i\phi/2}))}\right]\right\}$

Insert: $\left(e^{i\phi/2} + e^{-i\phi/2} \right) = 2 \cos \phi/2$

and

$$a = a_0^{1/2} / R^{1/2}$$

Whence: $$\frac{\epsilon^* - \epsilon_\infty}{\epsilon_0 - \epsilon_\infty} = R e^{i\phi} + \left\{ \frac{(1 - R e^{i\phi}) \cdot (1 + a e^{i\phi/2})}{1 + a^2 + 2a \cos \phi/2} \right\}$$

Now set $(1 + a^2 + 2a \cos \phi/2) = D$

Hence $$\frac{\epsilon^* - \epsilon_\infty}{\epsilon_0 - \epsilon_\infty} = \frac{1}{D} + R\left[1 - \frac{1}{D}\right] e^{i\phi} + \frac{a}{D} e^{i\phi/2} - \frac{aR}{D} e^{i3\phi/2}$$

Expanding exponentials, followed by equating real and imaginary terms yields for ϵ':

$$\frac{\epsilon' - \epsilon_\infty}{\epsilon_0 - \epsilon_\infty} = \frac{1}{D} + R\left[1 - \frac{1}{D}\right] \cos \phi + \frac{a}{D} \cos \phi/2 - \frac{aR}{D} \cos 3\phi/2$$

2. Reduction of result to a quadratic form:

In equation for ϵ' above set:

$$E = (\epsilon' - \epsilon_\infty) / \epsilon_0 - \epsilon_\infty$$

$$F = \cos \phi \quad G = \cos \phi/2 \quad H = \cos 3\phi/2$$

Then yields:

$$a^2 [E - RF] + a [2GE - 2RFG - G + RH] + (E - 1) = 0$$

Letting $A = [E - RF]$, $B = [2GE - 2RFG - G + RH]$ $C = [E - 1]$

yields $$a = \frac{-B \pm \sqrt{B^2 - 4AC}}{2A}$$

and since $a_0 = a^2 R$, all other terms are known so mathematically we may now test Glarum's approach.